Substituent Effect on the Mechanism of Alkaline Hypochlorite Oxidations of 2-Nitroanilines
&
Structural Determination of Agnotobenzaldehyde

A THESIS
SUBMITTED TO THE FACULTY OF THE GRADUATE SCHOOL
OF THE UNIVERSITY OF MINNESOTA
BY

Glen Charles Gullickson

IN PARTIAL FULFILLMENT OF THE REQUIREMENTS
FOR THE DEGREE OF
MASTER OF SCIENCE

Professor Wayland E. Noland

October, 2010

ACKNOWLEDGEMENTS

The following people deserve recognition for their contribution to this project:

Professor Wayland E. Noland, who has supported me throughout my thesis with his patience, encouragement, and knowledge, while allowing me the room to work in my own way.

My parents, for their consistent motivation and dedicated support throughout graduate school and during the completion this thesis.

My fiancée Anna, for her love, support, and patience throughout my graduate career.

Paul J. Erdman, for his preliminary work into Part I and data from synthesis of compound **3p** and said precursors in Part I.

Henrik van Lengerich, for the synthesis and use of compound **12** in Part II.

Dr. Nicholas P. Lanzatella for his advice, friendship, and motivation throughout my membership in the Noland group.

Dr. Victor G. Young, Jr. and the XCL staff for their assistance with diffractometer issues and recommendations on structure refinement questions.

Dr. Doyle Britton, for providing data collected on crystals of **4** and **12** in Part II, his help and expertise refining crystal structures, and advice in using software for graphical presentations of X-ray structures.

ABSTRACT

This thesis presents two separate topics, which contain their own compound numbering schemes. Each part starts compound numbering with 1 and progresses independently.

Benzofurazan 1-oxides and azobenzenes are both types of compounds that are of developing interest for their potential medical and material applications, respectively. Benzofurazan 1-oxides have many positive medicinal applications allowing them to potentially enhance the way current drugs work. Alternately, azobenzenes are of developing interest as molecular switches that could be used to develop nano-circuitry due to their ability to change conductivity through photo-induced isomerism. Both of these molecules are co-products in the hypochlorite oxidation of 2-nitroanilines; this study investigates the effect of varying functional groups at differing aromatic positions to determine what effects they have and proposes a mechanism that fits the observations.

"Agnotobenzaldehyde" was a solid isolated by Eugen Bamberger from the attempted reduction of 2-nitrobenzaldehyde to 2-nitrosobenzaldehyde. Though there has been some work over the years to attempt to determine the structure of agnotobenzaldehyde, the actual structure of agnotobenzaldehyde has remained a mystery for 104 years. This thesis presents the history of agnotobenzaldehyde, the reasons for the difficulty in determining its structure, and its final structural elucidation.

TABLE OF CONTENTS

ACKNOWLEDGEMENTS i
ABSTRACT ii
LIST OF TABLES iv
LIST OF FIGURES v
LIST OF SCHEMES vi
PART I. SUBSTITUENT EFFECTS ON THE MECHANISM OF ALKALINE HYPOCHLORITE OXIDATIONS OF 2-NITROANILINES 1
1.1 INTRODUCTION 1
1.2 STARTING MATERIALS 9
1.3 BLEACH OXIDATIONS 10
1.4 RESULTS AND DISCUSSION 12
1.5 CONCLUSION 24
1.6 FUTURE APPLICATIONS 25
1.7 EXPERIMENAL 26
PART II. STRUCTURAL DETERMINATION OF AGNOTOBENZALDEHYDE 50
2.1 BACKGROUND 50
2.2 INTRODUCTION 51
2.3 MATERIAL SYNTHESIS 54
2.4 RESULTS AND DISCUSSION 55
2.5 CRYSTALLOGRAPHY: EXPERIMENTAL 59
2.6 EXPERIMENAL 61
REFERENCES 65
APPENDIX 1. SPECTRAL DATA FOR PART II. 69
APPENDIX 2. X-RAY CRYSTALLOGRAPHIC DATA FOR COMPOUND 10 IN PART II. 74
APPENDIX 3. X-RAY CRYSTALLOGRAPHIC DATA FOR COMPOUND 12 IN PART II. 84

LIST OF TABLES

TABLE 1. SUMMARY OF BLEACH OXIDATION RESULTS..... 11
TABLE 2. CRYSTAL DATA AND STRUCTURE-REFINEMENT DETAILS 60

LIST OF FIGURES

FIGURE 1. METHODS TO FORM BENZOFURAZAN 1-OXIDES 1
FIGURE 2. TAUTOMERIC EQUILIBRIUM OF BENZOFURAZAN 1-OXIDES 2
FIGURE 3. VARIABLE THERMODYNAMIC STATES OBSERVED BY NMR 2
FIGURE 4. STERIC RESTRICTIONS IN SOLID STATE 3
FIGURE 5. PRELIMINARY AZOBENZENE FORMATION RESULTS 4
FIGURE 6. ACTIVE ANTITRYPANOSOMAL COMPOUNDS 4
FIGURE 7. CALCIUM CHANNEL MODULATOR HYBRIDS 5
FIGURE 8. NON-STEROIDAL ANTI-INFLAMMATORY HYBRID 6
FIGURE 9. COMMON AZO DYES 7
FIGURE 10. STATE ENERGIES OF PHENYLNITRENE RELATIVE TO GROUND STATE ($^3A_2$) ... 18
FIGURE 11. METHANOL HYDROGEN BONDING TO SINGLET STATES 19
FIGURE 12. $^1A_2$ RING CLOSURE AND EXPANSION 21
FIGURE 13. STUDY ON THE EFFECT OF FLUORO-SUBSTITUTION OF NITROANILINES TO FORM AZOBENZENES 25
FIGURE 14. STUDY ON THE REACTIVITY OF NUCLEOPHILES ON HALO-SUBSTITUTED BENZOFURAZAN 1-OXIDES 26
FIGURE 15. EARLY PROPOSED STRUCTURES FOR ANTHRANIL 51
FIGURE 16. BAMBERGER'S PROPOSED STRUCTURES FOR AGNOTOBENZALDEHYDE 52
FIGURE 17. PRODUCTS OF BAMBERGER'S ACETYLATION AND OXIDATION OF AGNOTOBENZALDEHYDE 52
FIGURE 18. BAKKE AND ENGAN'S PROPOSED STRUCTURES FOR AGNOTOBENZALDEHYDE 53
FIGURE 19. ANISOTROPIC DISPLACEMENT ELLIPSOIDS (50% PROBABILITY) FOR **10**. 56
FIGURE 20. ANISOTROPIC DISPLACEMENT ELLIPSOIDS (50% PROBABILITY) FOR **12**. 57

LIST OF SCHEMES

SCHEME 1. PROPOSED MECHANISM FOR ALKALINE HYPOCHLORITE OXIDATION 12
SCHEME 2. CHLORIDE EJECTION 14
SCHEME 3. PROPOSED ACETYLATION ROUTE OF AGNOTOBENZALDEHYDE 54
SCHEME 4. PROPOSED MECHANISM FOR AGNOTOBENZALDEHYDE FORMATION 58
SCHEME 5. ALTERNATE MECHANISM FOR AGNOTOBENZALDEHYDE FORMATION 59

PART I. SUBSTITUENT EFFECTS ON THE MECHANISM OF ALKALINE HYPOCHLORITE OXIDATIONS OF 2-NITROANILINES

1.1 Introduction

Benzo[1,2,5]oxadiazole 1-oxides, or benzofurazan 1-oxides (BFO), were first prepared by Noelting and Kohn in 1894 by thermal decomposition of azido-2-nitrobenzenes (Figure 1) [1]. Meigen and Normann in 1900 first reported that treatment of aromatic amines with neutral sodium hypochlorite produced azo-compounds in varying quantities [2]. The cyclization of 2-nitroanilines (**1**) to benzofurazan 1-oxides (**2**) through the use of alkaline sodium hypochlorite oxidation was first discovered by Green and Rowe in 1912 (Figure 1) [3]. The structural elucidation of benzofurazan 1-oxides and the mechanism of the Green-Rowe oxidation has been considerably challenging and has led to many publications on the topic since it was first reported in 1912.

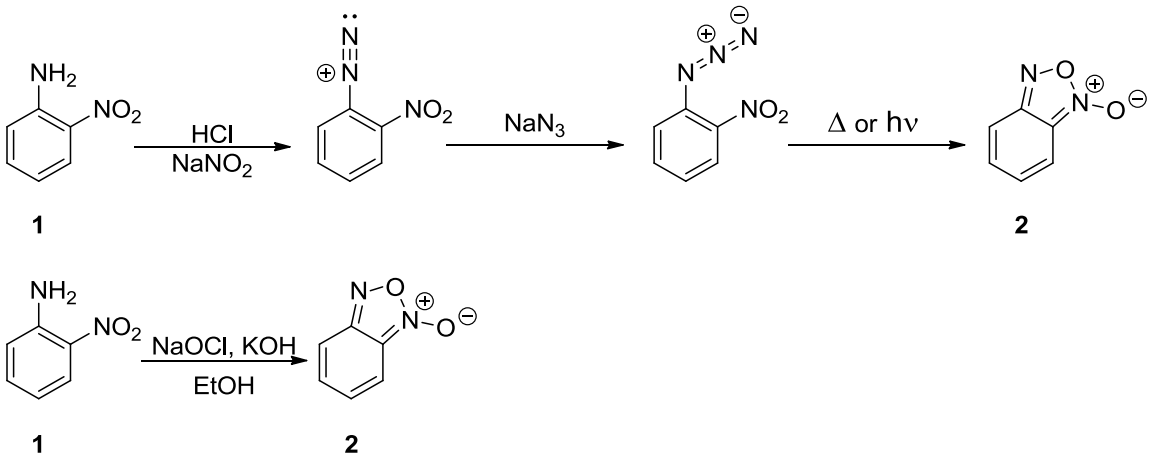

Figure 1. Methods to Form Benzofurazan 1-Oxides

Early complications in the structural elucidation stemmed from the experimental observation that only a single isomer would be obtained from reactions involving

substitutionally different isomeric 2-nitroanilines. This observation was rationalized by proposing that benzofurazan 1-oxides equilibrate between two forms by transition through a dinitroso intermediate while solvated (Figure 2) [4]. It was not until the 1960's, with the aid of variable temperature NMR, that this theory was confirmed [5]. Benzofurazan 1-oxide was cooled to -60 °C and the ^{1}H-NMR spectrum was collected, then it was warmed to 110 °C and multiple spectra were collected along the way [5]. The result of these experiments was that at low temperatures well defined peaks for a single isomer were observed, representing the *N*-oxide being in a single position, and when heated the peaks coalesced indicating rapid interconverson of the *N*-oxide between two forms (Figure 3).

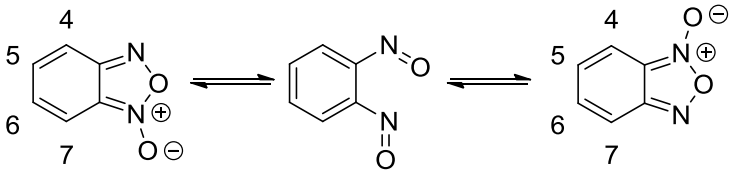

Figure 2. Tautomeric Equilibrium of Benzofurazan 1-Oxides

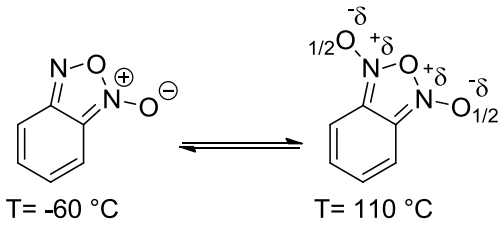

Figure 3. Variable Thermodynamic States Observed by NMR

In 1962, the Noland group reported their first results from collaboration with Dr. Doyle Britton to synthesize substituted benzofurazan 1-oxides and determine influences of steric interactions and electron-donating/withdrawing stabilization on the isomeric preference of benzofurazan 1-oxides in the solid state by X-ray crystallography [6]. In

2006 Paul Erdman, under Dr. Wayland Noland and in collaboration with Dr. Doyle Britton, presented and defended his thesis investigating substituted BFO isomerism. His results showed that steric interactions seemed to be the dominant influence determining which *N*-oxide isomer formed (Figure 4) [7].

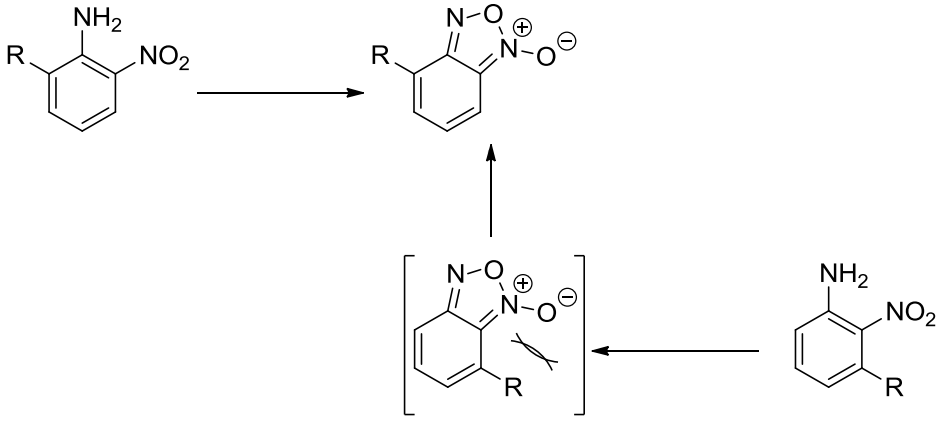

Figure 4. Steric Restrictions in Solid State

This project started off based on the observation that side-products of azobenzenes were consistently observed during the hypochlorite oxidation of specific substituted 2-nitroanilines (Figure 5). Christopher Jeffrey [8] and Paul Erdman [7] observed azobenzene **3 a-e** formation when attempting to oxidize aniline **1 a-e**, instead of the expected benzofurazan 1-oxide **2 a-e** (Figure 5). Upon exploration of this effect and repetition of these results, it was determined that azobenzenes were not the only product. The isolation of the expected benzofurazan 1-oxide (**4**) products could be accomplished, often in large quantities, depending on specific treatment techniques during the hypochlorite oxidation procedure, which will be covered in a later section.

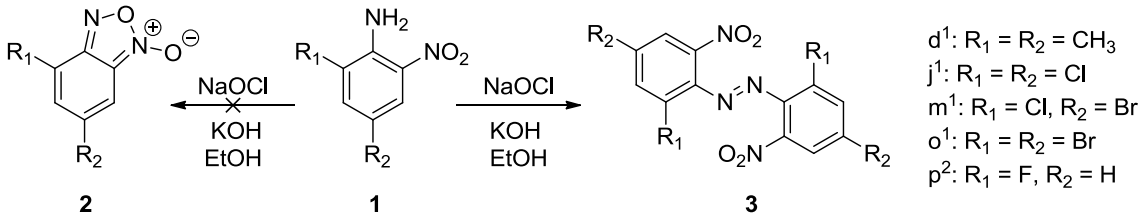

[1] Work by Christopher Jeffrey, 2003.
[2] Work by Paul Erdman, 2006.

Figure 5. Preliminary Azobenzene Formation Results (Compound Numbering and Lettering Based on *Table 1*, p.11)

In the last 40-50 years benzofurazan 1-oxides have grown in medicinal interest due to discoveries that these compounds possess interesting biological activities, most likely stemming from their equilibration through a 1,2-dinitrosobenzene. Benzofurazan 1-oxides have been evaluated to have antibacterial and antiprotozoan properties [9], antileukemic properties [10], and nitric oxide donor properties which effects vasodilation and platelet adherence inhibition [11,12].

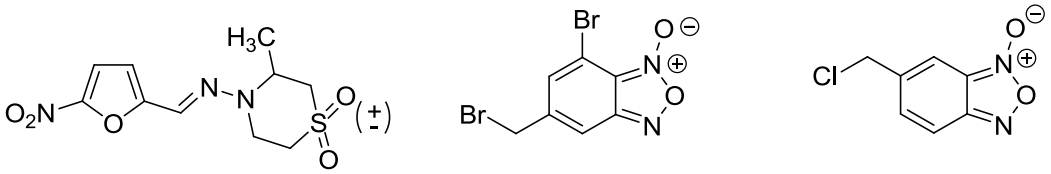

Nifurtimox® (Nfx)

4

5

Figure 6. Active Antitrypanosomal Compounds

Pharmaceutical studies in 2002 [13] and 2005 [14] investigated the activity of benzofurazan 1-oxides as an antitrypanosomal drug. The studies specifically focused on activity against *Trypanosoma cruzi*, the parasitic trypanosome that causes Chagas disease, a major third-world disease that is often fatal if untreated [13,14]. Nifurtimox® (Nfx, Figure 6) is one of the main drugs used to treat the disease currently; however, gastrointestinal and neurological side effects, in addition to a high relapse rate, makes the

disease difficult to treat with this drug. In these studies, over 30 benzofurazan 1-oxide derivatives were synthesized and screened against *T. cruzi*, with compounds **4** and **5** (Figure 6) having the highest activities. In the 2002 study, compound **4** had the highest activity out of the compounds screened with an IC_{50} of 6.3 μM, which was on the same order as Nfx (IC_{50} = 7.7 μM) [13]. Compound **5** had the highest activity out of the compounds screened in the 2005 study with an IC_{50} of 2.4 μM, which was on the same order as Nfx (IC_{50} = 6.7 μM) [14]. The studies also proposed that the use of these *N*-oxides will likely diminish or eliminate the undesirable side effects seen in Nfx, since the toxicity was probably due to the nitro group [13, 14]. The idea of substituting nitro components of current drugs with BFO analogs may provide interesting alternatives to a wide variety of drugs that probably already have undesired toxicities.

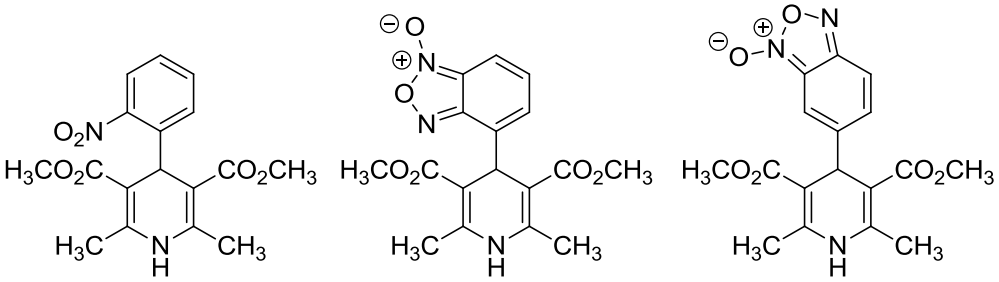

Figure 7. Calcium Channel Modulator Hybrids

In the last 10-20 years benzofurazan 1-oxide compounds have started to expand from their direct synthesis as active drugs to being combined with pharmaceutically active drugs to exploit the properties of the BFO moiety. The first application of hybridization of current drugs with BFOs was published in 1996 related to the derivatization of calcium channel blockers [15]. Nifedipine is a common

antihypertensive drug that was modified in this report by replacing the 2-nitrophenyl functionality with a BFO attached in the 4 or 6-positions of the combined systems to give compounds **6** and **7** (Figure 7). Compound **6** had the highest activity out of the compounds screened in this paper with an IC_{50} of 2.0 nM, which is on the same order as Nifedipine (IC_{50} = 1.1 nM) [15]. The goal of these modifications was to maintain potency of the base drug while adding the benefits of the BFO vasorelaxation. In this case, there was no substantial modification in the activity or vasorelaxation based on their rabbit basilar artery model [15].

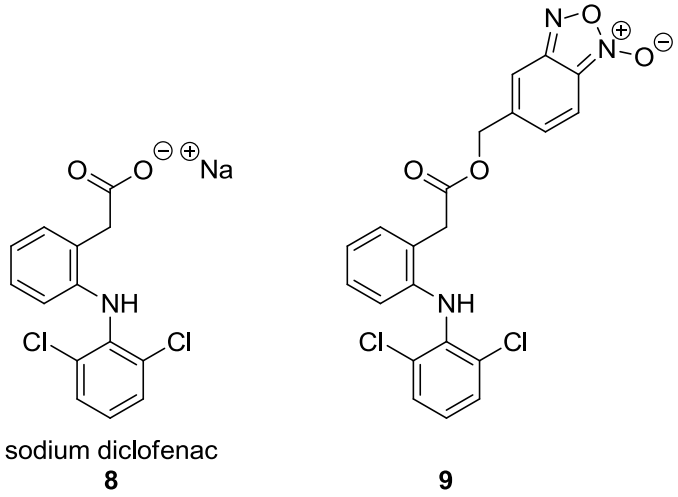

sodium diclofenac
8 **9**

Figure 8. Non-steroidal Anti-inflammatory Hybrid

Another study in 2010 investigated the combination of sodium diclofenac (**8**), a commonly used non-steroidal anti-inflammatory drug (NSAID), with benzofurazan 1-oxide (Figure 8) [16]. The problem with current NSAIDs is that their anti-inflammatory properties from COX-2 inhibition result in strong interference with ulcer healing [16]. The addition of the nitric oxide releasing benzofurazan 1-oxide functionality would hopefully aid in modulating gastric mucus production and result in NSAIDs with

diminished impact on ulcer healing. The study functionalized **8** by nucleophilic attack of the carboxylate on 5-bromomethylbenzo[1,2,5]oxadiazole 1-oxide to form **9** (Figure 8) [16]. Anti-inflammatory activity was modeled by in abdominal drug injection followed by induced inflammation in a rat's hind paw. Analytical ultracentrifugation of **8** versus **9** produced nearly identical treated to control volume ratios [2.01(31) versus 2.00(45) respectively], indicating no differences in anti-inflammatory activity [16]. The compounds were then evaluated for gastric effects by oral administration to rats. Treatment with **8** resulted in significant hemorrhagic lesions, where treatment with **9** showed much less extensive lesion formation when compared to control animals [16]. Lesion significance was based on an index scale presented in the study that weighted different observables [16]. Hybrid **9** showed approximately twice the lesion value of controls and a value three times lower than **8**. An *in vitro* nitric oxide release assay was also performed on **9** showing about a 0.4% nitrite release, which is moderate compared to the 2.5% release of a potent nitric oxide donor like (2*E*,3*E*)-4-ethyl-2-(hydroxyimino)-5-nitrohex-3-enamide [16].

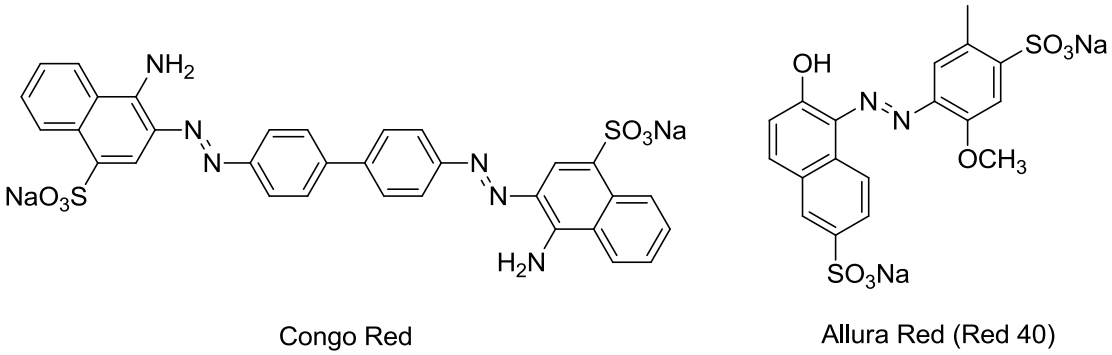

Congo Red

Allura Red (Red 40)

Figure 9. Common Azo Dyes

Aromatic azo compounds have a long history dating back to the 1880's as dyes for cotton, such as Congo Red (Figure 9), with later azo dyes developed for use on wool and silk [17]. Azo compounds are also used commonly as pH indicators due to their water solubility, which was built into many of their structures for ease of cloth dying, and due to their often sharp end point(s), which allows the azo dyes to be used as direct indicators of the pH of a solution at a specific point. Multiple dyes may also be combined on a strip of paper to allow accurate determination of the pH of a solution over a large range of acidities. More recently azo dyes have been incorporated as additives to foods for color enhancement and marketing. A common azo dye currently used as a food dye is Red #40 (Figure 9).

In the last 5-10 years there has been a great deal of interest and studies into aromatic azo compounds as light-driven molecular switches [18,19]. In 2004 Zhang *et al.* published a study on azobenzene as a molecular wire between two gold leads connected through a SCH_2 linkage. They found that a beam of light at 365 nm would convert the *trans*-isomer to the *cis*-configuration and that a beam of light at 420 nm was needed to reverse the isomerization. In the study zero-bias conductance was calculated for the trans-isomer to be about 21 μS[†], which is cited as a moderately good conductor, where the conductance of the *cis*-isomer was 2 orders of magnitude lower [18]. This energy gap allows the use of azobenzene as a molecular switch by effectively providing an on and off state.

[†] *Siemens*: SI derived unit of electric conductance, $S = \Omega^{-1} = m^{-2}*kg^{-1}*s^3*A^2$. (*IUPAC Compendium of Chemical Terminology 2nd Ed.* **1997**)

A theoretical paper in 2010 [20], by some of the same authors as the 2004 study, investigated the conductive characteristics of substituted azobenzenes. They found that *trans*-isomers with electron-donating groups displayed higher conductance potential, which varied depending on the substitution position, than azobenzene alone. Some of the derivatives that showed the largest energy gap in conductance were 2-nitro/2-amino co-dimer, 3-cyano dimer, and 2-nitro dimer, in which the energy difference between states was 1.5 to 3 times that of azobenzene [20]. The results from this study show that the energy gap between the *trans*- and *cis*-state can be enhanced through substitutional modification and that the characteristics of electronics that may use these switches can be carefully tuned by chemical modification of the azobenzene structure [20].

1.2 Starting Materials

Compounds **1a**, **1c**, and **1k** (Table 1) were commercial chemicals which were used without purification. Compounds **1b**, **1d-j**, **1l**, **1n**, and **1p** were synthesized from their un-nitrated analogs by nitration with nitric acid that usually produced two isomers of which only one was useful in this study. Compounds **1m** and **1o** were prepared by bromination of **1i** and **1l** respectively by dissolving in acetic acid and adding liquid bromine under nitrogen. Compound **1q** was prepared by iodination of **1a** by dissolving in dichloroethane at reflux and addition of 2 eq. of iodine monochloride. Compound **1p** was synthesized and the following hypochlorite oxidation was carried out by Paul J. Erdman. A detailed procedure for each synthesized starting material is provided in the Experimental Section.

1.3 Bleach Oxidations

Commercial "Blast" bleach was titrated every 6 months with an observed variance of ±0.004 M over the time of use. The procedure was a common iodometric titration where the bleach (2.00 mL) was diluted to 100.00 mL with deionized water and the diluted bleach (25.00 mL) was pipetted into a flask with potassium iodide (0.20 g) and 2 M hydrochloric acid (1.5 mL). This brown solution was titrated with standardized sodium thiosulfate (0.0200 M) from a buret. When the solution got very light brown, a saturated starch solution (2.0 mL) was added, causing the solution to turn bright blue and sodium thiosulfate was added until the blue solution turned colorless in 1 drop. The amount of standardized sodium thiosulfate used in the titration was then used to calculate the concentration of the commercial bleach (0.731(4) M).

Bleach oxidations were carried out with a consistent amount of 2-nitroaniline (0.240 mmol), volume of solvent (10.0 mL), temperature (82 °C for *tert*-butyl alcohol), and amount of base (0.480 mmol). The only variable that was left in each reaction was the amount of bleach used, which was determined for each reaction by disappearance of the fading color and excess of hypochlorite observed on starch/iodide paper. The only exceptions to this were reactions of compounds containing bromo- or iodo-substituents (Table 1, **1l-o** and **1q**)) , which were done at lower temperature (~40 °C) and altered addition procedures to prevent undesired side reactions at the bromo- or iodo-position. Compound numbering and yields can be found in *Table 1*.

Table 1. Summary of Bleach Oxidation Results

Aniline # 	Position relative to NH_2 (NO_2 = 6) 2	3	4	5	BFO # 	Yield %	Azo # 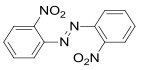	Yield %	Azo mol %
1a	H	H	H	H	**2a**	95	**3a**	1	2
1b	CH_3	H	H	H	**2b**	86	**3b**	2	5
1c	H	H	CH_3	H	**2c**	87	**3c**	3	6
1d	CH_3	H	CH_3	H	**2d**	84	**3d**	4	9
1e	H	OCH_3	H	H	**2e**	90	**3e**	2	4
1f	H	H	OCH_3	H	**2e**	88	**3f**	3	6
1g	H	CN	H	H	**2g**	84	**3g**	3	6
1h	H	H	CN	H	**2g**	86	**3h**	4	8
1i	Cl	H	H	H	**2i**	93	**3i**	6	12
1j	Cl	H	Cl	H	**2j**	91	**3j**	9	16
1k	H	Cl	Cl	H	**2k**	89	**3k**	8	14
1l	Br	H	H	H	**2l**	68[a]	**3l**	12[a]	26
1m	Cl	H	Br	H	**2m**	73[a]	**3m**	15[a]	29
1n	I	H	H	H	**2n**	38[a]	**3n**	17[a]	47
1o	Br	H	Br	H	**2o**	49[a]	**3o**	19[a]	44
1p	F	H	H	H	**2p**	0[b]	**3p**	40[b]	100
1q	I	H	I	H	**2q**	-	**3q**	-	-

[a] Modified procedure was used.

[b] Results by Paul Erdman.

Reactions with compounds **1 a-k** were pretty straightforward and recovered starting material held consistently between 1-5%; however, a sharp drop in product yield was observed with bromides and iodides. A variety of alcohols (methanol, ethanol, isopropyl alcohol, *tert*-butyl alcohol) were chosen in this study, with the added base being potassium hydroxide in all except *tert*-butyl alcohol. Variance in alkoxide had little effect on the yield of either product, though the initial color of the solution shifted more towards a light orange with weaker base and observation of the transitory red color was difficult in some cases with the weaker base. The main issue with the alkoxides appeared to be when they were used with bromides and iodides, which produced

substantially lowered yields. This sharp drop appeared to be related to the nucleophilicity of the alkoxide base, so that *tert*-butoxide was required to see any product. Even with *tert*-butoxide lower yields of BFO were obtained with little starting material recovered, so an alternate procedure was developed to minimize the rate and exposure to the base. In this procedure the temperature was lowered to ~40 °C, the base was added at the lower temperature and only directly before the hypochlorite solution was added, and quenching of the reaction was done immediately after the transitory color ceased. This modification increased the recovered yield by 20-40% with bromides and iodides, though there was still a noticeable drop in yields compared to other derivatives.

1.4 Results and Discussion

Scheme 1. Proposed Mechanism for Alkaline Hypochlorite Oxidation

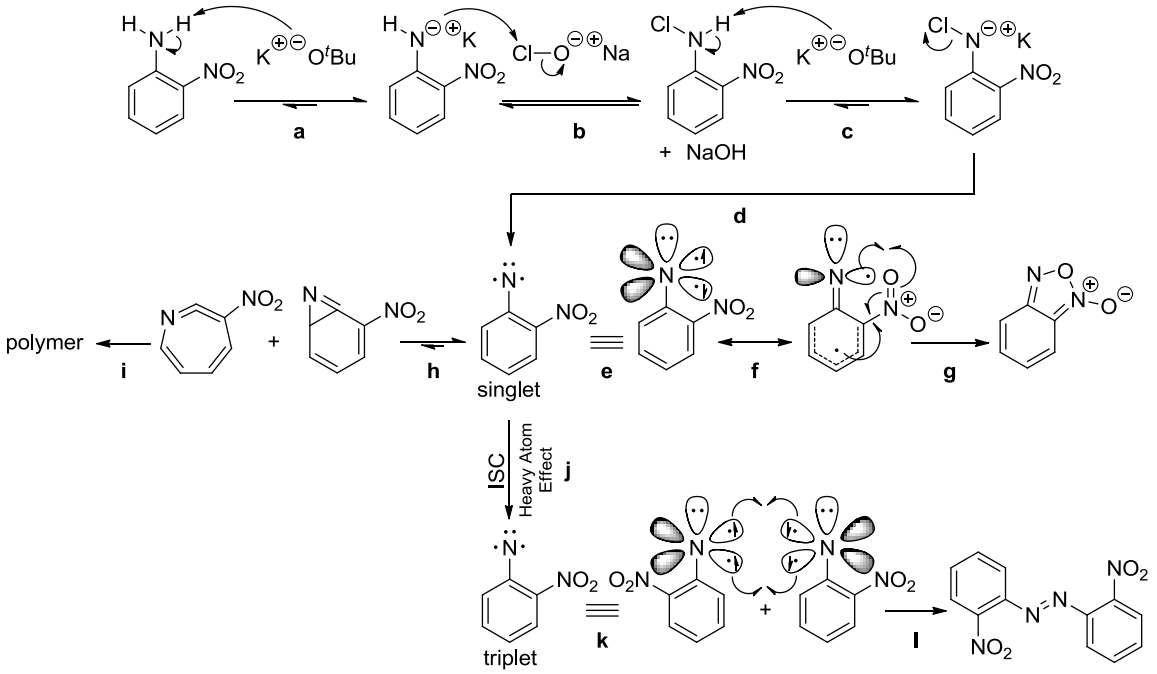

The investigation into the mechanism of the Green-Rowe oxidative cyclization was primarily begun by Dyall, an Australian chemist, around 1958 through 1984. The mechanism currently proposed in this thesis (Scheme 1, p. 12) is based on many of Dyall's reported observations and conclusions as well as new insight into the mechanism based on current information into nitrenes and experimental data presented within.

The mechanism starts out relatively simply with *tert*-butoxide removing a proton from the amino group of the 2-nitroaniline (Scheme 1, **a**, p. 12), which leads to the initial deep red color seen in the reaction. The next step involves nucleophilic attack by the nitrophenylamide on hypochlorite acting as a cationic chlorine source (Scheme 1, **b**, p. 12). This act of formation of the *N*-chloro-2-nitroaniline was experimentally justified by Dyall through monitoring the UV-VIS absorbance during this transition, synthesizing and characterizing *N*-chloro-2-nitroaniline by another route, and comparing the λ_{max} (376 nm) under similar conditions [21]. The *N*-chloroaniline is then deprotonated again by *tert*-butoxide (Scheme 1, **c**, p. 12), which gives the observed transitory red color seen after each drop of hypochlorite is added. This was also justified by Dyall through the addition of base (potassium *tert*-butoxide or lithium methoxide) to the aforementioned solution of *N*-chloro-2-nitroaniline and observing a λ_{max} (524 nm) [21b]. This can also be rationalized by the experimental observation that two equivalents of base is required to cause complete conversion and that the *N*-chlorination of the amino group should lower the pK_a of the remaining *N*-hydrogen. The subsequent steps become much more complex and will require in depth explanations for each step.

Scheme 2. Chloride Ejection

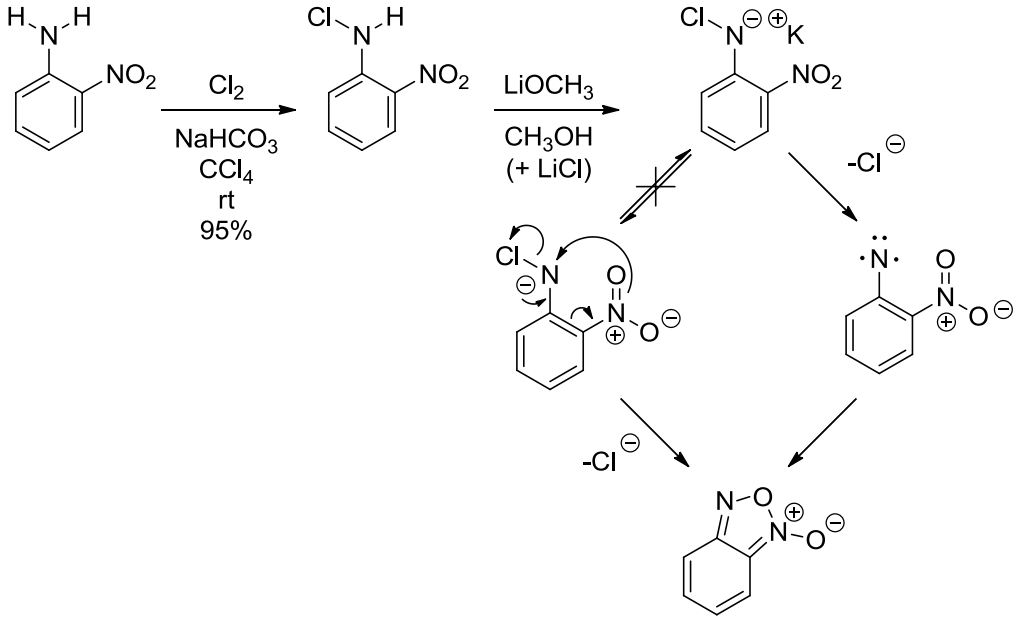

Step **d** (Scheme 1, p. 12) involves the irreversible loss of chloride to form a very short-lived phenylnitrene. In order to explain this step, it first must be known that the fading of the transient red color (*N*-chlorophenylamide) occurs at the same detectable rate as the formation of the benzofurazan 1-oxide [21b]. This implies that the loss of chloride is correlated to the rate-determining step; there are two reasonable methods of explaining this: (1) irreversible chloride loss resulting in a singlet phenylnitrene followed by a rapid ring closure or (2) reversible loss of chloride through an electrocyclic ring closure (Scheme 2). These two cases should be differentiable by determining if chloride concentration influences the rate of the reaction, implying the reversibility of the loss of chloride. In addition, placing bulky groups next to the amino and nitro groups should show an inhibition in the rate of formation of benzofurazan 1-oxide, for an electrocyclic ring closure mechanism, due to the out-of-plane distortion of the reactive groups caused by steric interactions [21b].

In order to identify which chloride ejection method was most reasonable, Dyall determined the rate of formation of benzofurazan 1-oxide by reaction of *N*-chloro-2-nitroanilne with lithium methoxide in methanol and comparing it with the same reaction with added lithium chloride as a chloride source; lithium nitrate was used as a control to provide equivalent ionic strength [21b]. Rates of the reactions for addition of lithium chloride and lithium nitrate were within the uncertainties of each other (0.196(2) s^{-1} and 0.191(9) s^{-1}, respectively) [21b]. These results indicate that the reaction rate is independent of chloride concentration, thus eliminating the reversible mechanism, or that the forward rate constant is so much larger than the reverse that the effect of chloride concentration is not differentiable.

The effects of placing sterically hindering methyl groups next to the amino and nitro groups, at 3- or 6- or 3,6-positions [7, 21b], seemed to have little or no effect on the observable rate of red color fading when we compared it to the same relative functionalities placed at 4- or 4,5-positions. Dyall also reported that the rate of product formation from 6-methyl-2-nitroaniline did not stand out from the rate determined for 5-methyl-2-nitroaniline (0.291 s^{-1} and 0.332 s^{-1} at 0 °C, respectively) when using potassium *tert*-butoxide as the base [21b]. In addition to these results, investigation by Platz *et al.* has shown a singlet phenylnitrene intermediate in the formation of benzofurazan 1-oxide from photolysis of azido-2-nitrobenzene [22]. It is also noteworthy that the study determined the lifetime of singlet 2-nitrophenylnitrene to be 8.3 ps before its ring closure to benzofurazan 1-oxide, indicating how small a component of the overall rate this step is compared to the loss of chloride [22].

Once a singlet phenylnitrene is formed there are three potential routes the reaction can take: (1) the singlet can react intra-molecularly with the nitro group to ring-close to a benzofurazan 1-oxide (Scheme 1, **e-g**, p. 12) [22]; (2) the singlet can ring-close to an adjacent *ortho*-position to form a benzazirine and/or undergo ring-expansion to form didehydroazepine which results in the isolation of polymers (Scheme 1, **h-i**, p. 12) [23,24]; or (3) undergo intersystem crossing (ISC), resulting in a triplet phenylnitrene which can inter-molecularly couple to form an azobenzene (Scheme 1, **j-l**, p. 12) [24,25]. In order to understand the routes and what determines preference for each route we must first understand more about nitrenes, specifically phenylnitrene. A nitrene is quite a bit different from a carbene, though until the late 1980's they were considered to have equivalent electronic states.

Phenylcarbene has two common low energy states, singlet and triplet, with triplet being the ground state. Singlet phenylcarbene has two non-degenerate nonbonding molecular orbitals (NBMOs) consisting of a 2p-π anti-bonding (AB or *) orbital and a hybridized σ orbital with both nonbonding electrons in the same σ orbital with anti-parallel spins [26]. Triplet phenylcarbene has similar geometry to the singlet, but the electrons are in a $\sigma\pi$ configuration, an open-shell configuration, with one electron in the σ orbital and the other in the π^* orbital with parallel spins [26]. The energy gap between these orbitals in phenylnitrene is very small (< 2 kcal/mol at 25 °C), permitting rapid

intersystem crossing[‡] between states ($k > 10^9\ s^{-1}$) facilitated by spin-orbit coupling [24,26].

Phenylnitrene has three interesting low energy states, a "closed shell" singlet (1^1A_1), an "open shell" singlet ($^1A_2$), and a triplet ($^3A_2$), with triplet being the ground state as in phenylcarbene (Figure 10). In all three states the lone pair of electrons on nitrogen occupies a 2s hybrid AO [24]. The highest energy state is a "closed shell" singlet state (1^1A_1), which looks similar to the singlet state of phenylcarbene, which has both electrons in a single 2p-σ orbital with anti-parallel spins [24]. The "open shell" singlet state ($^1A_2$) is quite different from 1^1A_1 and $^3A_2$ states, formally having one electron in the 2p-σ orbital and the other in the π orbital with anti-parallel spins (Scheme 1, **e**, p. 12) [24]. This orientation and anti-parallel spin state allows the π orbital of this state to delocalize the electron into the aromatic ring (Scheme 1, **f**, p. 12), lowing the energy of the state by ~12 kcal/mol with respect to 1^1A_1. This is allowed in only this state because the anti-parallel spin state of the electrons in separate orbitals allows their motions not to be correlated by the Pauli Exclusion Principle, allowing for decrease in Coulombic repulsion energy of like charges. These conditions result in an iminyl/cyclohexadienyl-like biradical (Figure 10) [24-27]. The ground state triplet ($^3A_2$), which looks similar to the triplet state of phenylcarbene, has one electron in the 2p-σ orbital and the other in the π orbital with parallel spins. Even though the triplet has a

[‡] *Intersystem crossing*: An isoenergetic radiationless transition between two electronic states having different multiplicities. It often results in a vibrationally excited molecular entity in the lower electronic state, which then usually deactivates to its lowest vibrational level. (*IUPAC Compendium of Chemical Terminology 2nd Ed.* **1997**)

similar configuration of electrons the fact the electrons have the same spin prevents delocalization.

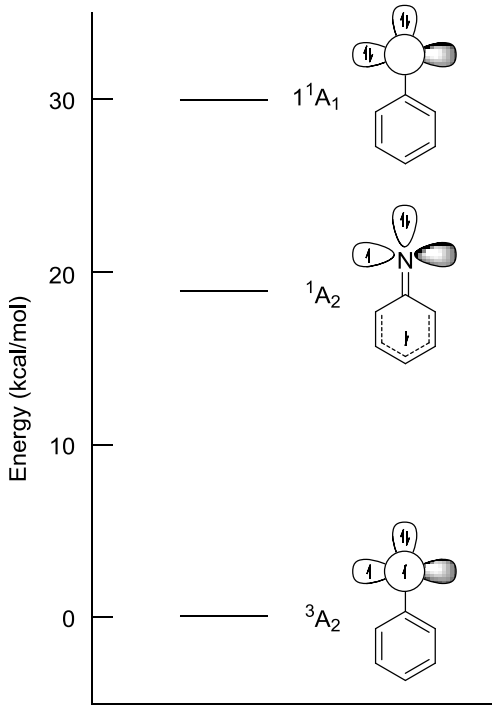

Figure 10. State Energies of Phenylnitrene Relative to Ground State ($^3A_2$) [24,28]

Intersystem crossing between $^1A_2$ and $^3A_2$ states is much more difficult for the phenylnitrene compared to the phenylcarbene. This is because ISC by spin-orbit interaction is forbidden in the phenylnitrene since the electrons are already in the same orbitals. [24,26]. Thus ISC is proposed to be facilitated by vibronic mixing between $^1A_2$ and 1^1A_1 states, where ISC by spin-orbit coupling is allowed in the "closed shell" singlet state (1^1A_1). In addition, there is a large energy gap (~18 kcal/mol, <2 kcal/mol for the phenylcarbene) between the phenylnitrene $^1A_2$ and $^3A_2$ states which makes ISC irreversible, unlike the phenylcarbene [24-28]. It has been shown that methanol can selectively enhance ISC for phenylnitrenes [29]. This capability is believed to happen

because alcohols could stabilize the "closed shell" singlet phenylnitrene state over the "open shell" singlet state, thus lowering the energy gap and allowing for a higher rate of ISC by spin-orbit coupling through the 1^1A_1 state to form the triplet (Figure 11). One can postulate that these effects would be diminished by the use of alcohols like *tert*-butyl alcohol because the higher pk_a, compared to methanol, lowers the hydrogen bond stabilization. Also the bulky nature of *tert*-butyl alcohol may interfere with the ability to hydrogen bond more than once to a specific location in space.

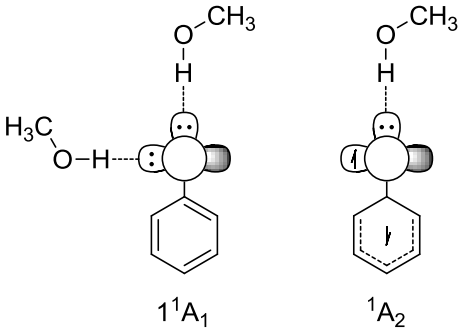

Figure 11. Methanol Hydrogen Bonding to Singlet States [29]

With the information presented above we can now rationalize each pathway that might be taken from the singlet phenylnitrene. Pathway **e-g** (Scheme 1, p. 12) is the action of the singlet phenylnitrene ($^1A_2$) rapidly ring closing by coupling of the cyclohexadienyl-like radical through the nitro group to the 2p-σ orbital of the iminyl-like radical to form benzofurazan 1-oxides. This pathway can be optimized by: (1) heating to increase the rate of *N*-chloro-2-nitrophenylamide consumption; (2) using over two equivalents of a strong base; (3) diluting the reaction/reactant to lower the probability of intermolecular coupling of the triplet. On point #1, heating seemed to drastically increase the fading rate of the *N*-chloro-2-nitrophenylamides; so much that at room temperature

some took over 5-15 minutes to fade per drop, which made the reaction very tedious with no benefits. On point #2, methoxide, ethoxide, isopropoxide, and *tert*-butoxide were tested and all worked similarly in most cases; however, the nucleophilicity of the base was found to be important in bromo- and iodo-substituted anilines (**1l-o**, **1q**). Even with *tert*-butoxide there seemed to be some issues (~25% yield of BFO), which could be partly alleviated by modifying the procedure by adding the base at around 40 °C, followed by immediate dropwise addition of sodium hypochlorite and immediate workup after the color fading ceased (~65% yield of BFO). However, even with modification the reaction of the diiodo compound (**1q**) was very messy under these conditions, producing many side products, not allowing isolation of any of the desired products. On point #3, it was found that dropwise addition of bleach followed by careful monitoring and waiting for color to fully dissipate after each drop produced the best yields of benzofurazan 1-oxides in all cases. It is my hypothesis that rapid addition of bleach causes increased concentration of phenylnitrene, which allows for buildup of triplet phenylnitrene concentration and promotes azobenzene formation. Even though ISC to the triplet is irreversible the triplet will abstract hydrogen if it is unable to intermolecularly couple, regenerating starting material.

Functionalization of 2-nitroanline with electron-withdrawing and donating groups (methoxy (**1e-f**) and cyano(**1g-h**)) in positions that could affect electron density at the nitrene or the nitro group by resonance seemed to have little or no influence on the yield of benzofurazan 1-oxide. However, both cyano derivatives did seem to cause the rate to go much slower than usual and the methoxy derivatives seemed to speed up the rate.

This is probably due to the relative inductive effects for each substituent, rather than resonance effects we were testing for, since the effect appeared to be dependent on the group and not on the position of substitution. The cyano group may have caused competitive stabilization of the cyclohexadienyl radical away from the nitro group and the methoxy group may have in turn increased the rate of ring closure. Only one 5-substituted benzofurazan 1-oxide isomer for each functional group type was observed, which is what was expected due to *N*-oxide migration.

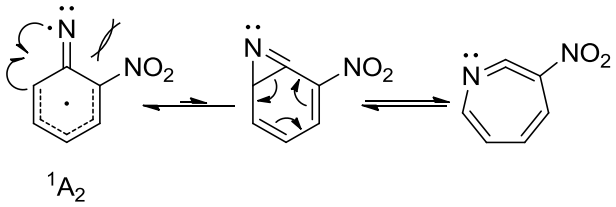

Figure 12. $^{1}A_{2}$ Ring Closure and Expansion

Pathway **h** and **i** (Scheme 1, p. 12) has been shown as a common pathway for unsubstituted phenylnitrene [24,26,30]; however, there is usually little polymer observed in hypochlorite oxidations of 2-nitroaniline. The ring closure occurs by radical coupling on the least hindered side to form a benzazirine, which rapidly relieves ring strain to form a didehydroazepine [24]. The reasons this may be observed less in this study are: (1) steric inhibition since many of our examples include 2,6-subsituted anilines, (2) the inductive effect of the nitro group cause the electron density of the aromatic ring to be localized closer to the nitro group, lowering the ability to couple at the less hindered side, and (3) the rate of ring closure to the nitro is likely much greater than this route and creates a 5-6 fused ring system versus the much more strained 3-6 fused ring system containing an unsaturated azirine (Figure 12). There has been no work in this study on

this route specifically, but it is possible this route may compete with azobenzene formation in cases where there is no 2-substitution.

Pathway **j-l** (Scheme 1, p. 12) involves intersystem crossing of a singlet phenylnitrene to a triplet followed by intermolecular radical termination by coupling with an opposite spin partner. In the optimized procedure, waiting for color to fade before each additional drop of hypochlorite, azobenzene formation was minimized in most cases; however, there was a clear trend that halogen substituents affected the yield of triplet phenylnitrene product. The trend seems to increase based on the number and size of the halogens present, except in the case of fluoride. The results from chloride, bromide, and iodide substituents are likely due to the heavy atom effect[§] on ISC [31]. The effect can either be due to the heavy atom intermolecularly interacting with a phenylnitrene or intramolecularly by influence of the delocalized radical in the $^1A_2$ state. Intermolecular interactions with correct orientations seem unlikely in a dilute solution, so the most likely cause is an intramolecular effect.

Yields of azobenzene appeared to increase from chloride to iodide substitution and from single to double substitution. However, there was an oddity in this trend where single substitution of fluorine (**1p**) produced exclusively azobenzene using the Green-Rowe method [3] and exclusively benzofurazan 1-oxide using the Noelting and Kohn method [1,7]. This observation implies that some factor in the Green-Rowe conditions influenced the ISC to the triplet. Fluorinated aromatic nitrenes have been studied quite a

[§] *Heavy atom effect*: The enhancement of the rate of a spin-forbidden process by the presence of an atom of high atomic number, which is either part of, or external to, the excited molecular entity. Mechanistically, it responds to a spin-orbit coupling enhancement produced by a heavy atom. (*IUPAC Compendium of Chemical Terminology 2nd Ed.* **1997**)

bit since they seem to have a unique ability to react with alkanes to give C-H insertion products when prepared from the azide [29,32]. The studies showed that a singlet phenylnitrene caused bond insertion, similar to the case of phenylcarbene, and that the triplet phenylnitrene reacted as it usually does by formation of azobenzene or by hydrogen abstraction. These results imply that either fluorine substitution causes change to the classic $^1A_2$ delocalized system or that fluorination lowers energy of the 1^1A_1 state such that it plays more of a role in phenylnitrene reactivity. From comparison of our results with the study, where singlet fluorine substituted phenylnitrenes behaved similar to the case of the singlet phenylcarbene, it is my hypothesis that fluorine substitution may lower the energy of the 1^1A_1 state consistent with our observations. This justified because in the study the $^1A_2$ state still facilitates ring closure to a benzazirine in an aprotic toluene solution, while methanol catalyzes ISC better than most phenylnitrenes due to the more accessible 1^1A_1 state (Figure 11, p. 19). This hypothesis is supported by an observation from Paul Erdman that when this reaction was performed in *tert*-butyl alcohol with *tert*-butoxide the yield of azobenzene obtained dropped to 6-15%, presumably due to the lack of energy state stabilization with *tert*-butyl alcohol relative to methanol [7]. Also part of the fluorinated phenylnitrene study supports this hypothesis through the observation that fluorine-substituted singlet phenylnitrenes predominately abstracted hydrogen when produced in methanol [32]. From this it is logical that the only observed product would be azobenzene in our case, since the only pathways accessible are azobenzene formation, ring closure/expansion with a compound that has both *ortho*-positions substituted causing

inhibition, and regeneration of starting material from both singlet and triplet states by hydrogen abstraction.

Previous observations that 2,4-dimethyl-6-nitroaniline (**1d**) produced predominantly azobenzene products (Figure 5) was shown not to be true with the optimized procedure. The observance of large amounts of azobenzene in this reaction is understandable with methyl substituted 2-nitroanilines since there is no observable color upon adding bleach in methoxide solution, which could lead to a larger buildup of phenylnitrene potentially giving increased azobenzene formation.

1.5 Conclusion

Variously substituted *o*-nitroanilines undergo ring closure to benzofurazan 1-oxide formation or 2,2'-dinitroazobenzene formation during modified Green-Rowe alkaline hypochlorite oxidations. Excellent yields of benzofurazan 1-oxides were obtained with non-bromo- or iodo-substituted anilines by following the optimized procedure listed above and in the Experimental Section. Low to moderate yields of azobenzenes were found to be obtained through careful treatment of halogenated o-nitroanilines, with fluorine-substituted derivatives showing remarkable trends favoring further investigation and optimization. The synthesis of benzofurazan 1-oxides or 2,2'-dinitroazobenzenes using this method, with the selection of a properly substituted *o*-nitroaniline for the desired product, provides larger over-all yields due to fewer steps being required and the synthesis can be done at lower costs compared to common reagents required for other methods.

1.6 FUTURE APPLICATIONS

The intriguing reactivity of fluoro-substituted 2-nitroanilines giving the comparatively large yields of azobenzene seen in *Table 1* is worth investigation. Investigation of how to optimize azobenzene formation would be worthy of note as it would provide an excellent method of forming substituted azobenzenes on a large scale with exclusive formation of product and recovery of starting material. In addition, it would be interesting to synthesize different fluoro-substituted nitroanilines, with fluoro- and nitro-functionality at different positions and/or with multiple substitutions. This will determine if 2-fluoro-6-nitroaniline (**1p**) has this behavior exclusively or if it is a general behavior of all fluoro-substituted nitroanilines (Figure 13).

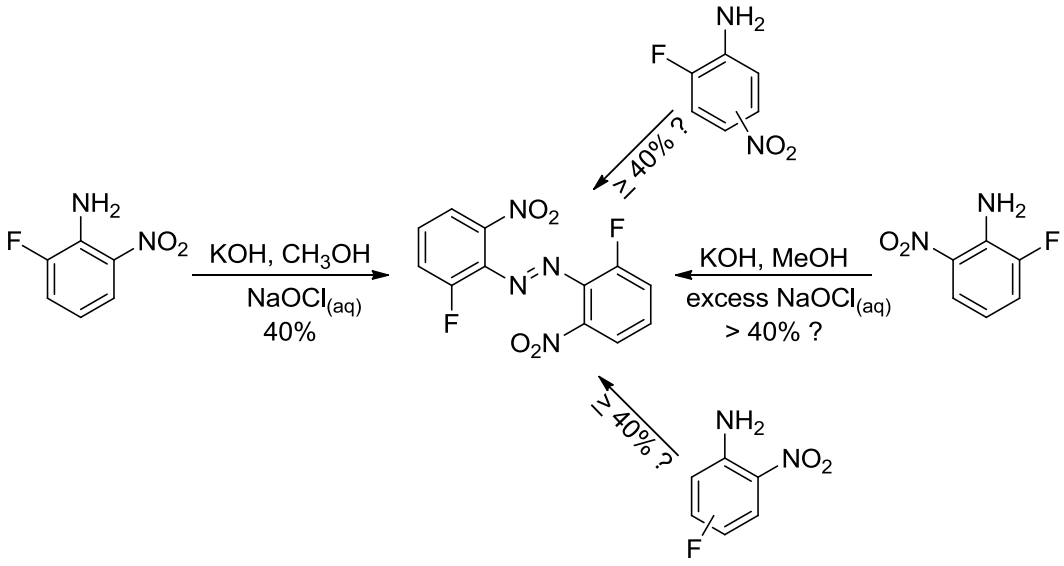

Figure 13. Study on the Effect of Fluoro-Substitution of Nitroanilines to Form Azobenzenes

Halo-substituted benzofurazan 1-oxides may provide easy access into derivatization with current drugs that have hydroxyl, amino, thio or similar groups that can be deprotonated and used as nucleophiles to displace the halides (Figure 14). Some

work in the Noland lab has already been done with fluoro-substituted benzofurazan 1-oxides showing good results with methoxide [7]. This work could be continued with different nucleophiles, with different steric restraints and/or nucleophilicity, to determine the limitations of using halo-substituted benzofurazan 1-oxides as derivatizing agents on drugs to potentially provide increased drug efficiency or reduce the side effects of a drug (Figure 8, p. 6).

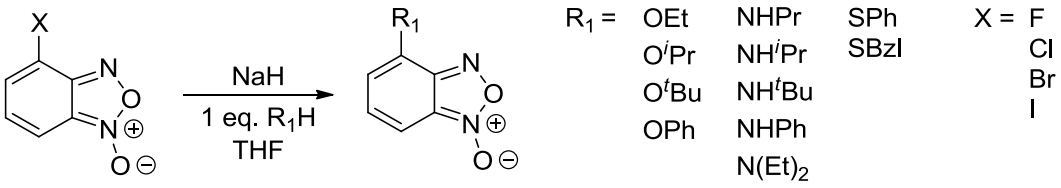

Figure 14. Study on the Reactivity of Nucleophiles on Halo-Substituted Benzofurazan 1-Oxides

1.7 Experimenal

General. Sodium hypochlorite solution used was a commercial product (Blast Bleach) at 0.731 M (iodometric titration) and pH ~10. All other solvents and reagents were also purchased and used as received unless otherwise stated. Thin-layer chromatography (TLC) was performed on plastic-backed pre-coated plates with 0.2 mm thick silica gel containing F_{254} indicator, eluting with the solvents indicated and visualized with a 254 nm UV lamp. Melting points were determined on a Fisher-Johns hot-stage melting point apparatus and are uncorrected. Infrared spectra were acquired on a 4000 FT-IR spectrometer. Nuclear magnetic resonance spectra chemical shifts (δ in ppm) were referenced to the solvent (dichloromethane, acetone, or methanol) [33] and ^{13}C spectra were proton-decoupled.

Nitration Method A (With Fuming Nitric Acid in Acetic Anhydride). The aniline derivative (0.100 mol) was added to acetic anhydride (75 mL) at 0 °C and the solution was stirred for 5 minutes. TLC with ethyl acetate and hexanes (1:1) was taken to ensure complete acetylation. Fuming nitric acid (0.150 mol, 90-93%) was added dropwise to the stirred solution while maintaining an internal temperature below 15 °C. The reaction solution was stirred for 30 minutes before being poured on ice (100 g). The resulting precipitate was collected by vacuum filtration and washed with a generous amount of water. The precipitate was added to a flask containing ice-cold sulfuric acid and allowed to warm to room temperature with stirring. After 3 hours of stirring at room temperature, TLC with ethyl acetate and hexanes (1:1) showed complete conversion of the *N*-acetyl product to the aniline derivative. The reaction solution was poured over ice (100 g) and extracted with ethyl acetate (3 x 20 mL), and the combined extracts were washed with saturated aqueous sodium bicarbonate until bubbling ceased and then with distilled water (30 mL). The ethyl acetate extract was dried over anhydrous magnesium sulfate, filtered, and the solvent evaporated on a rotating evaporator. In all cases where nitration produced a mixture of isomers, the bright yellow, orange, red, or brown solid mixture was separated quantitatively, based on ^{1}H-NMR, by Soxhlet extraction using hexanes over a period of 12-24 hours with the *o*-nitration products being recovered from the hexane solution.

Nitration Method B (With Sodium Nitrate in Sulfuric Acid on the N-acetyl derivative). The aniline derivative (0.100 mol) was added to acetic anhydride (75 mL) at 0 °C and the solution was stirred for 5 minutes. TLC with ethyl acetate and hexanes (1:1) was taken to

ensure complete acetylation. The solution was poured on ice (100 g) and the solid precipitate was recovered by vacuum filtration. The solid *N*-acetyl derivative was placed in a flask and dissolved in ice-cold sulfuric acid in an ice bath. A solution of sodium nitrate (0.100 mol) in the minimum amount of sulfuric acid required to dissolve it was added dropwise to the stirred solution while maintaining an internal temperature below 10 °C. The reaction was stirred until TLC showed complete nitration. Then the solution was warmed to room temperature and/or heated to 40 °C as needed to facilitate deacetylation. After being stirred for 1 hour, TLC with ethyl acetate and hexanes (1:1) showed complete *N*-deacetylation to the aniline derivative. The reaction solution was then poured on ice (100 g) and the resulting precipitate was collected by vacuum filtration and washed with a generous amount of water. In all cases where nitration produced a mixture of isomers, the bright yellow, orange, red, or brown solid mixture was separated quantitatively, based on ^{1}H-NMR, by Soxhlet extraction using hexanes over a period of 12-24 hours with *o*-nitration products being recovered from the hexane solution.

Oxidation Method A (With Unrestricted Exposure to Alkoxide). A modified procedure from Green and Rowe [3]: The 2-nitroaniline derivative (0.240 mmol) was dissolved in *tert*-butyl alcohol (6.00 mL) and with stirring the solution was heated to reflux. Then potassium *tert*-butoxide (0.480 mmol) was added, causing a color change to dark orange or dark red, and refluxed with stirring for 30 minutes. Sodium hypochlorite solution (~1.0 mmol, 0.731 M) was added dropwise, causing the solution to momentarily become deep red, which dissipated over time (5-90 seconds at reflux). The sodium hypochlorite

solution was added at a rate slow enough for the solution to go back to its original color after each drop was added. At the end of the dropwise addition the red color no longer developed and the solution was paler than when the addition started. The endpoint was determined to be when the color change no longer occurred and the solution tested positive for excess hypochlorite in a starch-iodide paper test. The *tert*-butyl alcohol was evaporated by passing an air stream over it. Then water was added (~10 mL) and the solution was extracted with dichloromethane (3 x 10 mL). The combined organic extracts were dried over anhydrous magnesium sulfate, filtered, and the solvent was evaporated on a rotating evaporator, leaving a pale yellow, orange, or red solid. Medium-pressure liquid chromatography (MPLC) was used to separate and/or purify the products.

Oxidation Method B (With Limited Exposure to Alkoxide). A modified procedure from Green and Rowe [3]: The 2-nitroaniline derivative (0.240 mmol) was dissolved in *tert*-butyl alcohol (6.00 mL) and with stirring the solution was heated to 40 °C. Then potassium *tert*-butoxide (0.480 mmol, 2eq.) was added, causing a color change to dark orange or dark red. Sodium hypochlorite solution was added immediately at a rate slow enough to allow the solution to go back to its original color after each drop was added. At the end of the dropwise addition the transient color no longer developed and the solution was paler than when the addition started. The reaction solution was cooled promptly in an ice bath and brought to a pH of 7 with 1 M hydrochloric acid. The solution was warmed to room temperature and the *tert*-butyl alcohol was evaporated by passing an air stream over it. Then water was added (~10 mL), and the solution was extracted with dichloromethane (3 x 10 mL). The combined organic extracts were dried

over anhydrous magnesium sulfate, filtered, and the solvent was evaporated on a rotating evaporator, leaving a pale yellow, orange, or red solid. MPLC was used to separate and/or purify the products.

Benzo[*c*][1,2,5]oxadiazole 1-oxide (2a) and **1,2-bis(2-nitrophenyl)diazene (3a).** Oxidation Method A was used with the aniline **1a** (33.2 mg, 0.240 mmol), giving **2a** (31.0 mg, 0.228 mmol, 95%) as pale yellow block crystals: m.p. 68-69 °C (lit. 70-71 °C [1]); ^{1}H-NMR (300 MHz, $CDCl_3$, δ) 7.52 (br s, 1H), 7.40 (br s, 1H), 7.28 (br s, 2H); ^{13}C-NMR (75 MHz, $CDCl_3$, δ) 132.43, 129.08, 118.11, 113.00; IR (KBr, cm^{-1}) 3098(w), 3086(w), 1659(w), 1616(s), 1588(s), 1538(s), 1486(s), 1443(m), 1430(w), 1423(m), 1353(m), 1284(w), 1257(w), 1252(w), 1202(w), 1147(m), 1127(m), 1048(w), 1016(s), 989(w), 975(w), 894(m), 836(m), 758(m), 748(s), 735(m), 673(m); and **3a** (0.7 mg, 0.005 mmol, 1%) as deep red needles: m.p. 191-193 °C (lit. 194-195 °C [2]); ^{1}H-NMR (300 MHz, $CDCl_3$, δ) 8.73 (dd, J = 6.9, 3.4 Hz, 4H), 7.83 (dd, J = 6.9, 3.4 Hz, 4H); IR (KBr, cm^{-1}) 3109(w), 1607(s), 1467(s), 1431(s), 1403(w), 1368(m), 1352(s), 1272(m), 1259(w), 1210(w), 1115(w), 1091(s), 1011(w), 961(w), 858(m), 807(m), 777(s), 766(s), 709(w), 669(w), 621(s).

2-Methyl-4-nitroaniline (11) and **2-methyl-6-nitroaniline (1b).** Nitration Method A was used with 2-methylaniline (**10**) (2141 mg, 19.98 mmol), giving **11** (508 mg, 3.34 mmol, 17%) as pale yellow needles: m.p. 129-130 °C (lit. 127-128 °C [34]); ^{1}H-NMR (300 MHz, $CDCl_3$, δ) 8.05 (s, 1H), 7.99 (d, J = 9.1 Hz, 1H), 6.61 (d, J = 8.9 Hz, 1H), 4.30 (br s, 2H), 2.22 (s, 3H); ^{13}C-NMR (75 MHz, $CDCl_3$, δ) 150.53, 138.87, 126.21, 123.88, 120.76, 112.83, 16.94; IR (KBr, cm^{-1}) 3475(s), 3364(s), 3249(m), 3229(w),

2940(w), 1635(s), 1601(m), 1583(m), 1510(s), 1475(s), 1468(w), 1441(w), 1382(w), 1312(s), 1294(s), 1276(s), 1203(w), 1155(w), 1101(s), 1041(w), 1015(w), 934(w), 893(w), 823(w), 814(w), 754(m), 712(w), 650(w); and **1d** (1784 mg, 11.72 mmol, 59%) as bright yellow needles: m.p. 96-97 °C (lit. 97 °C [35]); ^{1}H-NMR (300 MHz, $CDCl_3$, δ) 8.01 (d, *J* = 8.7 Hz, 1H), 7.25 (d, *J* = 6.6 Hz, 1H), 6.61 (t, *J* = 7.6 Hz, 1H), 6.13 (br s, 2H), 2.22 (s, 3H); ^{13}C-NMR (75 MHz, $CDCl_3$, δ) 143.27, 135.83, 131.97, 125.07, 124.02, 115.73, 17.27; IR (KBr, cm^{-1}) 3476(m), 3355(m), 2976(w), 1617(s), 1592(m), 1585(m), 1570(m), 1509(s), 1465(w), 1442(m), 1424(s), 1382(m), 1364(m), 1326(s), 1252(s), 1192(m), 1160(w), 1103(w), 1086(m), 1038(w), 1001(w), 954(w), 921(w), 891(w), 846(w), 791(w), 780(w), 737(s), 634(w).

4-Methylbenzo[*c*][1,2,5]oxadiazole 1-oxide (2b) and **1,2-bis(6-methyl-2-nitrophenyl)diazene (3b).** Oxidation Method A was used with **1b** (36.2 mg, 0.238 mmol), giving **2b** (31.0 mg, 0.206 mmol, 86%) as pale yellow block crystals: m.p. 57-58 °C (lit. 60 °C [38]); ^{1}H-NMR (300 MHz, $CDCl_3$, δ) 7.20 (d, *J* = 9.1 Hz, 1 H), 7.16 (dd, *J* = 9.0, 6.4 Hz, 1H), 7.12 (d, *J* = 6.5 Hz, 1H), 2.58 (s, 3 H); ^{13}C-NMR (75 MHz, $CDCl_3$, δ) 148.84, 130.57, 121.87, 117.31, 112.49, 15.62; IR (KBr, cm^{-1}) 3087(w), 2986(w), 1621(s), 1585(s), 1553(s), 1486(s), 1458(m), 1431(w), 1424(w), 1380(m), 1345(w), 1235(w), 1199(w), 1159(w), 1156(w), 1064(w), 1041(w), 1022(m), 1012(s), 992(w), 956(m), 907(w), 858(s), 832 (w), 783(w), 771(s), 744(w), 712(w), 635(m); HRMS *m/z* ($M + Na^+$) calcd 173.0322, found 173.0327; and **3b** (1.4 mg, 0.010 mmol, 2%) as deep red needles: m.p. 200-201 °C (lit. 199 °C [44]); ^{1}H-NMR (300 MHz, $CDCl_3$, δ) 8.68 (d, *J* = 6.7 Hz, 2H), 7.65-7.81 (m, 4H), 2.43 (s, 6H); IR (KBr, cm^{-1}) 2978(w), 1615(s),

1589(m), 1581(m), 1567(m), 1503(m), 1436(m), 1418(m), 1374(m), 1354(m), 1322(s), 1256(w), 1202(w), 1131(w), 1109(w), 1087(m), 1027(w), 1007(w), 956(w), 918(w), 889(w), 852(w), 788(w), 743(s), 635(w); HRMS *m/z* ($M + Na^+$) calcd 323.0751, found 323.0755.

5-Methylbenzo[*c*][1,2,5]oxadiazole 1-oxide (2c) and **1,2-bis(4-methyl-2-nitrophenyl)diazene (3c).** Oxidation Method A was used with **1c** (37.1 mg, 0.244 mmol), giving **2c** (31.3 mg, 0.209 mmol, 87%) as pale yellow block crystals: m.p. 96-97 °C (lit. 98 °C [10a]); 7.32 (s, 1 H), 7.29 (d, *J* = 8.8 Hz, 1H), 7.08 (d, *J* = 8.9 Hz, 1H), 2.43 (s, 3 H); ^{13}C-NMR (75 MHz, $CDCl_3$, δ) 151.48, 134.97, 114.04, 22.13; IR (KBr, cm^{-1}) 3067(w), 2956(w), 1619(s), 1595(s), 1528(s), 1490(s), 1454(m), 1426(w), 1419(w), 1378(m), 1343(w), 1232(w), 1189(w), 1054(w), 1046(w), 1028(m), 1014(s), 997(w), 947(m), 912(w), 861(s), 830 (w), 793(s), 738 (w), 638(m); HRMS *m/z* ($M + Na^+$) calcd 173.0322, found 173.0328; and **3c** (2.2 mg, 0.014 mmol, 3%) as deep red needles: m.p. 111-112 °C (lit. 114 °C [36]); ^{1}H-NMR (300 MHz, $CDCl_3$, δ) 8.72 (s, 2H), 8.34 (d, *J* = 7.8 Hz, 2H), 7.76 (d, *J* = 7.7 Hz, 2H) 2.32 (s, 6H); IR (KBr, cm^{-1}) 2918(w), 1695(s), 1669(m), 1511(s), 1467(w), 1403(m), 1376(w), 1355(w), 1332(s), 1276(m), 1242(m), 1202(m), 1181(m), 1159(m), 1097(m), 1045(w), 1031(w), 959(w), 919(m), 812(m), 778(w), 763(m), 685(w); HRMS *m/z* ($M + Na^+$) calcd 323.0751, found 323.0744.

2,4-Dimethyl-6-nitroaniline (1d). Nitration Method B was used with 2,4-dimethyl-aniline (**12**) (1005 mg, 8.294 mmol), giving **1d** (1153 mg, 6.938 mmol, 84%) as bright red needles: m.p. 67-68 °C (lit. 70 °C [37]); ^{1}H-NMR (300 MHz, $CDCl_3$, δ) 7.83 (d, *J* = 2.8 Hz, 1H), 7.12 (d, *J* = 2.9 Hz, 1H), 6.04 (br s, 2H), 2.25 (s, 3H), 2.21 (s, 3H); ^{13}C-

NMR (75 MHz, $CDCl_3$, δ) 141.43, 137.78, 132.08, 125.48, 125.19, 123.46, 20.14, 17.41; IR (KBr, cm^{-1}) 3485(s), 3473(s), 3369(s), 3081(w), 2978(w), 2945(w), 2925(w), 1638(m), 1596(m), 1589(m), 1515(s), 1472(w), 1431(m), 1422(m), 1405(m), 1388(m), 1376(m), 1363(m), 1332(s), 1257(s), 1233(s), 1158(w), 1084(w), 1023(w), 1017(w), 1008(w), 951(w), 898(w), 872(m), 856(m), 764(m).

4,6-Dimethylbenzo[*c*][1,2,5]oxadiazole 1-oxide (2d) and **1,2-bis(2,4-dimethyl-6-nitrophenyl)diazene (3d).** Oxidation Method A was used with aniline **1d** (39.2 mg, 0.236 mmol), giving **2d** (33.1 mg, 0.202 mmol, 84%) as pale yellow-orange block crystals: m.p. 106-108 °C (lit. 108-109 °C [38]); ^{1}H-NMR (300 MHz, $CDCl_3$, δ) [7.09 (s), 6.91 (s), 6.70 (s), 2H], [2.52 (s), 2.50 (s), 3H], [2.41 (s), 2.34 (s), 3H]; ^{13}C-NMR (75 MHz, $CDCl_3$, δ) 153.27, 140.36, 134.26, 116.56, 112.75, 107.41, 22.27, 15.90; IR (KBr, cm^{-1}) 2982(w), 2953(w), 2918(w), 1629(s), 1588(s), 1552(s), 1480(s), 1432(m), 1372(m), 1262(w), 1245(w), 1090(w), 1059(s), 1042(m), 1035(m), 1028(m), 1015(s), 977(w), 942(w), 911(w),861(w), 850(m), 836(m), 801(w),765(m), 745(w), 712(w); HRMS *m/z* ($M + Na^+$) calcd 187.0478, found 187.0479; and **3d** (3.2 mg, 0.019 mmol, 4%) as deep red block crystals: m.p. 254-255°C; ^{1}H-NMR (300 MHz, $CDCl_3$, δ) 7.29 (s, 2H), 7.23 (s, 2H), 2.51 (s, 6H), 2.42 (s, 6H); IR (KBr, cm^{-1}) 2926(w), 1611(m), 1533(s), 1437(w), 1386(m), 1371(s), 1306(w), 1265(w), 1243(w), 1224(w), 1023(w), 972(w), 861(w), 800(w), 762(m), 753(m); HRMS *m/z* ($M + Na^+$) calcd 351.1064, found 351.1050.

3-Methoxyaniline (13). 3-Aminophenol (**12**) (1.490 g, 13.65 mmol) was dissolved in anhydrous tetrahydrofuran (20 mL) at room temperature. Sodium hydride (60% dispersion in mineral oil) (0.655 g, 16.4 mmol) was added with stirring to the solution

and the solution was stirred for 30 minutes. Methyl iodide (2.328 g, 16.40 mmol) was added slowly to the solution over 10 minutes. The reaction mixture was stirred for 1 hour, then quenched with isopropyl alcohol, followed by water, until bubbling ceased. The solution was extracted with dichloromethane (3 x 25 mL), dried over anhydrous magnesium sulfate, and evaporated on a rotating evaporator. A slightly brown oil was recovered and purified by distillation under high vacuum (~0.02 torr) at around 70 °C, leaving **13** (1.529 g, 12.41 mmol, 91%) as a colorless oil: ^{1}H-NMR (300 MHz, $CDCl_3$, δ) 7.07 (t, *J* = 7.9 Hz, 1H), 6.33-6.36 (m, 2H), 6.25 (t, *J* = 2.3 Hz, 1H), 3.76 (s, 3H), 3.63 (br s, 2H).

3-Methoxy-4-nitroaniline (14) and **5-methoxy-2-nitroaniline (1e).** Nitration Method A was modified by first adding fuming nitric acid (0.947 g, 13.53 mmol) to acetic anhydride (5.0 mL) in an ice bath. This solution of acetyl nitrate (2.3 M) was added to a solution of **13** (1491 mg, 12.11 mmol) in acetic anhydride (13 mL) followed by *N*-deacetylation using ethanol/hydrochloric acid, giving **14** (0.434 mg, 2.58 mmol, 21%) as light brown power: m.p. 155-156 °C (lit. 169 °C [39], lit. 157.5-158 °C [40]); ^{1}H-NMR (300 MHz, $CDCl_3$, δ) 7.93 (d, *J* = 8.9 Hz, 1H), 6.20 (dd, *J* = 9.0, 2.1 Hz, 1H), 6.18 (d, *J* = 2.2 Hz, 1H), 4.29 (br s, 2H), 3.88 (s, 3H); IR (KBr, cm^{-1}) 3351(s), 3133(w), 3020(w), 1701(s), 1698(s), 1624(s), 1618(s), 1607(s), 1591(s), 1560(m), 1555(m), 1492(m), 1474(m), 1460(m), 1410(w), 1371(w), 1343(w), 1328(m), 1274(m), 1248(m), 1220(w), 1200(w), 1177(w), 1093(m), 1014(m), 955(w), 866(m), 849(w), 831(w), 819(w), 760(w), 754(m), 691(m), 674(w), 624(w); and **1e** (1.167 mg, 6.940 mmol, 57%) as bright yellow-orange needles: m.p. 126-127 °C (lit. 129 °C [41]); ^{1}H-NMR (300 MHz, $CDCl_3$, δ) 8.06

(d, *J* = 9.2 Hz, 1H), 6.23 (br s, 2H), 6.26 (dd, *J* = 9.3, 2.3 Hz, 1H), 6.17 (d, *J* = 2.4 Hz, 1H), 3.83 (s, 3H); IR (KBr, cm^{-1}) 3475(m), 3361(m), 1624(s), 1604(m), 1577(s), 1496(m), 1462(m), 1408(s), 1335(w), 1238(s), 1221(s), 1162(w), 1105(m), 1012(w), 945(w), 833(w), 801(w), 755(w), 737(w), 693(w), 630(w).

5-Methoxybenzo[*c*][1,2,5]oxadiazole 1-oxide (2e) and **1,2-bis(5-methoxy-2-nitrophenyl)diazene (3e).** Oxidation Method A was used with aniline **1e** (39.7 mg, 35.9 mmol), giving **2e** (35.9 mg, 0.216 mmol, 90%) as pale yellow block crystals: m.p. 116-117 °C (lit. 112-115 °C [42]); ^{1}H-NMR (300 MHz, $CDCl_3$, δ) 7.34 (d, *J* = 7.1 Hz, 1H), 6.97 (d, *J* = 7.3 Hz, 1H), 6.84 (s, 1H), 4.06 (s, 3H); ^{13}C-NMR (75 MHz, $CDCl_3$, δ) 161.83 , 152.16, 128.33, 114.76, 56.49; IR (KBr, cm^{-1}) 3095(m), 2958(w), 1621(s), 1571(m), 1542(s), 1492(s), 1438(m), 1356(w), 1322(m), 1294(w), 1257(m), 1208(m), 1186(w), 1128(w), 962(m), 916(m), 859(w), 786(m), 742(w), 688(w), 631(w), 614(w); HRMS *m/z* ($M + Na^+$) calcd 189.0271, found 189.0263; and **3e** (1.6 mg, 0.010 mmol, 2%) as deep orange-red needles: m.p. 250-252 °C; ^{1}H-NMR (300 MHz, $CDCl_3$, δ) 8.17 (d, *J* = 8.6 Hz, 2H), 7.68 (s, 2H), 7.26 (d, *J* = 8.7 Hz, 2H), 3.82 (s, 6H); IR (KBr, cm^{-1}) 2967(w), 1607(s), 1579(m), 1591(m), 1466(m), 1411(m), 1334(w), 1312(w), 1246(m), 1222(m), 1151(w), 1109(m), 1027(w), 956(w), 842(w), 775(w), 741(s), 632(w); HRMS *m/z* ($M + Na^+$) calcd 355.0649, found 355.0644.

4-Methoxy-2-nitroaniline (1f). Nitration Method A was used with 4-methoxyaniline hydrochloride (**15**) (881 mg, 5.52 mmol), giving **1f** (717 mg, 426 mmol, 77%) as bright yellow needles: m.p. 122-123 °C (lit. 123 °C [43]); ^{1}H-NMR (300 MHz, $CDCl_3$, δ) 7.46 (d, *J* = 3.0 Hz, 1H), 7.13 (dd, *J* = 9.0, 2.8 Hz, 1H), 6.82 (dd, *J* = 9.1, 2.9 Hz, 1H), 5.93 (br

s, 2H), 3.78 (s, 3H); ^{13}C-NMR (75 MHz, $CDCl_3$, δ) 150.85, 139.89, 131.37, 126.61, 119.03, 106.41, 55.65; IR (KBr, cm^{-1}) 3489(s), 3374(s), 3168(w), 3124(w), 2953(w), 2910(w), 1642(m), 1595(s), 1575(s), 1512(s), 1473(m), 1461(w), 1453(w), 1436(w), 1425(s), 1386(s), 1341(s), 1279(s), 1257(s), 1221(s), 1181(m), 1158(s), 1093(m), 1027(m), 938(w), 883(w), 841(s), 813(m), 783(m), 753(m).

5-Methoxybenzo[*c*][1,2,5]oxadiazole 1-oxide (2e)and **1,2-bis(4-methoxy-2-nitrophenyl)diazene (3f).** Oxidation Method A was used with aniline **1f** (40.4 mg, 0.243 mmol), giving **2e** (35.1 mg, 0.211 mmol, 88%) as pale yellow block crystals: m.p. 116-117 °C (lit. 112-115 °C [42]); ^{1}H-NMR (300 MHz, $CDCl_3$, δ) 7.34 (d, *J* = 7.1 Hz, 1H), 6.97 (d, *J* = 7.3 Hz, 1H), 6.84 (s, 1H), 4.06 (s, 3H); ^{13}C-NMR (75 MHz, $CDCl_3$, δ) 161.86, 152.19, 128.36, 114.79, 56.51; IR (KBr, cm^{-1}) 3095(m), 2958(w), 1621(s), 1571(m), 1542(s), 1492(s), 1438(m), 1356(w), 1322(m), 1294(w), 1257(m), 1208(m), 1186(w), 1128(w), 962(m), 916(m), 859(w), 786(m), 742(w), 688(w), 631(w), 614(w); HRMS *m/z* ($M + Na^+$) calcd 189.0271, found 189.0261; and **3f** (2.4 mg, 0.014 mmol, 3%) as deep orange needles: m.p. 254-256 °C (lit. 259 °C [44]); ^{1}H-NMR (300 MHz, $CDCl_3$, δ) 8.24 (d, *J* = 8.6 Hz, 2H), 7.64 (s, 2H), 7.15 (d, *J* = 8.5 Hz, 2H), 3.83 (s, 6H); IR (KBr, cm^{-1}) 2948(w), 1649(m), 1591(s), 1567(m), 1503(m), 1476(m), 1448(w), 1432(m), 1376(m), 1337(m), 1262(m), 1252(m), 1211(m), 1179(m), 1167(w), 1047(m), 1021(w), 949(w), 921(w), 838(m), 812(m), 778(m), 763(m), 635(w); HRMS *m/z* ($M + Na^+$) calcd 355.0649, found 355.0634.

3-Amino-4-nitrobenzonitrile (1g). Nitration Method A was used with 3-aminobenzonitrile (**16**) (622 mg, 5.27 mmol), giving **1g** (547 mg, 3.35 mmol, 64%) as

bright yellow-orange plates: m.p. 126-127 °C (lit. 128-131 °C [45]); ^{1}H-NMR (300 MHz, acetone-d_6, δ) 8.21(d, J = 8.6 Hz, 1H), 7.42 (d, J = 1.8 Hz, 1H), 6.68 (dd, J = 8.7, 1.7 Hz, 1H), 6.46 (br s, 2H); IR (KBr, cm^{-1}) 3393(m), 3315(m), 2925(w), 2854(w), 2248(w), 1680(s), 1648(s), 1613(s), 1589(s), 1551(m), 1485(w), 1384(w), 1319(w), 1304(w), 1260(w), 1174(w), 1100(w), 1038(w), 1019(w), 981(w), 899(w), 762(m), 684(w), 623(w).

5-Cyanobenzo[*c*][1,2,5]oxadiazole 1-oxide (2g) and **3,3'-(diazene-1,2-diyl)bis(4-nitrobenzonitrile) (3g).** Oxidation Method A was used with aniline **1g** (39.0 mg, 0.239 mmol), giving **2g** (32.5 mg, 0.202 mmol, 84%) as pale yellow-orange block crystals: m.p. 74.5-75.5 °C (lit. 75-76 °C [10d]); ^{1}H-NMR (300 MHz, $CDCl_3$, δ) 7.67 (br s, 1H), 7.44-7.53 (m, 2H); ^{13}C-NMR (75 MHz, $CDCl_3$, δ) 156.24, 146.63, 118.17; IR (KBr, cm^{-1}) 2918(w), 2886(w), 2246(w), 1679(m), 1646(s), 1598(s), 1582(s), 1546(s), 1453(w), 1427(w), 1323(m), 1295(w), 1256(w), 1146(m), 1131(w), 1037(w), 1012(m), 984(w), 896(w), 752(m), 633(w); HRMS *m/z* (M + Na$^+$) calcd 184.0118, found 184.0113; and **3g** (2.3 mg, 0.014 mmol, 3%) as deep red needles: m.p. 223-225 °C; ^{1}H-NMR (300 MHz, $CDCl_3$, δ) 8.49 (s, 2H), 8.41 (d, J = 8.4 Hz, 2H), 7.94 (d, J = 8.3 Hz, 2H); IR (KBr, cm^{-1}) 2967(w), 2245(w), 1683(s), 1653(m), 1612(m), 1577(m), 1544(m), 1479(w), 1401(w), 1378(w), 1315(w), 1239(m), 1165(w), 1109(w), 1034(m), 973(w), 882(w), 758(m), 677(w), 653(w), 622(w)HRMS *m/z* (M + Na$^+$) calcd 345.0343, found 345.0351.

4-Amino-3-nitrobenzonitrile (1h). Nitration Method B was used with 4-aminobenzonitrile (**17**) (2327 mg, 19.7 mmol), giving **1h** (2611 mg, 16.01 mmol, 81%) as bright yellow-orange plates: m.p. 161-162 °C (lit. 159-160 °C [46]); ^{1}H-NMR (300

MHz, CD_3OD, δ) 8.64 (d, *J* = 2.2 Hz, 1H), 7.81 (dd, *J* = 8.9, 2.2 Hz, 1H), 6.95 (d, *J* = 8.9 Hz, 1H); ^{13}C-NMR (75 MHz, CD_3OD, δ) 149.54, 135.01, 131.71, 127.59, 121.89, 119.88; IR (KBr, cm^{-1}) 3477(s), 3376(s), 3167(m), 2246(w), 1653(s), 1636(s), 1617(s), 1554(w), 1522(w), 1479(w), 1403(w), 1374(w), 1364(w), 1347(w), 1248(m), 1172(w), 1154(w), 1123(w), 1074(w), 918(w), 910(w), 903(w), 838(w), 826(w), 802(m), 756(w), 706(w), 677(w), 668(w), 622(w).

5-Cyanobenzo[*c*][1,2,5]oxadiazole 1-oxide (2g) and **4,4'-(diazene-1,2-diyl)bis(3-nitrobenzonitrile) (3h).** Oxidation Method A was used with aniline **1h** (39.8 mg, 0.244 mmol), giving **2g** (33.3 mg, 0.206 mmol, 86%) as pale orange block crystals: m.p. 74.5-75.5 °C (lit. 75-76 °C [10d]); ^{1}H-NMR (300 MHz, $CDCl_3$, δ) 7.66 (br s, 1H), 7.43- 7.52 (m, 2H); ^{13}C-NMR (75 MHz, $CDCl_3$, δ) 156.54, 146.83, 118.47; IR (KBr, cm^{-1}) 2918(w), 2886(w), 2246(w), 1679(m), 1646(s), 1599(s), 1582(s), 1546(s), 1453(w), 1427(w), 1322(m), 1295(w), 1256(w), 1146(m), 1132(w), 1037(w), 1012(m), 984(w), 896(w), 753(m), 632(w); HRMS *m/z* ($M + Na^+$) calcd 184.0118, found 184.0117; and **3h** (3.1 mg, 0.019 mmol, 4%) as deep red needles: m.p. 196-199 °C; ^{1}H-NMR (300 MHz, $CDCl_3$, δ) 8.62 (s, 1H), 8.41 (d, *J* = 8.1 Hz, 1H), 8.19 (d, *J* = 8.4, 1H); IR (KBr, cm^{-1}) 3067(w), 2242(w), 1603(s), 1563(m), 1524(m), 1469(w), 1403(w), 1372(w), 1357(w), 1346(w), 1251(m), 1161(w), 1118(w), 1084(m), 923(w), 847(w), 822(w), 805(m), 759(w), 708(w), 672(w), 669(w), 620(w); HRMS *m/z* ($M + Na^+$) calcd 345.0343, found 345.0335.

2-Chloro-4-nitroaniline (19) and **2-chloro-6-nitroaniline (1i).** Nitration Method A was used with 2-chloroaniline (**18**) (10.183 g, 79.82 mmol), giving **19** (3.641 g, 21.10 mmol, 26%) as pale yellow needles: m.p. 102-103 °C (lit. 104-105 °C [47]); ^{1}H-NMR (500

MHz, $CDCl_3$, δ) 8.19 (d, *J* = 2.5 Hz, 1H), 7.99 (dd, *J* = 9.0, 2.5 Hz, 1H), 6.77 (d, *J* = 9.0 Hz, 1H), 4.91 (br s, 2H); ^{13}C-NMR (126 MHz, $CDCl_3$, δ) 149.06, 138.68, 126.04, 124.45, 117.73, 113.78; IR (KBr, cm^{-1}) 3494(m), 3473(m), 3377(s), 3108(w), 1631(w), 1591(m), 1581(m), 1488(s), 1341(s), 1327(s), 1306(s), 1261(m), 1130(m), 907(w), 895(w), 823(w), 817(w), 745(m), 728(w), 645(w), 663(w); and **1i** (9.517 g, 55.15 mmol, 69%) as bright yellow needles: m.p. 74-74.5 °C (lit. 76 °C [48]); ^{1}H-NMR (500 MHz, $CDCl_3$, δ) 8.09 (dd, *J* = 8.7, 1.4 Hz, 1H), 7.53 (dd, *J* = 7.7, 1.4 Hz, 1H), 6.66 (dd, *J* = 8.7, 7.7 Hz, 1H), 6.56 (br s, 2H); ^{13}C-NMR (126 MHz, $CDCl_3$, δ) 141.53, 135.38, 125.26, 122.06, 115.83; IR (KBr, cm^{-1}) 3494(s), 3378(s), 3091(w), 1622(s), 1575(m), 1559(w), 1510(s), 1501(s), 1445(m), 1432(m), 1426(m), 1358(s), 1321(s), 1264(s), 1241(m), 1210(w), 1151(w), 1107(s), 1074(m), 977(w), 931(w), 877(w), 799(m), 746(s), 734(m), 705(w), 611(w).

4-Chlorobenzo[*c*][1,2,5]oxadiazole 1-oxide (2i) and **1,2-bis(2-chloro-6-nitrophenyl)diazene (3i).** Oxidation Method A was used with aniline **1i** (41.6 mg, 0.241 mmol), giving **2i** (38.1 mg, 0.223 mmol, 93%) as pale yellow block crystals: m.p. 76-77 °C (lit. 77-77.5 °C [49]); ^{1}H-NMR (300 MHz, acetone-d_6, δ) 7.68 (d, *J* = 6.3 Hz, 1H), 7.53 (d, *J* = 8.4 Hz, 1H), 7.39 (dd, *J* = 8.8, 7.0 Hz, 1H); ^{13}C-NMR (75 MHz, $CDCl_3$, δ) 136.35, 128.12, 115.27, 112.77, 110.45; IR (KBr, cm^{-1}) 3082(m), 2916(m), 2845(m), 1613(s), 1583(s), 1547(w), 1530(w), 1522(m), 1489(m), 1337(w), 1249(w), 1195(w), 1027(w), 1011(m), 932(m), 906(w), 850(m), 827(w); HRMS *m/z* ($M + Na^+$) calcd 192.9775, found 192.9768; and **3i** (4.9 mg, 0.029 mmol, 6%) as deep red-orange needles: m.p. 156-157 °C (lit. 158.5-159 °C [49]); ^{1}H-NMR (300 MHz, $CDCl_3$, δ) 8.21 (d, *J* = 8.2 Hz, 1H), 7.83 (d, *J* = 7.1 Hz, 1H), 7.63 (dd, *J* = 8.4, 7.2 Hz, 1H); IR (KBr, cm^{-1}) 3085(w),

1613(s), 1571(s), 1515(m), 1491(m), 1435(m), 1416(m), 1396(w), 1360(s), 1271(m), 1234(w), 1151(w), 1091(w), 1074(m) 916(w), 853(s), 771(w), 744(m), 737(m), 620(m); HRMS *m/z* ($M + Na^+$) calcd 362.9658 and 364.9629, found 362.9652 and 364.9636.

2,4-Dichloro-5-nitroaniline (21) and **2,4-dichloro-6-nitroaniline (1j).** Nitration Method B was used with 2,4-dichloroaniline (**20**) (2077 mg, 12.82 mmol), giving **21** (1099 mg, 5.307 mmol, 41%) as pale yellow needles: m.p. 104-105 °C (lit. 108 °C [50]); ^{1}H-NMR (500 MHz, $CDCl_3$, δ) 7.42 (s, 1H), 7.31 (d, *J* = 2.5 Hz, 1H), 4.41 (br s, 2H); ^{13}C-NMR (126 MHz, $CDCl_3$, δ) 142.57, 131.86, 123.48, 115.14, 113.83, 111.46; IR (KBr, cm^{-1}) 2298(m), 3322(m), 3215(m), 3094(w), 3053(w), 1641(s), 1631(s), 1595(m), 1565(s), 1530(s), 1478(s), 1389(m), 1357(s), 1316(s), 1281(m), 1142(m), 1110(m), 1076(m), 977(m), 884(s), 826(m), 756(w), 734(w), 678(w) ; and **1j** (975.3 mg, 4.711 mmol, 37%) as bright yellow needles: m.p. 99-100 °C (lit. 100 °C [51]); ^{1}H-NMR (500 MHz, $CDCl_3$, δ) 8.11 (d, *J* = 2.5 Hz, 1H), 7.54 (d, *J* = 2.5 Hz, 1H), 6.57 (br s, 2H); ^{13}C-NMR (126 MHz, $CDCl_3$, δ) 140.31, 135.25, 124.62, 122.79, 120.43; IR (KBr, cm^{-1}) 3475(s), 3361(s), 3087(w), 1633(s), 1587(w), 1550(m), 1503(s), 1453(m), 1395(m), 1353(m), 1321(m), 1256(m), 1228(m), 1143(m), 1113(w), 1086(w), 901(m), 876(m), 850(m), 765(m), 756(m), 729(m), 704(w), 668(w).

4,6-Dichlorobenzo[*c*][1,2,5]oxadiazole 1-oxide (2j) and **1,2-bis(2,4-dichloro-6-nitrophenyl)diazene (3j).** Oxidation Method A was used with aniline **1j** (50.3 mg, 0.243 mmol), giving **2j** (44.8 mg, 0.218 mmol, 91%) as pale yellow block crystals: m.p. 102-103.5 °C (lit. 107-108 °C [52]); ^{1}H-NMR (300 MHz, $CDCl_3$, δ) 7.36 (br s, 1H), 7.34 (br s, 1H); ^{13}C-NMR (75 MHz, $CDCl_3$, δ) 145.66, 133.16, 117.61, 115.04, 110.31, 108.76;

IR (KBr, cm^{-1}) 3085(w), 3072(w), 1614(s), 1572(s), 1528(s), 1482(s), 1439(w), 1430(w), 1374(w), 1364(w), 1322(w), 1216(w), 1189(w), 1160(w), 1091(w), 1053(m), 1027(s),959(w), 954(w), 905(w), 901(w), 866(w), 853(m), 727(s), 701(w), 668(w); HRMS *m/z* ($M + Na^+$) calcd 226.9386 and 228.9356, found 226.9390 and 228.9360; and **3j** (8.9 mg, 0.043 mmol, 9%) as deep red-orange needles: m.p. 232-233 °C; ^{1}H-NMR (300 MHz, $CDCl_3$, δ) 7.73 (br s, 2H), 7.59 (br s, 2H); IR (KBr, cm-1) 3080(m), 1583(s), 1541(s), 1435(w), 1396(w), 1362(s), 1281(w), 1224(w), 1161(w), 1091(m), 906(w), 864(s), 781(w), 754(m), 737(m), 690(m); HRMS *m/z* ($M + Na^+$) calcd 430.8879 and 432.8850 and 434.8820, found 430.8892 and 432.8864 and 434.8832.

5,6-Dichlorobenzo[*c*][1,2,5]oxadiazole 1-oxide (2k) and **1,2-bis(4,5-dichloro-6-nitrophenyl)diazene (3k).** Oxidation Method A was used with aniline **1k** (50.1 mg, 0.242 mmol), giving **2k** (43.8 mg, 0.214 mmol, 89%) as pale orange block crystals: m.p. 128-129 °C (lit. 130-131 °C [52]); ^{1}H-NMR (300 MHz, $CDCl_3$, δ) 8.12 (br s, 1H), 7.88 (br s, 1H); ^{13}C-NMR (75 MHz, $CDCl_3$, δ) 156.83, 142.71, 135.48, 122.32; IR (KBr, cm^{-1}) 3078(w), 3067(w), 1616(s), 1574(s), 1523(s), 1479(s), 1424(w), 1415(w), 1363(w), 1317(w), 1213(w), 1192(w), 1157(w), 1086(w), 1043(m), 1025(s),963(w), 948(w), 912(w), 858(w), 846(m), 725(s), 698(w), 662(w); HRMS *m/z* ($M + Na^+$) calcd 226.9386 and 228.9356, found 226.9387 and 228.9357; and **3k** (7.9 mg, 0.038 mmol, 8%) as deep red-orange needles: 236-238 °C; ^{1}H-NMR (300 MHz, $CDCl_3$, δ) 8.42 (br s, 1H), 8.26 (br s, 1H); IR (KBr, cm^{-1}) 3071(w), 1578(s), 1539(s), 1426(w), 1387(w), 1357(s), 1277(w), 1231(w), 1156(w), 1087(m), 911(w), 857(s), 772(w), 749(m), 733(m), 687(m); HRMS

m/z ($M + Na^+$) calcd 430.8879 and 432.8850 and 434.8820, found 430.8899 and 432.8871 and 434.8841.

2-Bromo-4-nitroaniline (23) and **2-bromo-6-nitroaniline (1l).** Nitration Method A was used with 2-bromoaniline (**22**) (2841 mg, 16.52 mmol), giving **23** (493 mg, 2.27 mmol, 14%) as pale yellow needles: m.p. 101-103 °C (lit. 104.5 °C [53]); ^{1}H-NMR (300 MHz, $CDCl_3$, δ) 8.38 (d, *J* = 8.9 Hz, 1 H), 8.04 (dd, *J* = 8.8 Hz, 2.4, 1 H), 6.74 (d, *J* = 2.3 Hz, 1 H), 4.17 (br s, 2 H); IR (KBr, cm^{-1}) 3485(m), 3372(m), 3094(w), 1620(s), 1583(s), 1485(s), 1416(m), 1338(m), 1314(m), 1250(m), 1205(w), 1121(m), 1051(w), 966(w), 895(m), 820(m), 744(s), 711(w), 664(w); and **1l** (1825 mg, 8.409 mmol, 51%) as bright yellow-orange needles: m.p. 71.5-72.5 °C (lit. 73-74 °C [54]); ^{1}H-NMR (500 MHz, $CDCl_3$, δ) 8.13 (dd, *J* = 8.6, 1.3 Hz, 1H), 7.69 (dd, *J* = 8.6, 1.4 Hz, 1H), 6.63 (br s, 2H), 6.60 (t, *J* = 8.7 Hz, 1H); ^{13}C-NMR (126 MHz, $CDCl_3$, δ) 142.31, 138.92, 126.06, 116.63, 113.92, 112.24; IR (KBr, cm^{-1}) 3484(m), 3369(m), 3089(w), 1616(s), 1502(s), 1495(s), 1426(m), 1354(m), 1316(m), 1271(m), 1260(s), 1242(m), 1200(w), 1151(w), 1090(m), 1071(w), 1043(w), 970(w), 928(w), 869(w), 814(w), 798(m), 745(s), 709(w), 705(w), 667(w).

4-Bromobenzo[*c*][1,2,5]oxadiazole 1-oxide (2l) and **1,2-bis(2-bromo-6-nitrophenyl)diazene (3l).** Oxidation Method B was used with aniline **1l** (52.1 mg, 0.240 mmol), giving **2l** (35.1 mg, 0.163 mmol, 68%) as pale orange block crystals: m.p. 100-102 °C (lit. 105 °C [55]); ^{1}H-NMR (300 MHz, $CDCl_3$, δ) 7.60 (d, *J* = 6.8 Hz, 1H), 7.36 (d, *J* = 9.0 Hz, 1H), 7.07 (dd, *J* = 8.7, 7.2 Hz, 1H); ^{13}C-NMR (75 MHz, $CDCl_3$, δ) 135.05, 129.02, 115.50, 113.83, 111.95; IR (KBr, cm^{-1}) 3030(w), 1612 (s), 1586(m), 1529(m),

1487(m), 1424(w),1331(w), 1231(w), 1201(w), 1028(w), 1009(w), 927(w), 911(m), 847(w), 811(w); HRMS *m/z* ($M + Na^+$) calcd 236.9270 and 238.9250, found 236.9262 and 238.9243; and **3l** (12.4 mg, 0.058 mmol, 12%) as deep red-orange needles: m.p. 163-165 °C; ^{1}H-NMR (300 MHz, $CDCl_3$, δ) 8.32 (d, *J* = 7.9 Hz, 1H), 8.03 (d, *J* = 6.8 Hz, 1H), 7.58 (dd, *J* = 8.1, 6.9 Hz, 1H); IR (KBr, cm^{-1}) 3087(w), 1615(s), 1510(m), 1493(m), 1431(m), 1387(w), 1321(s), 1272(m), 1254(m), 1153(w), 1091(m), 1073(w), 968(w), 916(w), 855(s), 794(m), 747(m), 660(w); HRMS *m/z* ($M + Na^+$) calcd 450.8648 and 452.8628 and 454.8607, found 450.8631 and 452.8611 and 454.8591.

4-Bromo-2-chloro-6-nitroaniline (1m). Aniline **1i** (1735 mg, 10.05 mmol) was dissolved in acetic acid (15 mL) and the reaction flask was purged with nitrogen. Bromine (1.05 mL, 20.5 mmol, d = 3.119 g/ml) was added dropwise, with stirring to the solution at room temperature, causing large quantities of an orange-brown solid to appear. The reaction was stirred for an additional 45 minutes, poured over ice (100 g), and the resulting orange-brown solid was recovered by suction filtration. The orange precipitate was purified by flash column chromatography using silica gel and eluted with 1:4 ethyl acetate/hexanes, giving **1m** (1673 mg, 6.653 mmol, 66%) as yellow-orange needles: m.p. 117-118 °C (lit. 114 °C [56]); ^{1}H-NMR (500 MHz, $CDCl_3$, δ) 8.25 (d, *J* = 2.3 Hz, 1H), 7.65 (d, *J* = 2.3 Hz, 1H), 6.59 (br s, 2H); IR (KBr, cm^{-1}) 3471(w), 3363(w), 3086(w), 1632(s), 1586(m), 1567(w), 1550(m), 1517(m), 1503(m), 1451(m), 1395(m), 1392(m), 1353(m), 1321(m), 1255(m), 1228(w), 1141(w), 1129(w), 1106(w), 1086(w), 1009(w), 900(w), 876(m), 849(w), 763(m), 757(m), 728(w), 707(w), 700(w).

6-Bromo-4-chlorobenzo[*c*][1,2,5]oxadiazole 1-oxide (2m) and **1,2-bis(4-bromo-2-chloro-6-nitrophenyl)diazene (3m).** Oxidation Method B was used with aniline **1m** (60.9 mg, 0.242 mmol), giving **2m** (43.7 mg, 0.175 mmol, 73%) as pale yellow block crystals: m.p. 97-98 °C; ^{1}H-NMR (300 MHz, $CDCl_3$, δ) 7.61 (s, 1H), 7.42 (s, 1H); ^{13}C-NMR (75 MHz, $CDCl_3$, δ)165.42, 134.81, 129.38, 128.26, 126.74; IR (KBr, cm^{-1}) 3081(w), 1616(s), 1569(m), 1525(w), 1476(m), 1372(w), 1321(w), 1217(w), 1182(w), 1083(m), 1024(m), 938(w), 906(w), 901(w), 851(w), 849(m), 817(w), 730(m), 704(w), 683(m); HRMS *m/z* ($M + Na^+$) calcd 270.8880 and 272.8860, found 270.8871 and 272.8850; and **3m** (18.0 mg, 0.072 mmol, 15%) as deep red-orange needles: m.p. 239-240 °C; ^{1}H-NMR (300 MHz, $CDCl_3$, δ) 7.92 (d, *J* = 2.1 Hz, 2H), 7.75(d, *J* = 2.1 Hz, 2H); IR (KBr, cm^{-1}) 3076(w), 2923(w), 2891(w), 2852(w), 1573(s), 1556(m), 1539(s), 1358(m), 1281(w), 1225(w), 1142(w), 1086(w), 906(w), 863(w), 843(w), 803(w), 776(w), 752(w), 733(w), 666(w); HRMS *m/z* ($M + Na^+$) calcd 518.7869 and 520.7848 and 522.7819, found 518.7861 and 520.7841 and 522.7811.

2-Iodo-4-nitroaniline (25) and **2-iodo-6-nitroaniline (1n).** Nitration Method A was modified by separately adding fuming nitric acid (0.270 g, 3.86 mmol) to acetic anhydride (2.0 mL) in an ice bath with stirring. This solution of acetyl nitrate (1.7 M) was added to a solution of 2-iodoaniline (**24**) (839 mg, 3.83 mmol) in acetic anhydride (13 mL), giving **25** (209 mg, 0.792 mmol, 21%) as light red needles: m.p. 107-108 °C (lit. 105.5 °C [57]); ^{1}H-NMR (300 MHz, $CDCl_3$, δ) 8.54 (d, *J* = 2.5 Hz, 1H), 8.02 (dd, *J* = 9.1, 2.4 Hz, 1H), 6.74 (d, *J* = 9.2 Hz), 4.85 (br s, 2H); IR (KBr, cm^{-1}) 3482(m), 3371(m), 3092(w), 1607(s), 1575(m), 1492(s), 1406(m), 1327(m), 1306(m), 1231(m),

1195(w), 1100(m), 1042(w), 954(w), 887(w), 810(w), 754(w), 721(w), 680(m); and **1n** (438 mg, 1.66 mmol, 43%) as bright red needles: m.p. 105-107 °C (lit. 108 °C [58]); ^{1}H-NMR (300 MHz, $CDCl_3$, δ) 8.16 (dd, *J* = 8.3, 1.4 Hz, 1H), 7.92 (dd, *J* = 7.3, 1.3 Hz, 1H), 6.65 (br s, 2H), 6.50 (dd, *J* = 8.4, 7.4 Hz, 1H); IR (KBr, cm^{-1}) 3448(m), 3345(m), 3058(w), 1611(s), 1569(m), 1551(m), 1521(w), 1509(w), 1491(s), 1427(s), 1342(s), 1310(s), 1253(s), 1138(w), 1076(m), 1051(w), 865(m), 807(w), 748(w), 719(w), 705(w), 667(w).

4-Iodobenzo[*c*][1,2,5]oxadiazole 1-oxide (2n) and **1,2-bis(2-iodo-6-nitrophenyl)diazene (3n).** Oxidation Method B was used with aniline **1n** (62.8 mg, 0.238 mmol), giving **2n** (23.9 mg, 0.091 mmol, 38%) as pale yellow-green block crystals: m.p. 120-121 °C; ^{1}H-NMR (300 MHz, $CDCl_3$, δ) 7.85 (d, *J* = 6.8 Hz, 1H), 7.37 (d, *J* = 8.9 Hz, 1H), 6.96 (dd, *J* = 8.9, 6.9 Hz, 1H); ^{13}C-NMR (75 MHz, $CDCl_3$, δ) 153.72, 142.01, 129.60, 114.84, 113.09, 83.12; IR (KBr, cm^{-1}) 3088(w), 1609(s), 1577(m), 1513(m), 1478(m), 1417(w), 1327(w), 1242(w), 1196(w), 1129(w), 1022(w), 1005(w), 900(s), 839(m), 805(m), 770(m), 734(m), 698(w); HRMS *m/z* ($M + Na^+$) calcd 284.9131, found 284.9125; and **3n** (21.4 mg, 0.082 mmol, 17%) as deep red needles: m.p. 177-179 °C; ^{1}H-NMR (300 MHz, $CDCl_3$, δ)8.29 (d, *J* = 8.0 Hz, 1H), 8.03 (d, *J* = 7.0 Hz, 1H), 7.52 (dd, *J* = 8.1, 6.9 Hz, 1H); IR (KBr, cm^{-1}) 3057(w), 1613(s), 1571(m), 1548(m), 1517(w), 1493(w), 1481(m), 1431(m), 1347(m), 1316(s), 1252(m), 1143(w), 1081(m), 1053(w), 923(w), 855(m), 798(w), 747(w), 660(m); HRMS *m/z* ($M + Na^+$) calcd 546.8371, found 546.8373.

2,4-Dibromo-6-nitroaniline (1o). Aniline **1l** (2106 mg, 9.704 mmol) was dissolved in acetic acid (16 mL) and the reaction flask was purged with nitrogen. Bromine (1.04 mL, 20.4 mmol, d = 3.119 g/ml) was added dropwise, with stirring to the solution at room temperature causing large quantities of dark orange solid to appear. The reaction was stirred for an additional 45 minutes, poured over ice (100 g), and the resulting dark orange solid was recovered by vacuum filtration. The orange precipitate was purified by flash column chromatography using silica gel and eluted with 1:4 ethyl acetate/hexanes, giving **1o** (1938 mg, 6.549 mmol, 67%) as bright yellow needles: m.p. 128-129 °C (lit. 127 °C [53]); ^{1}H-NMR (300 MHz, $CDCl_3$, δ) 8.23 (d, *J* = 2.9 Hz, 1H), 7.71 (d, *J* = 2.8 Hz, 1H), 6.42 (br s, 2H); ^{13}C-NMR (75 MHz, $CDCl_3$, δ) 141.52, 140.73, 132.87, 128.31, 112.56, 106.87; IR (KBr, cm^{-1}) 3467(s), 3356(s), 3088(m), 1627(s), 1578(w), 1564(w), 1547(m), 1501(s), 1445(m), 1389(m), 1346(s), 1321(m), 1258(s), 1227(m), 1118(m), 1101(m), 1077(m), 887(m), 878(s), 832(w), 761(m), 725(w), 705(w), 693(m).

4,6-Dibromobenzo[*c*][1,2,5]oxadiazole 1-oxide (2o) and **1,2-bis(2,4-dibromo-6-nitrophenyl)diazene (3o).** Oxidation Method B was used with aniline **1o** (72.2 mg, 34.6 mmol), giving **2o** (34.6 mg, 0.118 mmol, 49%) as pale yellow block crystals: m.p. 91.5-92 °C (lit. 92-93 °C [59]); ^{1}H-NMR (300 MHz, $CDCl_3$, δ) 7.67 (s, 1H), 7.57 (s, 1H); ^{13}C-NMR (75 MHz, $CDCl_3$, δ) 150.60, 138.48, 122.17, 115.47, 114.11, 112.94; IR (KBr, cm^{-1}) 3078(w), 1615(s), 1567(m), 1515(w), 1474(m), 1370(w), 1320(w), 1262(w), 1216(w), 1178(w), 1043(m), 1024(m), 930(w), 926(w), 903(w), 899(w), 854(w), 847(m), 820(w), 732(m), 701(w), 682(m), 675(m); HRMS *m/z* ($M + Na^+$) calcd 314.8375 and 316.8355 and 318.8334, found 314.8384 and 316.8364 and 318.8343; and **3o** (26.8 mg, 0.091

mmol, 19%) as deep red needles: m.p. 245-247 °C; ^{1}H-NMR (300 MHz, $CDCl_3$, δ) 8.12 (d, *J* = 2.1 Hz, 2H), 7.78 (d, *J* = 1.8 Hz, 2H); IR (KBr, cm^{-1}) 3073(w), 1569(s), 1541(s), 1426(w), 1357(m), 1279(w), 1265(w), 1217(w), 1200(w), 1132(m), 1086(w), 905(w), 892(w), 863(m), 833(w), 767(w), 749(w), 726(w), 659(w); HRMS *m/z* (M + Na^+) calcd 608.6838 and 610.6818 and 612.6797, found 608.6866 and 610.6846 and 612.6825.

2-Fluoro-6-nitroaniline (1p). *Procedure and data summarized from the Master's thesis of Paul Erdman* [7]. Nitration Method A was used with *N*-(2-fluoro-6-nitrophenyl)-acetamide (**26**) (2.90 g, 26.1 mmol), giving **1p** (1.22 g, 7.81 mmol, 30%) as bright yellow needles: m.p. 74.5-75 °C (lit. 75.5-76.5 °C [60]); ^{1}H-NMR (300 MHz, $CDCl_3$, δ) 7.94 (dt, *J* = 9.0, 1.5 Hz, 1H), 7.24 (ddd, *J* =10.8, 7.8, 1.5 Hz, 1H), 6.64 (ddd, *J* =8.7, 7.8, 5.4 Hz, 1H), 6.14 (br s, 2H).

1-Azido-6-fluoro-2-nitrobenzene (27). *Procedure and data summarized from the Master's thesis of Paul Erdman* [7]. Aniline **1p** (529 mg, 3.39 mmol) was dissolved in warm acetic acid (1.0 mL). A solution of sodium nitrite in concentrated sulfuric acid (6.63 mL, 5.34 mmol, 0.8056 M) was added over 10 minutes and the yellow solution was stirred for 1 hour. The yellow solution was added slowly to an aqueous solution of sodium azide (4.51 mL, 6.78 mmol, 1.52 M) and the solution was stirred for 1 hour. The solution was poured on ice (50 g), the mixture was extracted with chloroform (2 x 50 mL), and the extracts were evaporated under an air stream. The resulting yellow-red oil was purified by flash column chromatography using silica gel and eluted with 1:4 dichloromethane/hexanes, giving **27** (427 mg, 2.34 mmol, 81%) as a pale yellow oil: ^{1}H-

NMR (300 MHz, $CDCl_3$, δ) 7.69 (dt, *J* = 8.1, 1.5 Hz, 1H), 7.39 (ddd, *J* =10.8, 8.4, 1.8 Hz, 1H), 7.23 (dt, *J* =8.4, 5.1 Hz, 1H).

4-Fluorobenzo[*c*][1,2,5]oxadiazole 1-oxide (2p). *Procedure and data summarized from the Master's thesis of Paul Erdman* [7]. Azide **27** (426.8 mg, 2.177 mmol) was dissolved in toluene (50 mL) and refluxed for 18 hours, giving **2p** (301.9 mg, 1.959 mmol, 90%) as yellow-orange prisms: m.p. 42.5-43 °C; ^{1}H-NMR (300 MHz, $CDCl_3$, δ) 7.14-7.25 (br m, 2H), 7.00-7.05 (m, 1H).

1,2-Bis(2-fluoro-6-nitrophenyl)diazene (3p). *Procedure and data summarized from the Master's thesis of Paul Erdman* [7]. A procedure similar to Oxidation Method A was used with a solution of potassium hydroxide in methanol (0.084 g, 0.45 mmol, 4.7 M) as the base and solvent, with sodium hypochlorite solution (0.43 mL, 0.3 mmol, 5%) added to a solution of aniline **1p** (42.9 mg, 0.275 mmol) in methanol, giving **3p** (29.6 mg, 0.192 mmol, 40%) as deep red needles: m.p. 168-170 °C; ^{1}H-NMR (300 MHz, $CDCl_3$, δ) 7.79 (dt, *J* = 7.8, 1.5 Hz, 1H), 7.51-7.64 (m, 2H).

2,4-Diiodo-6-nitroaniline (1q). Aniline **1a** (2695 mg, 19.51 mmol) was dissolved in dichloroethane (10 mL) and warmed to 70 °C. Iodine monochloride (6703 mg, 41.29 mmol) was diluted with dichloroethane (10 mL) and added slowly to the stirred solution of **1a** over 45 minutes and the resulting solution was stirred for 2.5 hours more. The solution was washed with 5% sodium bisulfate (2 x 20 mL), brine (2 x 20 mL), and water (2 x 20 mL). The dichloroethane layer was separated, dried over anhydrous sodium sulfate, and evaporated on a rotating evaporator, leaving a red-orange solid. Flash column chromatography using silica gel and eluted with 1:8 ethyl acetate/hexanes gave

1q (4211 mg, 10.80 mmol, 55%) as bright yellow-orange needles: m.p. 103-104 °C (lit. 105.5 °C [61]); ^{1}H-NMR (300 MHz, $CDCl_3$, δ) 8.45 (d, *J* = 2.0 Hz, 1H), 8.14 (d, *J* = 2.0 Hz, 1H), 6.69 (br s, 2H); IR (KBr, cm^{-1}) 3452(m), 3342(m), 3080(w), 1613(s), 1543(m), 1532(m), 1488(s), 1439(m), 1376(m), 1343(m), 1316(m), 1301(w), 1257(m), 1243(m), 1117(w), 1086(m), 1041(w), 876(m), 826(w), 762(m), 712(w), 612(m).

4,6-Diiodobenzo[*c*][1,2,5]oxadiazole 1-oxide (2q) and **1,2-bis(2,4-diiodo-6-nitrophenyl)diazene (3q).** Oxidation Method B used with aniline **1q** (95.1 mg, 0.244 mmol) gave a large number of unidentified products from which neither **2q** nor **3q** were identified.

PART II. STRUCTURAL DETERMINATION OF AGNOTOBENZALDEHYDE

2.1 Background

Professor Dr. Eugen Bamberger (1857-1932) was born in Berlin, Germany, and started his academic career in 1875 at the University of Berlin studying medicine. The following summer of 1876 he went to the University of Heidelberg and worked in chemistry under Professor Dr. Robert Wilhelm Bunsen. The same year he returned to the University of Berlin, focused on chemistry, where he received his doctorate in 1880 for his work on derivatives of guanine under Professor Dr. August Wilhelm von Hofmann. In 1883 Bamberger went to the University of Munich, as an assistant to Professor Dr. Adolf von Baeyer, and earned the title of extraordinary professor of chemistry in 1891. In 1893 Bamberger accepted a position as professor of chemistry at the Swiss Federal Institute of Technology (Eidgenössische Technische Hochschule, ETH) in Zürich, Switzerland. It was at ETH Zürich where Bamberger spent the rest of his academic career; here he published the majority of his nearly 430 publications. In 1905 a neurologic condition left his right arm paralyzed, forcing Bamberger to relinquish his teaching position; however, he was allowed to continue his research for many years with the aid of an assistant. Eventually, he could no longer continue his work and from then on he lived in the Ticino region of southern Switzerland. Despite the move and his medical condition, Bamberger continued to write up his unpublished earlier work. He

continued publishing his work, along with commentaries on other author's publications, through 1931, one year before his death in 1932 at the age of 75 [62].

2.2 Introduction

The discovery of anthranil, around 1882, prompted controversy over the structure of the compound, which resulted in a large number of publications that debated the topic. Bamberger and Professor Dr. Gustav Heller (1866-1946), a German chemist at the University of Leipzig, had many polemical discussions over the structure of anthranil [63]. Heller supported, and vigorously defended, the lactam structure **1** for anthranil (Figure 15), which was originally proposed and assigned by anthranil discoverers Friedländer and Enriques. Bamberger initially proposed and used the tricyclic structure **2** for anthranil in his publications; however, he later claimed that structure **2** should be regarded as equivalent to **3** (Figure 15) [64].

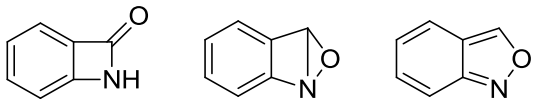

1 **2** **3**

Figure 15. Early Proposed Structures for Anthranil

In the first decade of the 1900's the finding that anthranil was the anhydride of 2-hydroxylaminobenzaldehyde (**5**) (Scheme 3, p. 54) prompted Bamberger to attempt to prepare the compound [65]. In 1906 Bamberger published his discovery of a strange solid product when he attempted to synthesize **5** through the reduction of 2-nitrobenzaldehyde (**4**) by shaking in chilled aqueous ammonium chloride and ether with the gradual addition of zinc dust [66]. Bamberger referred to the compound as

agnotobenzaldehyde, coming from the combination of the Greek word ἄγνωτος (agnotos), meaning unknown, and benzaldehyde [66,67]. Bamberger utilized elemental analysis together with a Landsberger-Lehner [68] molecular weight determination to establish that agnotobenzaldehyde had the molecular formula $C_{14}H_{12}N_2O_5$. Bamberger proposed that agnotobenzaldehyde was formed through some combination of **5** and unreacted **4**. From all this information he suggested structures **6** and **7** (Figure 16) [66]. These structures are based on the nucleophilic attack of either the aldehyde or nitro group of unreacted **4** by the lone pair of the nitrogen from hydroxylamine **5**.

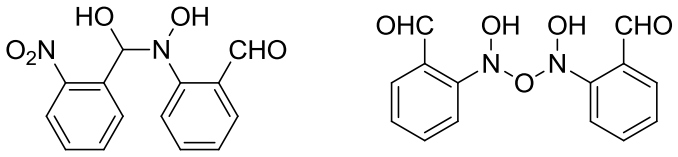

6 **7**

Figure 16. Bamberger's Proposed Structures for Agnotobenzaldehyde

8 **9**

Figure 17. Products of Bamberger's Acetylation and Oxidation of Agnotobenzaldehyde

In 1918, during a time when Bamberger was no longer able to continue his research, he published his last paper related to agnotobenzaldehyde [65]. In this publication, Bamberger treated agnotobenzaldehyde with acetic anhydride at 0 °C, which produced precursor **4** and a white solid that he suspected to be *N*-acetyl-*o*-hydroxyl-aminobenzaldehyde (Figure 17, **8**) [65]. Bamberger was able to carefully add a solution

of calcium hypochlorite in water to **8**, which produced 2-nitrosobenzaldehyde (**9**) (Figure 17) [65]. This procedure remains one of the most common ways to synthesize **9** due to its relatively simple procedure and low cost of reagents.

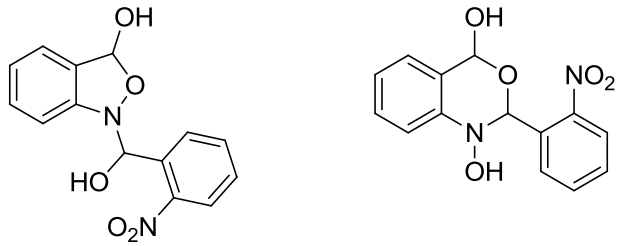

10 **11**

Figure 18. Bakke and Engan's Proposed Structures for Agnotobenzaldehyde

A one and a half page communication by Heller and Herrmann in 1927 [69], on the reaction of agnotobenzaldehyde with aniline or 4-methylaniline to produce 2-nitro-*N*-benzylideneanilines, was the last publication related to agnotobenzaldehyde until 1978. Then Bakke and Engan published a short communication where they utilized ^{1}H-NMR, IR, and MS to analyze 2-nitrosobenzaldehyde and the intermediates formed using Bamberger's method [70]. In this communication, Bakke and Engan refuted Bamberger's proposal that **7** was a likely structure for agnotobenzaldehyde based on their spectroscopic evidence [70]. Instead, Bakke and Engan proposed that Bamberger's alternate structure (Figure 16, **6**) is a reactive intermediate which is in equilibrium with the true structure of agnotobenaldehyde [70]. Based on this proposal, one of the hydroxyls in **6** could add to the aldehyde to form a five-membered ring (**10**) and/or a six-membered ring hemiacetal (**11**) (Figure 18) [69]. Bakke and Engan were also the first to recognize that agnotobenzaldehyde has different spectra in solid state or solution phase.

In addition to structural corrections for agnotobenzaldehyde, Bakke and Engan showed that the acetylation of agnotobenzaldehyde produced a compound with cyclic structure **12**, as well as an equivalent of starting material **4**, instead of **8** (Figure 17, p. 52) proposed by Bamberger (Scheme 3).

Scheme 3. Proposed Acetylation Route of Agnotobenzaldehyde

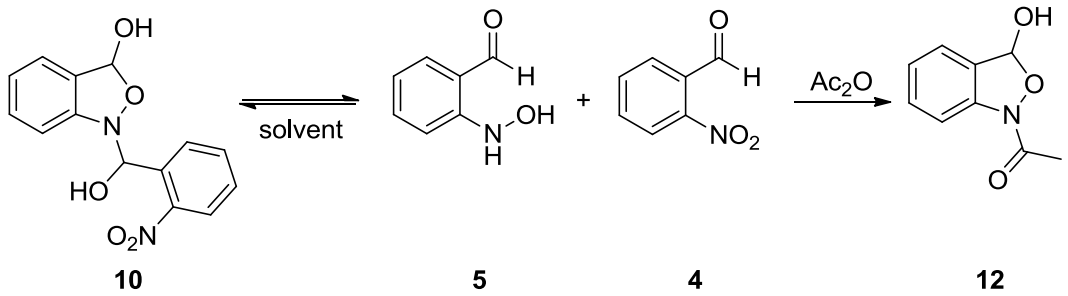

10 **5** **4** **12**

The most recent publication related to agnotobenzaldehyde was by Muchowski and Maddox in 2005 [71]. This publication focused on hydroxylamines and the isolation of **5** from a slight modification of Bamberger's method. Muchowski and Maddox's modification optimized recovery of **5**; but overreduction to anthranil and 2-amino-benzaldehyde prevented the formation of agnotobenzaldehyde [71]. Muchowski and Maddox never managed to isolate **5**, but they were able to identify and assign the ^{1}H-NMR and ^{13}C-NMR spectra from the mixture.

2.3 Material Synthesis

2-Nitrobenzaldehyde was prepared by following a procedure by Davey and Gwilt [72], with minor modifications. Their procedure of dissolving benzaldehyde in acetic anhydride followed by adding fuming nitric acid was followed as published; however, the length of time stirring after adding nitric acid was lowered to 2 hours based on TLC

analysis and not left overnight at room temperate. Then, it was worked up directly as stated in their procedure.

In our present work, Bamberger's original procedure for the preparation of agnotobenzaldehyde was largely followed, but there was some optimization of the reagent preparation and reaction conditions. It was found that the quality of zinc metal greatly affected the yield and the cleanness of the reaction. Thus, granular zinc was ground in a mortar and pestle, instead of using zinc dust. It was also found that light and temperature affected the rate of decomposition of the product. The decomposition of agnotobenzaldehyde was much faster in solution. A solution of agnotobenzaldehyde decomposed completely overnight in the light at room temperature, but could be kept in the dark at -25 ^{o}C for a few days before most of it had decomposed. However, dry crystalline agnotobenzaldehyde showed little decomposition over a month in the light at room temperature.

2.4 Results and Discussion

Characterization of agnotobenzaldehyde began about 1906 with Bamberger's determination of its molecular formula by elemental analysis and molecular weight determination. In 1978 Bakke and Engan determined that agnotobenzaldehyde had different spectra as a solid or in solution [70]. An IR spectrum of the solid fused with potassium bromide showed no carbonyl, but when it was dissolved in acetonitrile, bands consistent with starting material **4** and hydroxylamine **5** appeared. Dissociation of agnotobenzaldehyde can also be observed with ^{1}H-NMR which gives a spectrum that contains starting material **4** and hydroxylamine **5**. In addition, there is a small amount of

an unknown compound, or mixture of compounds, appearing near the baseline of the spectrum, at a ratio of approximately 5:1.

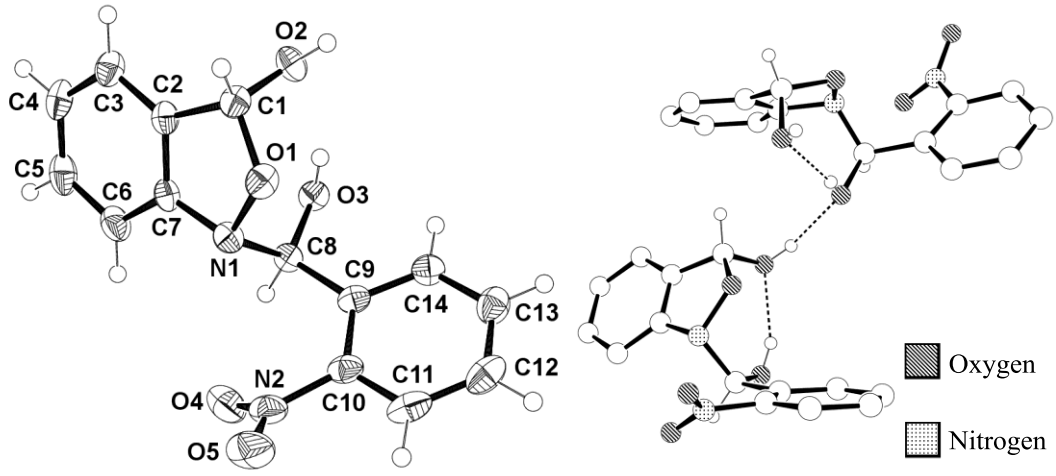

Figure 19. Left: Anisotropic displacement ellipsoids (50% probability) for **10**.
Right: Hydrogen bonding H•••O interactions are shown with dashed lines.

A crystal of agnotobenzaldehyde was used to analyze its solid state structure by X-ray diffraction. The crystal structure of agnotobenzaldehyde was determined to be *rac*-(3*R*)-1-((*S*)-hydroxy(2-nitrophenyl)methyl)-1,3-dihydro-2,1-benzisoxazol-3-ol (**10**) (Figure 19) with agreement between the crystallographic model and the experimental X-ray diffraction data of 96.36% (R = 0.0364). Compound **10** has extensive intramolecular (2.003 Å) and intermolecular (1.942 Å) hydrogen bonding between hydroxyls that continues as a chain though the entire crystal lattice, orthogonal to the *b* face. This hydrogen bonding locks the molecule into two enantiomorphic configurations, instead of the four possible stereoisomers due to the two chiral centers. It is probable that this extensive, strong hydrogen bond system is what causes agnotobenzaldehyde to slowly fall out of aprotic solvents and remain in this stable form even though 10% or less is possibly observed by ^{1}H-NMR when fully dissolved. Bond lengths and angles for the

2,1-benzisoxazol-like portion are consistent with an aromatic benzene ring fused to an isoxazole with little or no delocalization into the isoxazole portion like 2,1-benzisoxazol.

The crystal structure of acetylated agnotobenzaldehyde was determined to be *rac*-(*R*)-1-(3-hydroxy-2,1-benzisoxazol-1(3*H*)-yl)ethanone (**12**) (Figure 20) with agreement between the crystallographic model and the experimental X-ray diffraction data of 96.66% (R = 0.0334). Compound **12** has two strong intermolecular hydrogen bonds between hydroxyls with contact distances of 1.902 Å. The similarity between the heterocyclic ring systems **10** and **12** indicates that this five membered ring form is the more stable configuration for these compounds to form from hydroxylamine **5**.

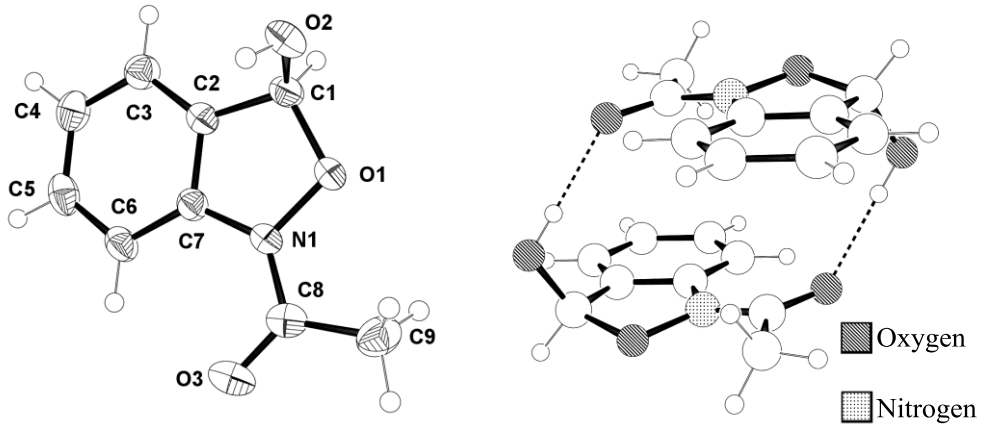

Figure 20. Left: Anisotropic displacement ellipsoids (50% probability) for **12**.
Right: Hydrogen bonding H•••O interactions are shown with dashed lines.

The mechanism for formation of compound **10** can be rationalized in different ways: (1) hydroxylamine **5** is in equilibrium with a ring closed form that occurs from intramolecular nucleophilic attack of the aldehyde by the hydroxylamine hydroxyl, which then finds a molecule of **4** in solution and the remaining amino nitrogen carries out intermolecular nucleophilic attack on the aldehyde of **4** to make **10** (Scheme 4); or (2) the amino nitrogen of hydroxylamine **5** carries out intermolecular nucleophilic attack on the

aldehyde first to form intermediate **6**, which undergoes ring closure by intramolecular nucleophilic attack on the aldehyde by the one of the remaining hydroxyls to produce **10** (Scheme 5). The mechanism proposed in *Scheme 4* could be the primary route because the rate and probability of intramolecular ring closure will be higher than an intermolecular event. In addition, the observance of exclusively a five-membered ring hemiacetal (**10**) and no six-membered ring hemiacetal (**11**) is justified best by *Scheme 4* since a six-membered ring hemiacetal (**11**) (Figure 18, p. 53) would have been the expected major product of ring closure. This can be justified due to inductive decrease in the nucleophilicity of the hydroxylamine hydroxyl and the potential stabilization of a six-membered ring (**11**) compared to a five-membered ring (**10**) (Figure 18, p. 53). Computations using GAMESS with a RHF/6-21G basis set produced results with compound **11** 8.6 kcal/mol lower in energy than compound **10**. Repeated computations using GAMESS with a RHF/STO-5G basis set produced similar results with compound **11** 3.6 kcal/mol lower in energy than compound **10**. However, it can be argued that compound **11** would not have as strong an intramolecular hydrogen bond in its crystal structure, preventing it from precipitating and accumulating in any measurable quantity.

Scheme 4. Proposed Mechanism for Agnotobenzaldehyde Formation

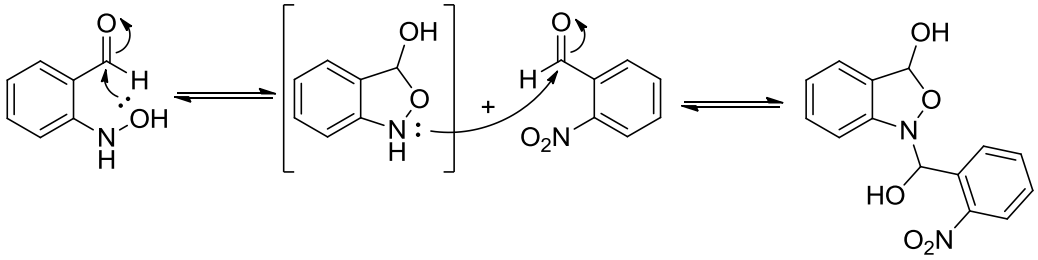

5 **4** **10**

Scheme 5. Alternate Mechanism for Agnotobenzaldehyde Formation

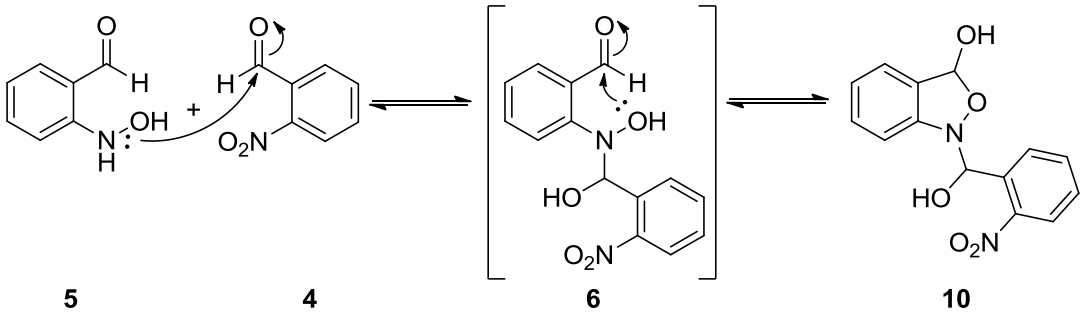

5 **4** **6** **10**

2.5 Crystallography: Experimental

For the three compounds given in *Table 2*, data were collected on a *Siemens* or *Bruker SMART* area detector diffractometer for a data collection at -100 °C [73]. A preliminary set of cell constants was calculated from reflections harvested from three sets of 20 frames. These initial sets of frames were oriented such that orthogonal wedges of reciprocal space were surveyed. The data collection was carried out using MoKα radiation (graphite monochromator) with a detector distance of 5 cm. A randomly oriented region of reciprocal space was surveyed to the extent of one sphere and to a resolution of 0.84 Å. Four major sections of frames were collected with 0.30º steps in ω at four different ϕ settings and a detector position of -28º in 2θ. The intensity data were corrected for absorption and decay using SADABS [74]. Final cell constants were calculated from the xyz centroids of strong reflections from the actual data collection after data reduction was done with SAINT [75]. The structure was solved using Bruker SHELXTL and refined using SHELXL-97 [76]. The space groups were determined based on systematic absences and intensity statistics. A direct-methods solution was calculated which provided most non-hydrogen atoms from the electron density map.

Full-matrix least squares / difference Fourier cycles were performed which located the remaining non-hydrogen atoms. All non-hydrogen atoms were refined with anisotropic displacement parameters.

Table 2. Crystal Data and Structure-Refinement Details

	4	**10**	**12**
Empirical formula	$C_7H_5NO_3$	$C_{14}H_{12}N_2O_5$	$C_9H_9NO_3$
Crystal system	monoclinic	orthorhombic	triclinic
Space group	$P2_1$	$Pbca$	$P\bar{1}$
a /Å	7.5557(15)	13.8066(14)	7.313(4)
b /Å	3.8736(8)	8.4412(9)	7.465(4)
c /Å	11.343(2)	22.8320(24)	9.487(6)
α/°	90	90	67.09(4)
β/°	90.26(3)	90	68.70(4)
γ/°	90	90	61.36(3)
V/Å^3	331.98(11)	2660.9(5)	408.6(4)
Z	2	8	2
D_{calc}/g cm^{-3}	1.512	1.439	1.456
F(000)	156	1200	188
Crystal size/mm	0.50 × 0.15 × 0.10	0.50 × 0.20 × 0.15	0.45 × 0.35 × 0.30
μ/mm^{-1}	0.121	0.111	0.111
Temp./K	174(2)	173(2)	173(2)
wavelength/Å	0.71073	0.71073	0.71073
θ Range/°	1.80 to 27.53	1.78 to 25.07	2.39 to 27.52
hkl Range	$-9 < h < 9$	$-16 < h < 16$	$-9 < h < 9$
	$0 < k < 5$	$-9 < k < 10$	$-9 < k < 9$
	$0 < l < 14$	$-27 < l < 27$	$-12 < l < 12$
Reflections: collected, unique, observed (I>2σ(I))	3886, 861, 738	20102, 2357, 1712	4864, 1860, 1634
$R(F)$	0.0334	0.0364	0.0334
$wR(F^2)$ all data	0.0868	0.1035	0.0903
Goodness-of-fit	1.043	1.038	1.044
max/min resid. dens./e Å^{-3}	0.174, -0.145	0.207, -0.194	0.238, -0.145
CCDC No.[a]	788556	788554	788555

a) Crystallographic data have been deposited with the *Cambridge Crystallographic Data Centre* (CCDC). Copies of the data can be obtained, free of charge, on application to the CCDC via *www.ccdc.cam.ac.uk/data_request/cif*, by emailing *data_request@ccdc.cam.ac.uk* , or by contacting The Cambridge Crystallographic Data Centre, 12, Union Road, Cambridge CB2 1EZ, UK; fax: +44 1223 336033.

Crystals were grown from solvent combinations listed for each compound in the

Experimental Section. Crystals of **12** were provided by Henrik van Lengerich and X-ray crystal data collections for **4** and **12** were performed by Prof. Emer. Doyle Britton.

2.6 Experimenal

General. Solvents and reagents were purchased and used as received. Thin-layer chromatography was performed on plastic-backed pre-coated plates with 0.2 mm thick alumina containing F_{254} indicator eluting with the solvents indicated and visualized with a 254 nm UV lamp. Melting points were obtained on a Fisher-Johns hot-stage melting point apparatus and are not corrected. Infrared spectra were acquired on a 4000 FT-IR spectrometer. Nuclear magnetic resonance spectra chemical shifts (δ in ppm) were referenced to the solvent (dichloromethane or acetone) [33] and ^{13}C spectra were proton-decoupled.

2-nitrobenzaldehyde (4). Freshly distilled benzaldehyde (20.382 g, 192.06 mmol) was added to acetic anhydride (200 mL) and cooled to -10 °C in a salt-ice bath. Fuming nitric acid (9.00 mL, 214 mmol, *d* 1.50) was added slowly to a stirred solution over 15 min and stirred for an additional 2 h. The solution was poured on ice (200 g) and the resulting solid was recovered by vacuum filtration. The solid was thoroughly washed with water and recrystallized from methanol, producing large block crystals of (4-nitrophenyl)methylene diacetate (15.527 g, 61.321 mmol, 32%). m.p. 124-125 °C (lit. 125 °C [77]) ^1H-NMR (300 MHz, acetone-d_6, δ) 8.32 (d, J = 8.9 Hz, 2H), 7.85 (d, J = 8.6 Hz, 2H), 7.74 (s, 1H), 2.15 (s, 6H).

Evaporation of the mother liquor and recrystallization from toluene-hexanes produced white needles of **4** (11.463 g, 75.854 mmol, 39%). m.p. 40-42 °C (lit. 43.5-44.5 °C [78]);

^{1}H-NMR (300 MHz, $CDCl_3$, δ) 10.44 (s, 1 H), 8.13 (ddd, *J* = 7.5, 1.6, 0.9 Hz, 1 H), 7.97 (ddd, *J* = 7.2, 2.1, 0.9 Hz, 1 H), 7.81 (dt, *J* = 7.4, 2.2 Hz, 1 H), 7.76 (dt, *J* = 7.4, 2.1 Hz. 1H); ^{1}H-NMR (300 MHz, acetone-d_6, δ) 10.36 (s, 1H), 8.23 – 8.11 (m, 1H), 8.00 – 7.86 (m, 3H).

***rac*-(3*R*)-1-((*S*)-hydroxy(2-nitrophenyl)methyl)-1,3-dihydro-2,1-benzisoxazol-3-ol (10).** **4** (0.251 g, 1.66 mmol) was dissolved in diethyl ether (5 mL) and combined with ammonium chloride (0.157 g, 2.94 mmol) in water (5 mL). The reaction flask was covered with aluminum foil and cooled in an ice-water bath. Zinc granules (0.421 g, 6.44 mmol) were ground with a mortar and pestle and added slowly to a vigorously stirred solution over a period of 10 min; the internal temperature never exceeded 10 °C. The mixture was stirred for an additional 15 min at 0 °C. The zinc-containing residue was removed by vacuum filtration and the filtrate was extracted with ether (2 x 10 mL). The ether extracts were combined, dried over anhydrous magnesium sulfate for 2 h in the dark, and the drying agent was removed by vacuum filtration. The ether mother liquor was reduced in volume to 2 mL by evaporation facilitated by passing an air flow over the solution for 15 min. The concentrated solution was covered with aluminum foil and cooled in a freezer to -25 °C for 12 h. From this, a solid had formed in the container which was isolated by filtration, wished with cold ether, and placed on a pump vacuum to remove any remaining solvent. The product (**10**) was a fluffy white microcrystalline solid (0.186 g, 0.645 mmol, 78%), used for NMR and IR analysis. A portion of the microcrystalline solid (~20 mg) was recrystallized by vapor diffusion using ethyl acetate and hexanes at -25 °C in the dark. After a week, clear, colorless needles were produced,

which were used for X-ray crystal structure analysis. m.p. 97-98 °C (lit. 98.5-99 °C [66]); ^{1}H-NMR (500 MHz, acetone-d_6, δ) 10.36 (s, 1H, CHO-**4**), 9.90 (s, 1H, CHO-**5**), 9.77 (s, 1H, NH-**5**), 8.32 (s, 1H, OH-**5**), 8.17 (dd, *J* = 6.8, 1.9 Hz, 1H, H3-**4**), 8.00 – 7.89 (m, 3H, H4,5,6-**4**), 7.70 (dd, *J* = 7.7, 1.4 Hz, 1H, H6-**5**), 7.54 (dt, *J* = 7.5, 1.4 Hz, 1H, H4-**5**), 7.34 (d, *J* = 8.5 Hz, 1H, H3-**5**), 6.91 (dt, *J* = 7.4, 1.3 Hz, 1H, H5-**5**); IR (KBr, cm^{-1}) 3321(bs), 3267(bs), 3081(w), 3029(w), 2967(w), 2924(w), 2867(w), 1609(m), 1578(w), 1526(s), 1468(m), 1446(w), 1412(w), 1354(s), 1314(w), 1333(w), 1286(w), 1242(w), 1224(w), 1187(m), 1113(w), 1087(w), 1049(m), 1035(m), 1019(m), 1003(m), 937(m), 920(m), 887(w), 858(w), 831(w), 789(w), 784(w), 768(m), 755(w), 734(m), 726(w), 709(m), 682(w), 672(w), 638(w), 607(w).

***rac*-(*R*)-1-(3-hydroxy-2,1-benzisoxazol-1(3*H*)-yl)ethanone (12).** Compound **10** (1.1059 g, 3.8365 mmol) was finely ground in a mortar and pestle and transferred into a reaction flask covered with aluminum foil. The solid was dissolved in a minimal amount of toluene (1.50 mL) and the flask was placed in an ice-water bath. Acetic anhydride (0.605 g, 5.93 mmol) was added dropwise over 10 min, with stirring; additional toluene was required to facilitate stirring due to the formation of a white precipitate. The flask was sealed in a vacuum desiccator and placed in a freezer for 20 h. The precipitate was recovered by vacuum filtration and wished with a small amount of cold toluene, leaving compound **12** as a white crystalline solid (0.4806 g, 2.682 mmol, 70%). m.p. 125-126 °C (lit. 126.5-127 °C [65]); ^{1}H-NMR (500 MHz, acetone-d_6, δ) 7.74 (d, *J* = 8.0 Hz, 1H, C6-H), 7.48 (d, *J* = 7.6 Hz, 1H, C3-H), 7.43 (t, *J* = 7.7 Hz, 1H, C5-H), 7.22 (t, *J* = 7.5 Hz, 1H, C4-H), 6.69 (s, 1H, C1-H), 6.67 (s, 1H, OH), 2.24 (s, 3H, CH_3). ^{13}C-NMR (75 MHz,

acetone-d_6, δ) 167.46, 137.73, 130.69, 129.36, 125.27, 124.33, 114.36, 100.00, 21.80; IR (KBr, cm^{-1}) 3311(s), 2984(m), 2875(w), 1641(s), 1602(s), 1488(s), 1464(s), 1438(s), 1357(m), 1330(w), 1302(w), 1269(w), 1192(m), 1153(w), 1112(m), 1088(s), 1052(s), 1024(m), 1010(s), 933(s), 895(s), 864(w), 761(s), 744(m), 728(m), 689(w), 648(m), 618(w).

REFERENCES

[1] Noelting, E.; Kohn, A. *Chem.-Ztg.* **1894**, *18*, 1095.

[2] Meigen, W.; Normann, W. *Ber. Dtsch. Chem. Ges.* **1900**, *33*, 2711-2717. *J. Chem. Soc. Abstr.* **1900**, *78(1)*, 702.

[3] Green, A. G.; Rowe, F. M. *J. Chem. Soc.* **1912**, *101*, 2433-2459.

[4] a) Auwers, K. V. *Liebigs Ann. Chem.* **1927**, *453*, 211-238. b) Hammick, D. L.; Edwards, W. A. M.; Steiner, E. R. *J. Chem. Soc.* **1931**, 3308-3313.

[5] a) Mallory, F. B.; Wood, C. S. *P. Natl. Acad. Sci. U.S.A.* **1961**, *47*, 697-700. b) Katritzky, A. R.; Oesne, S.; Harris, R. K. *Chem. Ind.-London* **1961**, 990-992. c) Englert, G. *Z. Elektrochem. Angew. P.* **1961**, *65*, 854-863. d) Englert, G. *Z. Naturforsch.* **1961**, *16b*, 413-414. e) Englert, G. *Fresen. Z. Anal. Chem.* **1961**, *181*, 447-455.

[6] Britton, D.; Noland, W. E. *J. Org. Chem.* **1962**, *27*, 3218-3223.

[7] Erdman, P. J. *Master of Science Thesis (with W.E. Noland)*, University of Minnesota, Minneapolis, MN, **2006**.

[8] Jeffery, C. S. *Unpublished Work (with W.E. Noland)*, University of Minnesota, Minneapolis, MN, **2003**.

[9] Calvino, R.; Mortarini, V.; Gasco, A.; Sanfilippo, A.; Ricciardi, M. L. *Eur. J. Med. Chem.-Chim. Ther.*, **1980**, *15*, 485-487.

[10] a) Ghosh, P. B.; Whitehouse, M. W. *J. Med. Chem.* **1968**, *11(2)*, 305-311. b) Whitehouse, M. W.; Gosh, P. B. *Biochem. Pharmacol.*, **1968**, *17(1)*, 158-161. c) Gosh, P. B.; Whitehouse, M. W. *J. Med. Chem.*, **1969**, *12*, 505-507. d) Gosh, P. B.; Ternai, B.; Whitehouse, M. W. *J. Med. Chem.*, **1972**, *15*, 255-260.

[11] a) Ghosh, P. B.; Everitt, B. J. *J. Med. Chem.*, **1974**, *17(2)*, 203-206. b) Medana, C.; Di Stilo, A.; Visentin, S.; Fruttero, R.; Gasco, A.; Ghigo, D.; Bosia, A. *Pharm. Res.*, **1999**, *16(6)*, 956-960. c) Granik, V. G.; Kaminka, M. É.; Grigor'ev, N. B.; Severina, I. S.; Kalinkina, M. A.; Makarov, V. A.; Levina, V. I. *Khim. Farm. Zh.*, **2002**, *36*, 523-527.

[12] a) Ghigo, D.; Heller, R.; Calvino, R.; Alessio, P.; Fruttero, R.; Gasco, A.; Bosia, A.; Pescarmona, G. *Biochem. Pharmacol.*, **1992**, *43(6)*, 1281-1288. b) Calvino, R.; Fruttero, R.; Ghigo, D.; Bosia, A.; Pescarmona, G.; Gasco, A. *J. Med. Chem.*, **1992**, *35(17)*, 3296-3300. c) Ferioli, R.; Fazzini, A.; Folco, G.C.; Fruttero, R.; Calvino, R.; Gasco, A.; Bongrani, S.; Civelli, M. *Pharmacol. Res.*, **1993**, *28(3)*, 203-212. d) Medana, C.; Ermondi, G.; Fruttero, R.; Di Stilo, A.; Ferretti, C.; Gasco, A. *J. Med. Chem.*, **1994**, *37(25)*, 4412-4416. e) Hecker, M.; Vorhoff, W.; Bara, A. T.; Mordvintcev, P. I.; Busse, R. *N.-S. Arch. Pharmacol.*, **1995**, *351(4)*, 426-432.

[13] Aguirre, G.; Cerecetto, H.; Di Maio, R.; González, M.; Porcal, W.; Seoane, G.; Ortega, M. A.; Aldana, I.; Monge, A.; Denicola, A. *Arch. Pharm. Pharm. Med. Chem.* **2002**, *335*, 15-21.

[14] Aguirre, G.; Boiani, L.; Cerecetto, H.; Di Maio, R.; González, M.; Porcal, W.; Denicola, A.; Möller, M.; Thomson, L.; Tórtora, V. *Bioorgan. Med. Chem.* **2005**, *13*, 6324-6335.

[15] Gasco, A. M.; Ermondi, G.; Fruttero, R.; Gasco, A. *Eur. J. Med. Chem.*, **1996**, *31*, 3-10.
[16] Sérgio de Carvalho, P.; Maróstica, M.; Gambero, A.; Pedrazzoli, J., Jr. *Eur. J. Med. Chem.* **2010**, *45(6)*, 2489-2493.
[17] "Azo dye" *Encyclopædia Britannica*. Encyclopædia Britannica Online. *http://www.britannica.com/EBchecked/topic/46918/azo-dye*. (accessed 8/10/2010, 2010).
[18] Zhang, C.; Du, M.-H.; Cheng, H.-P.; Roitberg, A. E.; Krause, J. L. *Phys. Rev. Lett.* **2004**, *92*, 158301/1-158301/4.
[19] Venkataraman, L.; Park, Y. S.; Whalley, A. C.; Nuckolls, C.; Hybertsen, M. S.; Steigerwald, M. L. *Nano Lett.* **2007**, *7(11)*, 502-506.
[20] Palma, J. L.; Cao, C.; Zhang, X.-G.; Krstić, P. S.; Krause, J. L.; Cheng, H.-P. *J. Phys. Chem.* **2010**, *114*, 1655-1662.
[21] a) Chapman, K. J.; Dyall, L. K. *Aust. J. Chem.* **1976**, *29*, 367-374. b) Chapman, K. J.; Dyall, L. K.; Frith, L. K. *Aust. J. Chem.* **1984**, *37*, 341-354. c) Dyall, L. K. *Aust. J. Chem.* **1984**, *37*, 2013-2026.
[22] McCulla, R. D.; Burdzinski, G.; Platz, M. S. *Org. Lett.* **2006**, *8(8)*, 1637-1640.
[23] a) Schrock, A. K.; Schuster, G. B. *J. Am. Chem. Soc.* **1984**, *106(18)*, 5228-5234. b) Shields, C. J.; Chrisope, D. R.; Schuster,G. B.; Dixon, A. J.; Poliakoff, M.; Turner, J. J. *J. Am. Chem. Soc.* **1987**, *109(15)*, 4723-4726. c) Li, Y.-Z.; Kirby, J. P.; George, M. W.; Poliakoff, M.; Schuster,G. B. *J. Am. Chem. Soc.* **1988**, *110(24)*, 8092-8098.
[24] Borden, W. T.; Gritsan, N. P.; Hadad, C. M.; Karney, W. L.; Kemnitz, C. R.; Platz, M. S. *Acc. Chem. Res.* **2000**, *33*, 765-771.
[25] Leyva, E.; Platz, M. S.; Persy, G.; Wirz, J. *J. Am. Chem. Soc.* **1986**, *108(13)*, 3783-3790.
[26] Platz, M. S. *Acc. Chem. Res.* **1995**, *28*, 487-492.
[27] Hrovat, D. A; Waali, E. E.; Borden, W. T. *J. Am. Chem. Soc.* **1992**, *114*, 8698-8699.
[28] Parasuk, V.; Cramer, C. J. *Chem. Phys. Lett.* **1996**, *260*, 7-14.
[29] Poe, R.; Schnapp. K.; Young, M. J. T.; Grayzar, J.; Platz, M. S. *J. Am. Chem. Soc.* **1992**, *114*, 5054-5067.
[30] Johnson, W. T. G.; Sullivan, M. B.; Cramer, C. J. *Int. J. Quantum Chem.* **2001**, *85*, 492-508.
[31] Anastassiou, A. G. *J. Am. Chem. Soc.* **1966**, *88(10)*, 2322-2324.
[32] Young, M. J. T; Platz, M. S. *J. Org. Chem.* **1991**, *56*, 6403-6406.
[33] Gottlieb, H. E.; Kotlyar, V.; Nudelman, A. *J. Org. Chem.* **1997**, *62(21)*, 7512-7515.
[34] Beilstein, F.; Kuhlberg *Liebigs Ann. Chem.* **1871**, *158*, 344.
[35] Lellmann; Wuerthner *Liebigs Ann. Chem.* **1885**, *228*, 143.
[36] Janovsky, J. V. *Monatsh. Chem.* **1889**, *10*, 585-601.
[37] Willgerodt, C.; Schmierer, F. *Ber. Dtsch. Chem. Ges.* **1905**, *38*, 1472-1478.
[38] Zincke, T.; Schwarz, P. *Liebigs Ann. Chem.* **1899**, *307*, 28-49.
[39] Reverdin, F.; Widmer, K. *Ber. Dtsch. Chem. Ges.* **1913**, *46*, 4072-4074.

[40] Shine, H. J.; Cheng, J. D. *J. Org. Chem.* **1971**, *36(19)*, 2787-2790.
[41] Bantlin, A. *Ber. Dtsch. Chem. Ges.* **1878**, *11*, 2099-2107.
[42] Mallory, F. B.; Varimbi, S. P. *J. Org. Chem.* **1963**, *28*, 1656-1662.
[43] Haehle, F. H. *J. Prakt. Chem.- Leipzig* **1891**, *43(2)*, 74.
[44] Lothrop, W. C. *J. Am. Chem. Soc.* **1942**, *64*, 1698-1700.
[45] Makosza, M.; Bia-lecki, M. *J. Org. Chem.* **1998**, *63(15)*, 4878-4888.
[46] Borsche, W.; Stackmann, L.; Makaroff, J. *Ber. Dtsch. Chem. Ges.* **1916**, *49*, 2222-2243.
[47] Beilstein, F.; Kurbatow, A. *Liebigs Ann. Chem.* **1876**, *182*, 108.
[48] Lobry de Bruyn, A. F. H. *Recl. Trav. Chim. Pay-Bas* **1917**, *36*, 126-166.
[49] Dyall, L. K.; Pausacker, K. H. *Aust. J. Chem.* **1958**, *11*, 491-508.
[50] Artini, E. *Z. Kristallogr. Minera.* **1911**, *46*, 407-414.
[51] Witt, O. N. *Ber. Dtsch. Chem. Ges.* **1875**, *8*, 1226-1276.
[52] Boulton, A. J.; Gripper Gray, A. C.; Katritzky, A. R. *J. Chem. Soc. B* **1967**, *9*, 909-911.
[53] Koerner, W. *Gazz. Chim. Ital.* **1874**, *4*, 341.
[54] Meldola, R.; Streatfeild, F. H. *J. Chem. Soc.* **1898**, *73*, 681-690.
[55] Tappi, G.; Forni, P. V. *Ann. Chim. App.* **1949**, *39*, 338-343.
[56] Orton, K. J. P. *J. Chem. Soc.* **1902**, *81*, 490-495.
[57] Michael; Norton *Ber. Dtsch. Chem. Ges.* **1878**, *11*, 109.
[58] Kapil, R. S. *J. Chem. Soc.* **1959**, 4127-4128.
[59] Moje, W. *J. Org. Chem.* **1964**, *29(12)*, 3722-3723.
[60] Liedholm, B. *Acta Chem. Scand. Ser. B* **1976**, *30*, 141-149.
[61] Michael; Norton *Ber. Dtsch. Chem. Ges.* **1878**, *11*, 109.
[62] Blangey, L. *Helv. Chim. Acta* **1933**, *16*, 644-685.
[63] "Prof. Dr. phil. Gustav Heller" Professorenkatalog der Universität Leipzig - Die Professoren-Datenbank für Leipzig. *http://www.uni-leipzig.de/unigeschichte/professorenkatalog/leipzig/Heller_423.html* (accessed 2/9/2010, 2010).
[64] (a) Speroni, G. In *Physico-Chemical Properties of Isoxazole;* Wiley-Interscience: New York, 1962; Vol. 17, p. 177-222. (b) Wuensch, K. H.; Boulton, A. J. *Adv. Heterocycl. Chem.* **1967**, *8*, 277-379.
[65] Bamberger, E. *Ber. Dtsch. Chem. Ges.* **1918**, *51*, 613-629. *J. Chem. Soc. Abstr.* **1918**, *114(1)*, 346-347.
[66] Bamberger, E. *Ber. Dtsch. Chem. Ges.* **1906**, *39*, 4252-4276. *J. Chem. Soc. Abstr.* **1907**, *92(1)*, 163-164.
[67] Woodhouse, S. C. *English-Greek dictionary: a vocabulary of the Attic language;* Routledge & K. Paul: London, 1910 (1979 reprint); p. 923-924.
[68] Meyer, R.; Jaeger, P. *Ber. Dtsch. Chem. Ges*, **1903**, *36*, 1555-1560.
[69] Heller, G.; Herrmann, H. *Ber. Dtsch. Chem. Ges, Abt. A.* **1927**, *60(1)*, 912-913.
[70] Bakke, J.M.; Engan, H-J *Acta Chem. Scand. B* **1978**, *32*, 230-231.
[71] Muchowski, J. M.; Maddox, M. L. *J. Mex. Chem. Soc.* **2005**, *49(1)*, 24-31.
[72] Davey, W.; Gwilt, J. R. *J. Chem. Soc.* **1950**, 204-208.
[73] SMART V5.054, *Bruker Analytical X-Ray Systems*, Madison, WI, USA, 2001.

[74] Blessing, R. *Acta Cryst.* **1995**, *A51*, 33-38.
[75] SAINT+ V6.45, *Bruker Analytical X-Ray Systems*, Madison, WI, USA, 2003.
[76] SHELXTL V6.14, *Bruker Analytical X-Ray Systems*, Madison, WI, USA, 2000.
[77] Thiele, J.; Winter, E. *Liebigs Ann. Chem.* **1900**, *311*, 353-362.
[78] Gabriel, S.; Meyer, R. *Ber. Dtsch. Chem. Ges*, **1881**, *14*, 830.

APPENDIX 1. SPECTRAL DATA FOR PART II

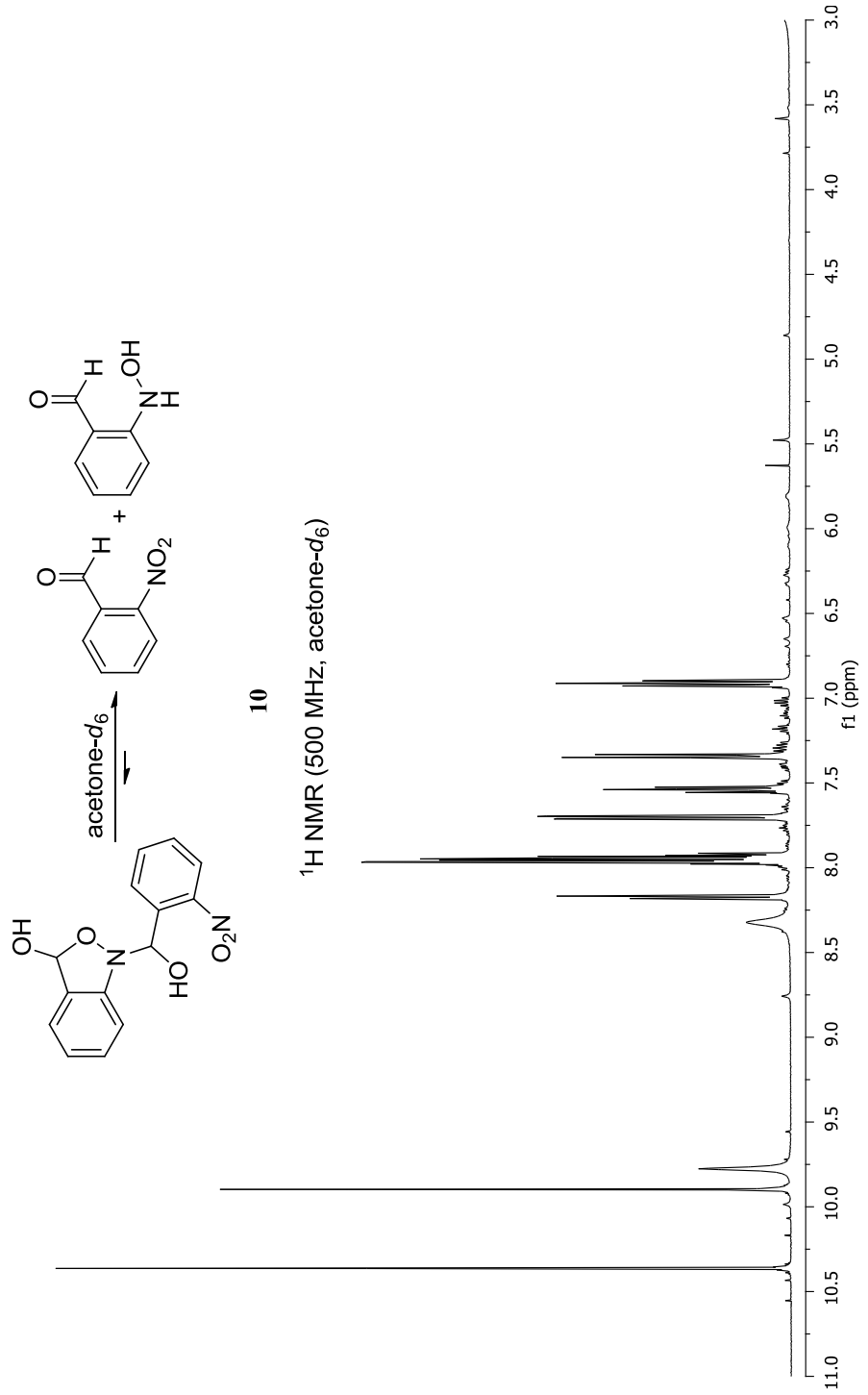

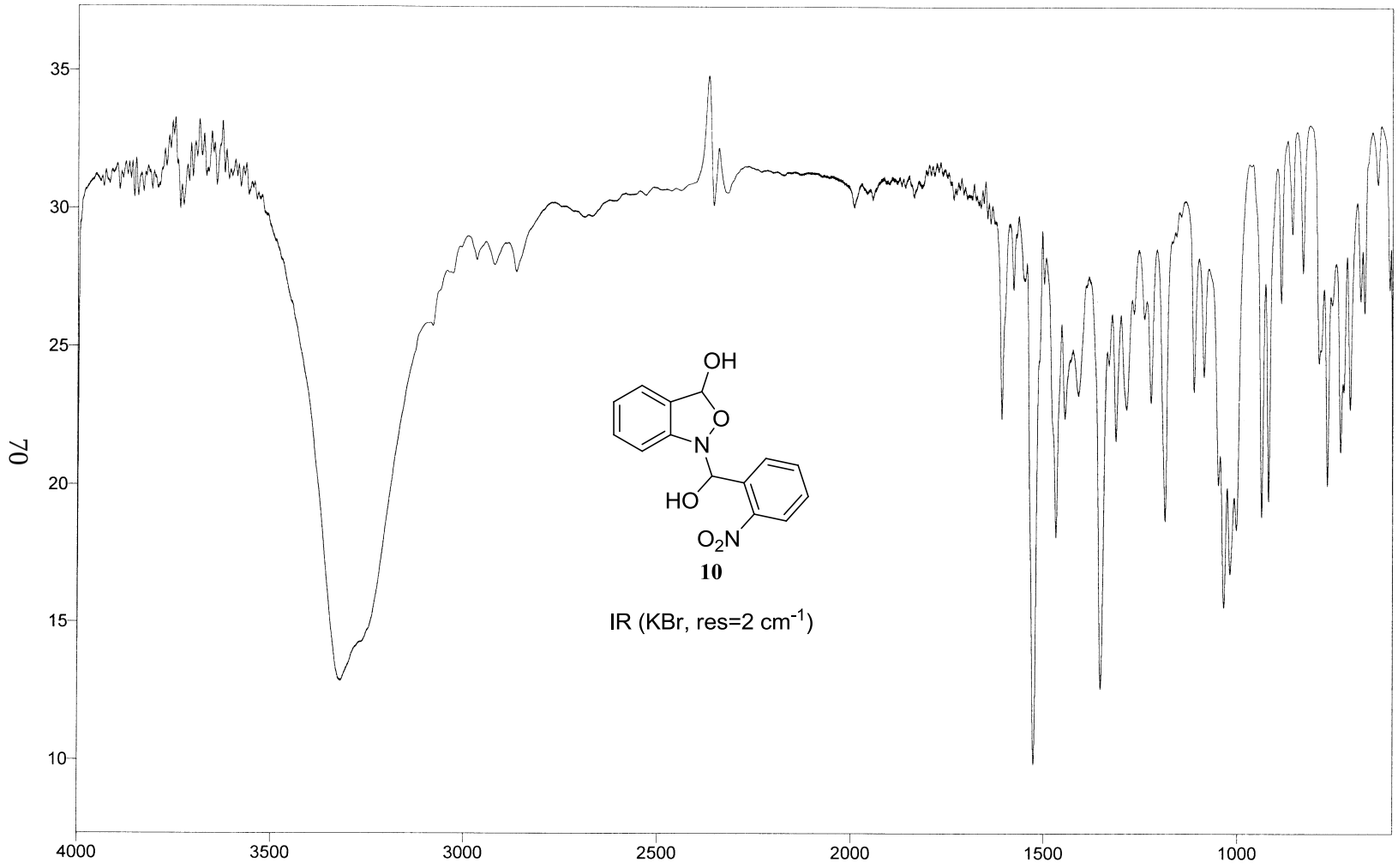

10

IR (KBr, res=2 cm^{-1})

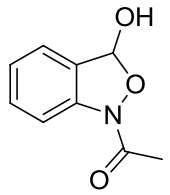

12

^{1}H NMR (500 MHz, acetone-d_6)

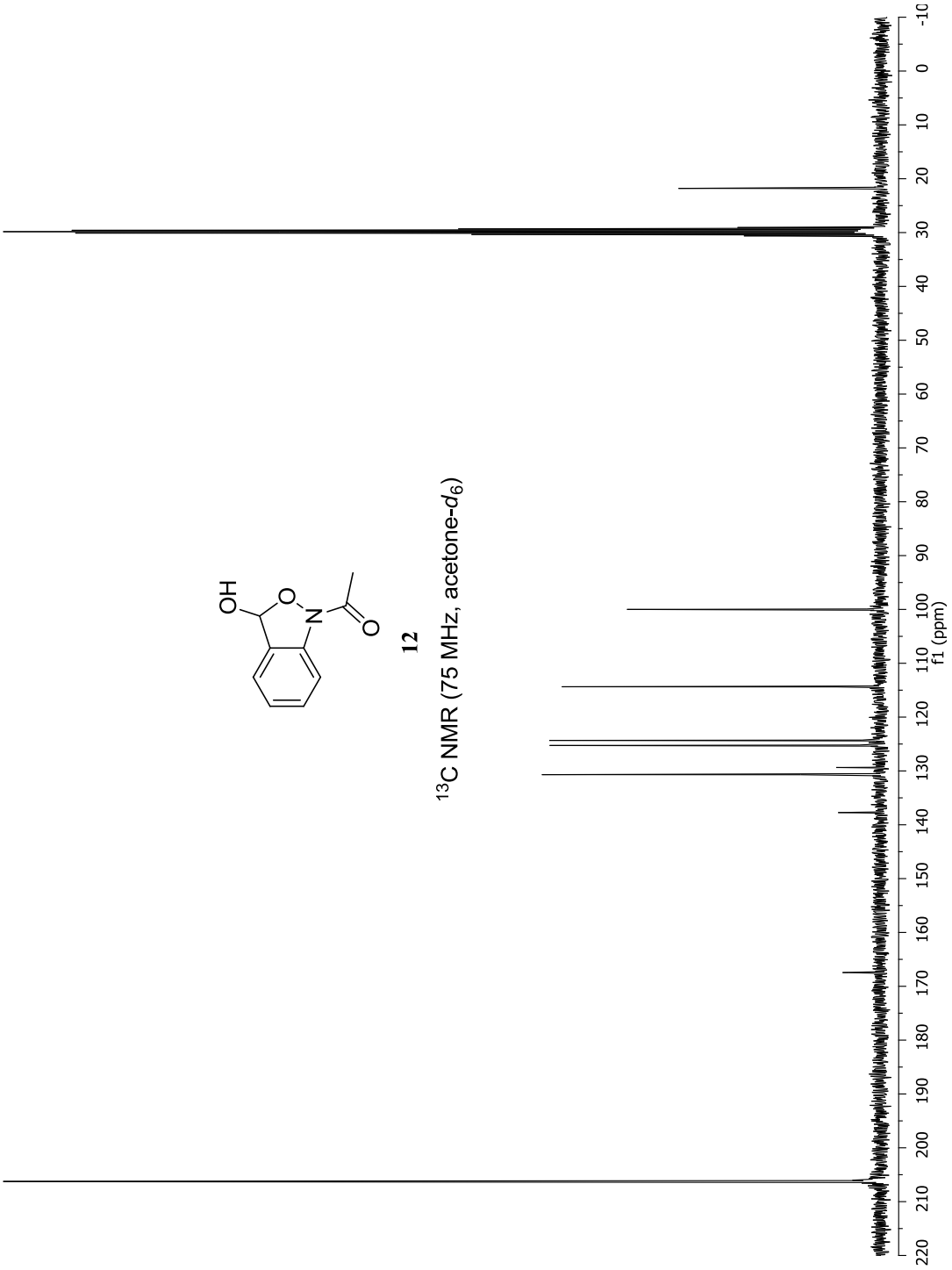
OH
O
N
O
12
^{13}C NMR (75 MHz, acetone-d_6)
f1 (ppm)
220
210
200
190
180
170
160
150
140
130
120
110
100
90
80
70
60
50
40
30
20
10
0
-10

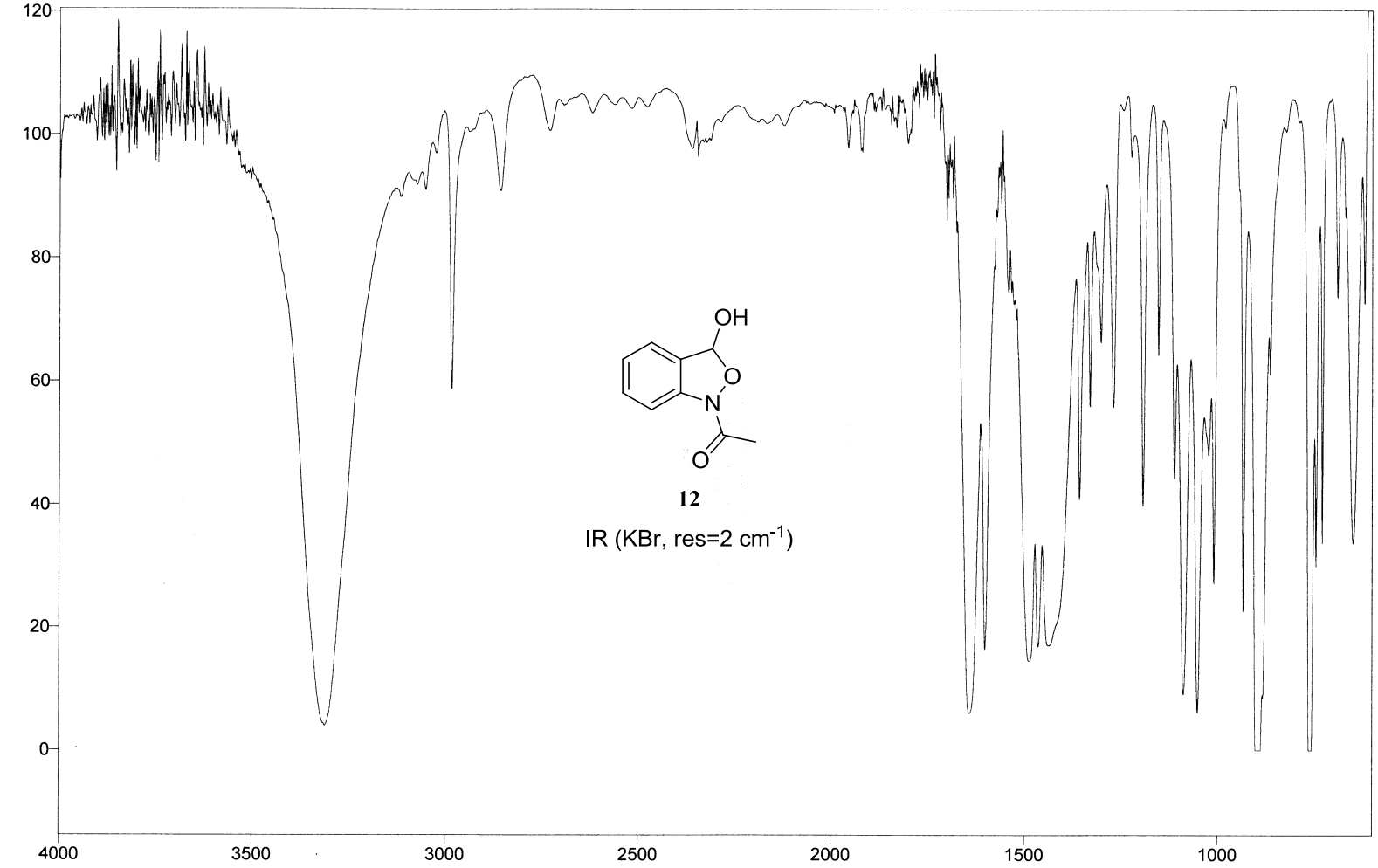

12

IR (KBr, res=2 cm^{-1})

APPENDIX 2. X-RAY CRYSTALLOGRAPHIC DATA FOR COMPOUND 10 IN PART II.

```
data_09094
_audit_creation_method          SHELXL-97
_chemical_name_systematic
rac-(1R)-((1S)-hydroxy(2-nitrophenyl)methyl-1,3-dihydrobenzo[c]isoxazol-3-ol
_chemical_name_common           Agnotobenzaldehyde
_chemical_formula_moiety        'C14 H12 N2 O5'
_chemical_formula_sum           'C14 H12 N2 O5'
_chemical_properties_physical   photo-sensitive
_exptl_crystal_recrystallization_method
'vapor diffusion of hexane into ethyl acetate at 248 K in a closed vial'
_chemical_melting_point         372

_exptl_crystal_description      Needle
_exptl_crystal_colour           Colorless

_diffrn_ambient_temperature     173(2)
_diffrn_ambient_pressure        101.32
_chemical_formula_weight        288.26

loop_
_atom_type_symbol
_atom_type_description
_atom_type_scat_dispersion_real
_atom_type_scat_dispersion_imag
_atom_type_scat_source
C C 0.0033 0.0016 'International Tables Vol C Tables 4.2.6.8 and 6.1.1.4'
H H 0.0000 0.0000 'International Tables Vol C Tables 4.2.6.8 and 6.1.1.4'
N N 0.0061 0.0033 'International Tables Vol C Tables 4.2.6.8 and 6.1.1.4'
O O 0.0106 0.0060 'International Tables Vol C Tables 4.2.6.8 and 6.1.1.4'

_symmetry_cell_setting          orthorhombic
_symmetry_space_group_name_H-M   'P b c a'
_symmetry_space_group_name_Hall  '-P 2ac 2ab'
_symmetry_int_tables_number     61
```

```
loop_
_symmetry_equiv_pos_as_xyz
'x, y, z'
'-x+1/2, -y, z+1/2'
'-x, y+1/2, -z+1/2'
'x+1/2, -y+1/2, -z'
'-x, -y, -z'
'x-1/2, y, -z-1/2'
'x, -y-1/2, z-1/2'
'-x-1/2, y-1/2, z'

_cell_length_a                 13.8066(14)
_cell_length_b                 8.4412(9)
_cell_length_c                 22.832(2)
_cell_angle_alpha              90.00
_cell_angle_beta               90.00
_cell_angle_gamma              90.00
_cell_volume                   2660.9(5)
_cell_formula_units_Z          8
_cell_measurement_temperature  173(2)
_cell_measurement_reflns_used  3650
_cell_measurement_theta_min    2.31
_cell_measurement_theta_max    23.84
_exptl_crystal_size_max        0.50
_exptl_crystal_size_mid        0.20
_exptl_crystal_size_min        0.15
_exptl_crystal_density_meas    ?
_exptl_crystal_density_diffrn  1.439
_exptl_crystal_density_method  'not measured'
_exptl_crystal_F_000           1200
_exptl_absorpt_coefficient_mu  0.111
_exptl_absorpt_correction_type  multi-scan
_exptl_absorpt_correction_T_min  0.8605
_exptl_absorpt_correction_T_max  0.9837
_exptl_absorpt_process_details  'SADABS, R. Blessing, 1995'

_exptl_special_details
;
 ?
;
_diffrn_radiation_probe        x-ray
_diffrn_radiation_type         MoK\a
_diffrn_radiation_wavelength   0.71073
```

```
_diffrn_source                 'normal-focus sealed tube'
_diffrn_radiation_monochromator  graphite
_diffrn_measurement_device_type  'Bruker SMART Platform CCD'
_diffrn_measurement_method       'area detector, omega scans per phi'
_diffrn_detector_area_resol_mean ?
_diffrn_standards_number        ?
_diffrn_standards_interval_count ?
_diffrn_standards_interval_time  ?
_diffrn_standards_decay_%       ?
_diffrn_reflns_number           20102
_diffrn_reflns_av_R_equivalents  0.0513
_diffrn_reflns_av_sigmaI/netI    0.0280
_diffrn_reflns_limit_h_min       -16
_diffrn_reflns_limit_h_max       16
_diffrn_reflns_limit_k_min       -9
_diffrn_reflns_limit_k_max       10
_diffrn_reflns_limit_l_min       -27
_diffrn_reflns_limit_l_max       27
_diffrn_reflns_theta_min         1.78
_diffrn_reflns_theta_max         25.07
_reflns_number_total            2357
_reflns_number_gt               1712
_reflns_threshold_expression     >2sigma(I)

_computing_data_collection       'Bruker SMART'
_computing_cell_refinement       'Bruker SMART'
_computing_data_reduction        'Bruker SAINT'
_computing_structure_solution    'Bruker SHELXTL'
_computing_structure_refinement  'SHELXL-97 (Sheldrick, 1997)'
_computing_molecular_graphics    'Bruker SHELXTL'
_computing_publication_material  'Bruker SHELXTL'

_refine_special_details
;
 Refinement of F^2^ against ALL reflections.  The weighted R-factor wR and
 goodness of fit S are based on F^2^, conventional R-factors R are based
 on F, with F set to zero for negative F^2^. The threshold expression of
 F^2^ > 2sigma(F^2^) is used only for calculating R-factors(gt) etc. and is
 not relevant to the choice of reflections for refinement.  R-factors based
 on F^2^ are statistically about twice as large as those based on F, and R-
 factors based on ALL data will be even larger.
;

_refine_ls_structure_factor_coef Fsqd
```

_refine_ls_matrix_type full
_refine_ls_weighting_scheme calc
_refine_ls_weighting_details
'calc w=1/[\s^2^(Fo^2^)+(0.0413P)^2^+1.7567P] where P=(Fo^2^+2Fc^2^)/3'
_atom_sites_solution_primary direct
_atom_sites_solution_secondary difmap
_atom_sites_solution_hydrogens geom
_refine_ls_hydrogen_treatment constr
_refine_ls_extinction_method none
_refine_ls_extinction_coef ?
_refine_ls_number_reflns 2357
_refine_ls_number_parameters 192
_refine_ls_number_restraints 0
_refine_ls_R_factor_all 0.0637
_refine_ls_R_factor_gt 0.0364
_refine_ls_wR_factor_ref 0.1035
_refine_ls_wR_factor_gt 0.0853
_refine_ls_goodness_of_fit_ref 1.038
_refine_ls_restrained_S_all 1.038
_refine_ls_shift/su_max 0.000
_refine_ls_shift/su_mean 0.000

loop_
_atom_site_label
_atom_site_type_symbol
_atom_site_fract_x
_atom_site_fract_y
_atom_site_fract_z
_atom_site_U_iso_or_equiv
_atom_site_adp_type
_atom_site_occupancy
_atom_site_symmetry_multiplicity
_atom_site_calc_flag
_atom_site_refinement_flags
_atom_site_disorder_assembly
_atom_site_disorder_group
O1 O 0.38128(10) 0.16275(15) 0.36935(6) 0.0307(3) Uani 1 1 d . . .
O2 O 0.21969(10) 0.24592(17) 0.36306(6) 0.0335(4) Uani 1 1 d . . .
H2 H 0.1911 0.1748 0.3821 0.050 Uiso 1 1 calc R . .
O3 O 0.34036(9) 0.47037(16) 0.41614(6) 0.0289(3) Uani 1 1 d . . .
H3 H 0.2992 0.3993 0.4096 0.043 Uiso 1 1 calc R . .
O4 O 0.63731(11) 0.3883(2) 0.40140(7) 0.0498(5) Uani 1 1 d . . .
O5 O 0.68900(12) 0.1541(2) 0.42317(8) 0.0554(5) Uani 1 1 d . . .
N1 N 0.44611(11) 0.29857(19) 0.36090(7) 0.0277(4) Uani 1 1 d . . .

N2 N 0.63222(12) 0.2644(3) 0.42935(8) 0.0380(5) Uani 1 1 d . . .
C1 C 0.29815(14) 0.1789(2) 0.33209(8) 0.0291(5) Uani 1 1 d . . .
H1 H 0.2798 0.0749 0.3143 0.035 Uiso 1 1 calc R . .
C2 C 0.33157(14) 0.2928(2) 0.28628(8) 0.0268(5) Uani 1 1 d . . .
C3 C 0.29014(16) 0.3384(2) 0.23347(9) 0.0337(5) Uani 1 1 d . . .
H3A H 0.2329 0.2890 0.2194 0.040 Uiso 1 1 calc R . .
C4 C 0.33473(17) 0.4578(3) 0.20197(9) 0.0382(5) Uani 1 1 d . . .
H4 H 0.3078 0.4912 0.1657 0.046 Uiso 1 1 calc R . .
C5 C 0.41800(18) 0.5290(3) 0.22260(9) 0.0417(6) Uani 1 1 d . . .
H5 H 0.4472 0.6109 0.2001 0.050 Uiso 1 1 calc R . .
C6 C 0.46036(16) 0.4844(3) 0.27532(9) 0.0371(5) Uani 1 1 d . . .
H6 H 0.5176 0.5338 0.2894 0.045 Uiso 1 1 calc R . .
C7 C 0.41492(14) 0.3643(2) 0.30641(8) 0.0267(4) Uani 1 1 d . . .
C8 C 0.43469(14) 0.4059(2) 0.41106(8) 0.0258(4) Uani 1 1 d . . .
H8 H 0.4806 0.4962 0.4053 0.031 Uiso 1 1 calc R . .
C9 C 0.46510(14) 0.3191(2) 0.46647(8) 0.0264(4) Uani 1 1 d . . .
C10 C 0.55574(14) 0.2480(3) 0.47380(9) 0.0306(5) Uani 1 1 d . . .
C11 C 0.57945(16) 0.1609(3) 0.52306(10) 0.0390(6) Uani 1 1 d . . .
H11 H 0.6409 0.1107 0.5258 0.047 Uiso 1 1 calc R . .
C12 C 0.51355(18) 0.1474(3) 0.56813(10) 0.0404(6) Uani 1 1 d . . .
H12 H 0.5296 0.0896 0.6025 0.048 Uiso 1 1 calc R . .
C13 C 0.42429(17) 0.2183(3) 0.56286(9) 0.0371(5) Uani 1 1 d . . .
H13 H 0.3786 0.2099 0.5938 0.045 Uiso 1 1 calc R . .
C14 C 0.40065(15) 0.3019(2) 0.51266(9) 0.0305(5) Uani 1 1 d . . .
H14 H 0.3383 0.3488 0.5097 0.037 Uiso 1 1 calc R . .

loop_
_atom_site_aniso_label
_atom_site_aniso_U_11
_atom_site_aniso_U_22
_atom_site_aniso_U_33
_atom_site_aniso_U_23
_atom_site_aniso_U_13
_atom_site_aniso_U_12
O1 0.0387(8) 0.0221(7) 0.0313(7) 0.0047(6) -0.0027(6) -0.0014(6)
O2 0.0339(8) 0.0301(8) 0.0367(8) 0.0058(7) 0.0077(6) -0.0046(7)
O3 0.0296(8) 0.0257(7) 0.0316(8) 0.0001(6) -0.0011(6) 0.0058(6)
O4 0.0361(9) 0.0555(12) 0.0578(11) -0.0025(9) 0.0104(8) -0.0063(8)
O5 0.0382(9) 0.0664(12) 0.0616(11) -0.0250(10) -0.0048(8) 0.0230(9)
N1 0.0290(9) 0.0229(9) 0.0314(9) 0.0002(7) 0.0019(7) -0.0018(7)
N2 0.0268(10) 0.0468(12) 0.0405(11) -0.0171(10) -0.0059(8) 0.0018(10)
C1 0.0339(11) 0.0256(11) 0.0278(10) 0.0000(9) -0.0012(9) -0.0020(9)
C2 0.0329(11) 0.0222(10) 0.0251(10) -0.0007(8) 0.0044(8) 0.0010(9)
C3 0.0437(12) 0.0306(12) 0.0269(11) -0.0029(9) 0.0005(9) -0.0014(10)

C4 0.0563(15) 0.0357(12) 0.0225(10) 0.0027(9) 0.0034(10) 0.0011(11)
C5 0.0566(15) 0.0364(12) 0.0320(12) 0.0075(10) 0.0131(11) -0.0049(12)
C6 0.0386(12) 0.0360(12) 0.0367(12) 0.0013(10) 0.0093(10) -0.0086(10)
C7 0.0302(11) 0.0250(10) 0.0250(10) -0.0005(9) 0.0067(8) 0.0021(9)
C8 0.0257(10) 0.0233(10) 0.0284(10) -0.0004(8) 0.0009(8) 0.0019(9)
C9 0.0275(10) 0.0213(10) 0.0304(10) -0.0042(8) -0.0053(8) 0.0002(9)
C10 0.0280(10) 0.0308(11) 0.0330(11) -0.0110(9) -0.0068(9) 0.0010(9)
C11 0.0386(12) 0.0337(12) 0.0447(13) -0.0102(10) -0.0182(11) 0.0100(11)
C12 0.0551(15) 0.0296(12) 0.0364(12) 0.0019(10) -0.0160(11) 0.0019(11)
C13 0.0461(13) 0.0327(12) 0.0325(11) 0.0036(10) -0.0023(10) -0.0038(11)
C14 0.0299(11) 0.0272(11) 0.0343(11) 0.0003(9) -0.0022(9) 0.0022(9)

_geom_special_details
;
All esds (except the esd in the dihedral angle between two l.s. planes)
are estimated using the full covariance matrix. The cell esds are taken
into account individually in the estimation of esds in distances, angles
and torsion angles; correlations between esds in cell parameters are only
used when they are defined by crystal symmetry. An approximate (isotropic)
treatment of cell esds is used for estimating esds involving l.s. planes.
;

loop_
_geom_bond_atom_site_label_1
_geom_bond_atom_site_label_2
_geom_bond_distance
_geom_bond_site_symmetry_2
_geom_bond_publ_flag
O1 C1 1.435(2) . ?
O1 N1 1.467(2) . ?
O2 C1 1.412(2) . ?
O2 H2 0.8400 . ?
O3 C8 1.416(2) . ?
O3 H3 0.8400 . ?
O4 N2 1.227(3) . ?
O5 N2 1.226(2) . ?
N1 C7 1.429(2) . ?
N1 C8 1.469(2) . ?
N2 C10 1.471(3) . ?
C1 C2 1.493(3) . ?
C1 H1 1.0000 . ?
C2 C7 1.378(3) . ?
C2 C3 1.389(3) . ?
C3 C4 1.383(3) . ?

C3 H3A 0.9500 . ?
C4 C5 1.380(3) . ?
C4 H4 0.9500 . ?
C5 C6 1.390(3) . ?
C5 H5 0.9500 . ?
C6 C7 1.388(3) . ?
C6 H6 0.9500 . ?
C8 C9 1.521(3) . ?
C8 H8 1.0000 . ?
C9 C14 1.388(3) . ?
C9 C10 1.398(3) . ?
C10 C11 1.383(3) . ?
C11 C12 1.378(3) . ?
C11 H11 0.9500 . ?
C12 C13 1.375(3) . ?
C12 H12 0.9500 . ?
C13 C14 1.385(3) . ?
C13 H13 0.9500 . ?
C14 H14 0.9500 . ?

loop_
_geom_angle_atom_site_label_1
_geom_angle_atom_site_label_2
_geom_angle_atom_site_label_3
_geom_angle
_geom_angle_site_symmetry_1
_geom_angle_site_symmetry_3
_geom_angle_publ_flag
C1 O1 N1 109.61(13) . . ?
C1 O2 H2 109.5 . . ?
C8 O3 H3 109.5 . . ?
C7 N1 O1 103.53(14) . . ?
C7 N1 C8 114.03(15) . . ?
O1 N1 C8 108.31(14) . . ?
O5 N2 O4 123.4(2) . . ?
O5 N2 C10 117.8(2) . . ?
O4 N2 C10 118.70(18) . . ?
O2 C1 O1 110.78(15) . . ?
O2 C1 C2 109.28(16) . . ?
O1 C1 C2 103.26(15) . . ?
O2 C1 H1 111.1 . . ?
O1 C1 H1 111.1 . . ?
C2 C1 H1 111.1 . . ?
C7 C2 C3 120.79(18) . . ?

C7 C2 C1 107.83(17) . . ?
C3 C2 C1 131.23(18) . . ?
C4 C3 C2 118.0(2) . . ?
C4 C3 H3A 121.0 . . ?
C2 C3 H3A 121.0 . . ?
C5 C4 C3 120.7(2) . . ?
C5 C4 H4 119.6 . . ?
C3 C4 H4 119.6 . . ?
C4 C5 C6 121.9(2) . . ?
C4 C5 H5 119.1 . . ?
C6 C5 H5 119.1 . . ?
C7 C6 C5 116.8(2) . . ?
C7 C6 H6 121.6 . . ?
C5 C6 H6 121.6 . . ?
C2 C7 C6 121.80(19) . . ?
C2 C7 N1 111.84(17) . . ?
C6 C7 N1 126.36(19) . . ?
O3 C8 N1 113.55(15) . . ?
O3 C8 C9 111.77(15) . . ?
N1 C8 C9 108.78(15) . . ?
O3 C8 H8 107.5 . . ?
N1 C8 H8 107.5 . . ?
C9 C8 H8 107.5 . . ?
C14 C9 C10 115.97(18) . . ?
C14 C9 C8 120.38(17) . . ?
C10 C9 C8 123.61(18) . . ?
C11 C10 C9 122.5(2) . . ?
C11 C10 N2 116.19(18) . . ?
C9 C10 N2 121.29(19) . . ?
C12 C11 C10 119.7(2) . . ?
C12 C11 H11 120.2 . . ?
C10 C11 H11 120.2 . . ?
C13 C12 C11 119.3(2) . . ?
C13 C12 H12 120.3 . . ?
C11 C12 H12 120.3 . . ?
C12 C13 C14 120.4(2) . . ?
C12 C13 H13 119.8 . . ?
C14 C13 H13 119.8 . . ?
C13 C14 C9 122.1(2) . . ?
C13 C14 H14 118.9 . . ?
C9 C14 H14 118.9 . . ?

loop_
_geom_torsion_atom_site_label_1

_geom_torsion_atom_site_label_2
_geom_torsion_atom_site_label_3
_geom_torsion_atom_site_label_4
_geom_torsion
_geom_torsion_site_symmetry_1
_geom_torsion_site_symmetry_2
_geom_torsion_site_symmetry_3
_geom_torsion_site_symmetry_4
_geom_torsion_publ_flag
C1 O1 N1 C7 -17.66(18) . . . . ?
C1 O1 N1 C8 103.73(16) . . . . ?
N1 O1 C1 O2 -96.64(16) . . . . ?
N1 O1 C1 C2 20.25(18) . . . . ?
O2 C1 C2 C7 102.67(18) . . . . ?
O1 C1 C2 C7 -15.3(2) . . . . ?
O2 C1 C2 C3 -72.8(3) . . . . ?
O1 C1 C2 C3 169.2(2) . . . . ?
C7 C2 C3 C4 -0.3(3) . . . . ?
C1 C2 C3 C4 174.7(2) . . . . ?
C2 C3 C4 C5 0.1(3) . . . . ?
C3 C4 C5 C6 0.0(3) . . . . ?
C4 C5 C6 C7 0.1(3) . . . . ?
C3 C2 C7 C6 0.4(3) . . . . ?
C1 C2 C7 C6 -175.64(18) . . . . ?
C3 C2 C7 N1 -179.14(17) . . . . ?
C1 C2 C7 N1 4.8(2) . . . . ?
C5 C6 C7 C2 -0.3(3) . . . . ?
C5 C6 C7 N1 179.20(19) . . . . ?
O1 N1 C7 C2 7.5(2) . . . . ?
C8 N1 C7 C2 -109.93(18) . . . . ?
O1 N1 C7 C6 -172.00(18) . . . . ?
C8 N1 C7 C6 70.5(2) . . . . ?
C7 N1 C8 O3 51.8(2) . . . . ?
O1 N1 C8 O3 -62.86(18) . . . . ?
C7 N1 C8 C9 176.93(15) . . . . ?
O1 N1 C8 C9 62.27(18) . . . . ?
O3 C8 C9 C14 4.1(3) . . . . ?
N1 C8 C9 C14 -122.07(19) . . . . ?
O3 C8 C9 C10 -178.25(17) . . . . ?
N1 C8 C9 C10 55.6(2) . . . . ?
C14 C9 C10 C11 2.1(3) . . . . ?
C8 C9 C10 C11 -175.65(19) . . . . ?
C14 C9 C10 N2 -176.90(18) . . . . ?
C8 C9 C10 N2 5.4(3) . . . . ?

O5 N2 C10 C11 32.7(3) . . . . ?
O4 N2 C10 C11 -145.7(2) . . . . ?
O5 N2 C10 C9 -148.25(19) . . . . ?
O4 N2 C10 C9 33.3(3) . . . . ?
C9 C10 C11 C12 -2.6(3) . . . . ?
N2 C10 C11 C12 176.48(19) . . . . ?
C10 C11 C12 C13 1.3(3) . . . . ?
C11 C12 C13 C14 0.3(3) . . . . ?
C12 C13 C14 C9 -0.8(3) . . . . ?
C10 C9 C14 C13 -0.4(3) . . . . ?
C8 C9 C14 C13 177.39(18) . . . . ?

_diffrn_measured_fraction_theta_max 1.000
_diffrn_reflns_theta_full 25.07
_diffrn_measured_fraction_theta_full 1.000
_refine_diff_density_max 0.207
_refine_diff_density_min -0.194
_refine_diff_density_rms 0.043

APPENDIX 3. X-RAY CRYSTALLOGRAPHIC DATA FOR COMPOUND 12 IN PART II.

```
data_15377
_audit_creation_method          SHELXL-97
_chemical_name_systematic
rac-(R)-1-(3-hydroxy-2,1-benzisoxazol-1(3H)-yl)ethanone
_chemical_formula_moiety        'C9 H9 N O3'
_chemical_formula_sum           'C9 H9 N O3'
_chemical_melting_point         400

_exptl_crystal_description      prism
_exptl_crystal_colour           colorless

_diffrn_ambient_temperature     173(2)
_chemical_formula_weight        179.17

loop_
_atom_type_symbol
_atom_type_description
_atom_type_scat_dispersion_real
_atom_type_scat_dispersion_imag
_atom_type_scat_source
C C 0.0033 0.0016 'International Tables Vol C Tables 4.2.6.8 and 6.1.1.4'
H H 0.0000 0.0000 'International Tables Vol C Tables 4.2.6.8 and 6.1.1.4'
N N 0.0061 0.0033 'International Tables Vol C Tables 4.2.6.8 and 6.1.1.4'
O O 0.0106 0.0060 'International Tables Vol C Tables 4.2.6.8 and 6.1.1.4'

_symmetry_cell_setting          triclinic
_symmetry_space_group_name_H-M   'P -1'
_symmetry_space_group_name_Hall  '-P 1'
_symmetry_int_tables_number     2

loop_
_symmetry_equiv_pos_as_xyz
'x, y, z'
'-x, -y, -z'

_cell_length_a                  7.313(4)
_cell_length_b                  7.465(4)
```

```
_cell_length_c                  9.487(6)
_cell_angle_alpha               67.09(4)
_cell_angle_beta                68.70(4)
_cell_angle_gamma               61.36(3)
_cell_volume                    408.6(4)
_cell_formula_units_Z           2
_cell_measurement_temperature   173(2)
_cell_measurement_reflns_used   3373
_cell_measurement_theta_min     2.3832
_cell_measurement_theta_max     27.4293
_exptl_crystal_size_max         0.45
_exptl_crystal_size_mid         0.35
_exptl_crystal_size_min         0.30
_exptl_crystal_density_meas     ?
_exptl_crystal_density_diffrn   1.456
_exptl_crystal_density_method   'not measured'
_exptl_crystal_F_000            188
_exptl_absorpt_coefficient_mu   0.111
_exptl_absorpt_correction_type  multi-scan
_exptl_absorpt_correction_T_min 0.94
_exptl_absorpt_correction_T_max 0.98
_exptl_absorpt_process_details  'SADABS, R. Blessing, 1995'

_exptl_special_details
;
 ?
;
_diffrn_radiation_probe         x-ray
_diffrn_radiation_type          MoK\a
_diffrn_radiation_wavelength    0.71073
_diffrn_source                  'normal-focus sealed tube'
_diffrn_radiation_monochromator graphite
_diffrn_measurement_device_type 'Bruker SMART Platform CCD'
_diffrn_measurement_method      'area detector, omega scans per phi'
_diffrn_detector_area_resol_mean ?
_diffrn_standards_number        ?
_diffrn_standards_interval_count ?
_diffrn_standards_interval_time ?
_diffrn_standards_decay_%       ?
_diffrn_reflns_number           4864
_diffrn_reflns_av_R_equivalents 0.0144
_diffrn_reflns_av_sigmaI/netI   0.0153
_diffrn_reflns_limit_h_min      -9
_diffrn_reflns_limit_h_max      9
```

```
_diffrn_reflns_limit_k_min       -9
_diffrn_reflns_limit_k_max       9
_diffrn_reflns_limit_l_min       -12
_diffrn_reflns_limit_l_max       12
_diffrn_reflns_theta_min         2.39
_diffrn_reflns_theta_max         27.52
_reflns_number_total             1860
_reflns_number_gt                1634
_reflns_threshold_expression     >2sigma(I)

_computing_data_collection       'SMART, Bruker'
_computing_cell_refinement       'SAINT, Bruker'
_computing_data_reduction        'SAINT, Bruker'
_computing_structure_solution    'SHELXL-97 (Sheldrick, 1997)'
_computing_structure_refinement  'SHELXL-97 (Sheldrick, 1997)'
_computing_molecular_graphics    'SHELXTL, Bruker'
_computing_publication_material  ?

_refine_special_details
;
 Refinement of F^2^ against ALL reflections.  The weighted R-factor wR and
 goodness of fit S are based on F^2^, conventional R-factors R are based
 on F, with F set to zero for negative F^2^. The threshold expression of
 F^2^ > 2sigma(F^2^) is used only for calculating R-factors(gt) etc. and is
 not relevant to the choice of reflections for refinement.  R-factors based
 on F^2^ are statistically about twice as large as those based on F, and R-
 factors based on ALL data will be even larger.
;

_refine_ls_structure_factor_coef Fsqd
_refine_ls_matrix_type           full
_refine_ls_weighting_scheme      calc
_refine_ls_weighting_details
'calc w=1/[\s^2^(Fo^2^)+(0.0454P)^2^+0.0857P] where P=(Fo^2^+2Fc^2^)/3'
_atom_sites_solution_primary     direct
_atom_sites_solution_secondary   difmap
_atom_sites_solution_hydrogens   geom
_refine_ls_hydrogen_treatment    constr
_refine_ls_extinction_method     SHELXL
_refine_ls_extinction_coef       0.039(7)
_refine_ls_extinction_expression Fc^*^=kFc[1+0.001xFc^2^\l^3^/sin(2\q)]^-1/4^
_refine_ls_number_reflns         1860
_refine_ls_number_parameters     127
_refine_ls_number_restraints     0
```

_refine_ls_R_factor_all 0.0387
_refine_ls_R_factor_gt 0.0334
_refine_ls_wR_factor_ref 0.0903
_refine_ls_wR_factor_gt 0.0870
_refine_ls_goodness_of_fit_ref 1.044
_refine_ls_restrained_S_all 1.044
_refine_ls_shift/su_max 0.000
_refine_ls_shift/su_mean 0.000

loop_
_atom_site_label
_atom_site_type_symbol
_atom_site_fract_x
_atom_site_fract_y
_atom_site_fract_z
_atom_site_U_iso_or_equiv
_atom_site_adp_type
_atom_site_occupancy
_atom_site_symmetry_multiplicity
_atom_site_calc_flag
_atom_site_refinement_flags
_atom_site_disorder_assembly
_atom_site_disorder_group
C1 C 0.37412(18) 0.61515(17) 0.17385(13) 0.0304(2) Uani 1 1 d . . .
H1 H 0.3090 0.6869 0.0799 0.037 Uiso 1 1 calc R . .
C2 C 0.52759(17) 0.70611(16) 0.15526(12) 0.0282(2) Uani 1 1 d . . .
C3 C 0.69927(19) 0.72337(18) 0.03524(14) 0.0348(3) Uani 1 1 d . . .
H3 H 0.7336 0.6774 -0.0549 0.042 Uiso 1 1 calc R . .
C4 C 0.82137(19) 0.80961(19) 0.04909(15) 0.0387(3) Uani 1 1 d . . .
H4 H 0.9403 0.8237 -0.0326 0.046 Uiso 1 1 calc R . .
C5 C 0.77059(19) 0.87528(18) 0.18169(15) 0.0374(3) Uani 1 1 d . . .
H5 H 0.8559 0.9342 0.1887 0.045 Uiso 1 1 calc R . .
C6 C 0.59941(18) 0.85748(17) 0.30388(15) 0.0336(3) Uani 1 1 d . . .
H6 H 0.5660 0.9015 0.3948 0.040 Uiso 1 1 calc R . .
C7 C 0.47859(16) 0.77194(16) 0.28706(13) 0.0282(2) Uani 1 1 d . . .
C8 C 0.19891(19) 0.75067(17) 0.53630(13) 0.0322(3) Uani 1 1 d . . .
C9 C 0.0081(2) 0.6959(2) 0.60931(15) 0.0425(3) Uani 1 1 d . . .
H9A H -0.0087 0.6396 0.5392 0.064 Uiso 0.31(3) 1 calc PR . .
H9B H -0.1194 0.8231 0.6271 0.064 Uiso 0.38(3) 1 calc PR . .
H9C H 0.0268 0.5891 0.7097 0.064 Uiso 0.37(3) 1 calc PR . .
H9D H -0.0588 0.7282 0.7114 0.064 Uiso 0.56(3) 1 calc PR . .
H9E H 0.0519 0.5448 0.6236 0.064 Uiso 0.68(3) 1 calc PR . .
H9F H -0.0943 0.7787 0.5410 0.064 Uiso 0.71(3) 1 calc PR . .
N1 N 0.29684(15) 0.73763(16) 0.38794(11) 0.0328(2) Uani 1 1 d . . .

```
O1 O 0.21020(13) 0.67729(15) 0.31008(10) 0.0378(2) Uani 1 1 d . . .
O2 O 0.45956(14) 0.39894(12) 0.19506(10) 0.0366(2) Uani 1 1 d . . .
H2 H 0.5450 0.3396 0.2549 0.055 Uiso 1 1 calc R . .
O3 O 0.26916(15) 0.80967(13) 0.60288(10) 0.0409(2) Uani 1 1 d . . .

loop_
_atom_site_aniso_label
_atom_site_aniso_U_11
_atom_site_aniso_U_22
_atom_site_aniso_U_33
_atom_site_aniso_U_23
_atom_site_aniso_U_13
_atom_site_aniso_U_12
C1 0.0345(6) 0.0351(6) 0.0276(5) -0.0112(4) -0.0068(4) -0.0159(5)
C2 0.0305(5) 0.0274(5) 0.0297(5) -0.0081(4) -0.0089(4) -0.0117(4)
C3 0.0366(6) 0.0364(6) 0.0319(6) -0.0091(5) -0.0044(5) -0.0168(5)
C4 0.0341(6) 0.0383(6) 0.0413(6) -0.0049(5) -0.0044(5) -0.0195(5)
C5 0.0353(6) 0.0306(6) 0.0528(7) -0.0066(5) -0.0170(5) -0.0161(5)
C6 0.0347(6) 0.0308(5) 0.0435(6) -0.0136(5) -0.0142(5) -0.0121(5)
C7 0.0269(5) 0.0273(5) 0.0326(5) -0.0100(4) -0.0082(4) -0.0094(4)
C8 0.0390(6) 0.0248(5) 0.0288(5) -0.0060(4) -0.0109(5) -0.0079(4)
C9 0.0464(7) 0.0433(7) 0.0332(6) -0.0093(5) 0.0006(5) -0.0214(6)
N1 0.0320(5) 0.0440(5) 0.0337(5) -0.0190(4) -0.0048(4) -0.0184(4)
O1 0.0337(4) 0.0581(5) 0.0382(5) -0.0248(4) -0.0022(3) -0.0253(4)
O2 0.0468(5) 0.0350(4) 0.0389(5) -0.0112(3) -0.0142(4) -0.0196(4)
O3 0.0576(6) 0.0378(5) 0.0329(4) -0.0107(3) -0.0167(4) -0.0170(4)

_geom_special_details
;
 All esds (except the esd in the dihedral angle between two l.s. planes)
 are estimated using the full covariance matrix.  The cell esds are taken
 into account individually in the estimation of esds in distances, angles
 and torsion angles; correlations between esds in cell parameters are only
 used when they are defined by crystal symmetry.  An approximate (isotropic)
 treatment of cell esds is used for estimating esds involving l.s. planes.
;

loop_
_geom_bond_atom_site_label_1
_geom_bond_atom_site_label_2
_geom_bond_distance
_geom_bond_site_symmetry_2
_geom_bond_publ_flag
C1 O2 1.3812(16) . ?
```

C1 O1 1.4597(17) . ?
C1 C2 1.4985(16) . ?
C1 H1 1.0000 . ?
C2 C3 1.3753(19) . ?
C2 C7 1.3848(17) . ?
C3 C4 1.3897(18) . ?
C3 H3 0.9500 . ?
C4 C5 1.388(2) . ?
C4 H4 0.9500 . ?
C5 C6 1.383(2) . ?
C5 H5 0.9500 . ?
C6 C7 1.3916(16) . ?
C6 H6 0.9500 . ?
C7 N1 1.3998(16) . ?
C8 O3 1.2355(15) . ?
C8 N1 1.3456(17) . ?
C8 C9 1.489(2) . ?
C9 H9A 0.9800 . ?
C9 H9B 0.9800 . ?
C9 H9C 0.9800 . ?
C9 H9D 0.9800 . ?
C9 H9E 0.9800 . ?
C9 H9F 0.9800 . ?
N1 O1 1.4222(13) . ?
O2 H2 0.8400 . ?

loop_
_geom_angle_atom_site_label_1
_geom_angle_atom_site_label_2
_geom_angle_atom_site_label_3
_geom_angle
_geom_angle_site_symmetry_1
_geom_angle_site_symmetry_3
_geom_angle_publ_flag
O2 C1 O1 111.57(10) . . ?
O2 C1 C2 115.44(10) . . ?
O1 C1 C2 102.82(9) . . ?
O2 C1 H1 108.9 . . ?
O1 C1 H1 108.9 . . ?
C2 C1 H1 108.9 . . ?
C3 C2 C7 120.73(11) . . ?
C3 C2 C1 129.86(10) . . ?
C7 C2 C1 109.37(10) . . ?
C2 C3 C4 118.39(12) . . ?

C2 C3 H3 120.8 . . ?
C4 C3 H3 120.8 . . ?
C5 C4 C3 120.37(12) . . ?
C5 C4 H4 119.8 . . ?
C3 C4 H4 119.8 . . ?
C6 C5 C4 121.92(11) . . ?
C6 C5 H5 119.0 . . ?
C4 C5 H5 119.0 . . ?
C5 C6 C7 116.73(12) . . ?
C5 C6 H6 121.6 . . ?
C7 C6 H6 121.6 . . ?
C2 C7 C6 121.86(11) . . ?
C2 C7 N1 108.28(10) . . ?
C6 C7 N1 129.85(11) . . ?
O3 C8 N1 118.78(12) . . ?
O3 C8 C9 123.94(11) . . ?
N1 C8 C9 117.27(11) . . ?
C8 C9 H9A 109.5 . . ?
C8 C9 H9B 109.5 . . ?
H9A C9 H9B 109.5 . . ?
C8 C9 H9C 109.5 . . ?
H9A C9 H9C 109.5 . . ?
H9B C9 H9C 109.5 . . ?
C8 C9 H9D 109.5 . . ?
H9A C9 H9D 141.1 . . ?
H9B C9 H9D 56.3 . . ?
H9C C9 H9D 56.3 . . ?
C8 C9 H9E 109.5 . . ?
H9A C9 H9E 56.3 . . ?
H9B C9 H9E 141.1 . . ?
H9C C9 H9E 56.3 . . ?
H9D C9 H9E 109.5 . . ?
C8 C9 H9F 109.5 . . ?
H9A C9 H9F 56.3 . . ?
H9B C9 H9F 56.3 . . ?
H9C C9 H9F 141.1 . . ?
H9D C9 H9F 109.5 . . ?
H9E C9 H9F 109.5 . . ?
C8 N1 C7 132.28(10) . . ?
C8 N1 O1 118.44(10) . . ?
C7 N1 O1 109.28(9) . . ?
N1 O1 C1 107.44(9) . . ?
C1 O2 H2 109.5 . . ?

```
loop_
_geom_torsion_atom_site_label_1
_geom_torsion_atom_site_label_2
_geom_torsion_atom_site_label_3
_geom_torsion_atom_site_label_4
_geom_torsion
_geom_torsion_site_symmetry_1
_geom_torsion_site_symmetry_2
_geom_torsion_site_symmetry_3
_geom_torsion_site_symmetry_4
_geom_torsion_publ_flag
O2 C1 C2 C3 67.85(16) . . . . ?
O1 C1 C2 C3 -170.43(11) . . . . ?
O2 C1 C2 C7 -110.03(11) . . . . ?
O1 C1 C2 C7 11.70(11) . . . . ?
C7 C2 C3 C4 -0.39(17) . . . . ?
C1 C2 C3 C4 -178.06(11) . . . . ?
C2 C3 C4 C5 0.32(18) . . . . ?
C3 C4 C5 C6 0.17(18) . . . . ?
C4 C5 C6 C7 -0.56(17) . . . . ?
C3 C2 C7 C6 -0.02(16) . . . . ?
C1 C2 C7 C6 178.09(10) . . . . ?
C3 C2 C7 N1 179.47(10) . . . . ?
C1 C2 C7 N1 -2.43(12) . . . . ?
C5 C6 C7 C2 0.48(16) . . . . ?
C5 C6 C7 N1 -178.88(11) . . . . ?
O3 C8 N1 C7 2.74(19) . . . . ?
C9 C8 N1 C7 -178.33(11) . . . . ?
O3 C8 N1 O1 -177.66(9) . . . . ?
C9 C8 N1 O1 1.27(15) . . . . ?
C2 C7 N1 C8 171.23(11) . . . . ?
C6 C7 N1 C8 -9.3(2) . . . . ?
C2 C7 N1 O1 -8.39(12) . . . . ?
C6 C7 N1 O1 171.04(11) . . . . ?
C8 N1 O1 C1 -163.65(10) . . . . ?
C7 N1 O1 C1 16.03(12) . . . . ?
O2 C1 O1 N1 107.91(11) . . . . ?
C2 C1 O1 N1 -16.40(11) . . . . ?
_diffrn_measured_fraction_theta_max 0.986
_diffrn_reflns_theta_full        27.52
_diffrn_measured_fraction_theta_full 0.986
_refine_diff_density_max         0.238
_refine_diff_density_min         -0.145
_refine_diff_density_rms         0.034
```